

Treatment Effect of Budesonide in 5xFAD mouse model of Alzheimer's disease

Doctoral thesis
to obtain a doctorate (PhD)
from the Faculty of Medicine
of the University of Bonn

Yang Xu
from Tianjin, China

2025

Written with authorization of
the Faculty of Medicine of the University of Bonn

First reviewer: Prof. Dr. Anja Schneider

Second reviewer: Prof. Dr. Mikael Simons

Day of oral examination: 11.02.2025

From the German Center for Neurodegenerative Diseases

Table of Contents

List of abbreviations	5
1. Introduction.....	9
1.1 Alzheimer's disease (AD).....	9
1.1.1 Symptoms and diagnosis of AD	9
1.1.2 Pathology of AD	11
1.1.3 Therapy.....	20
1.2 Glucocorticoids.....	25
1.2.1 Glucocorticoid biology	25
1.2.2 Hormetic function of GCs	26
1.2.3 Clinical application of GCs	29
1.2.4 GCs in neuroinflammation.....	30
1.2.5 GCs are associated with reduced dementia risk	33
1.3 Project plan	34
1.3.1 Aim of project	34
1.3.2 Experimental plan	35
2. Materials and methods	39
2.1 Materials.....	39
2.1.1 Compounds, consumables.....	39
2.1.2 Buffers and solutions.....	40
2.1.3 Antibodies	41
2.1.4 Software.....	43
2.1.5 Equipment.....	44
2.2 Methods	44
2.2.1 Generation of 5xFAD mouse line	44
2.2.2 Drug delivery of Budesonide	45
2.2.3 Tissue preparation	49
2.2.4 Immunohistochemically staining	49
2.2.5 Microscopy and imaging processing.	50
2.2.6 Behavior experiments	52

2.2.7	Statistical analysis.....	55
3.	Results.....	56
3.1	Organ distribution of Budesonide	56
3.2	Effects of inhaler Budesonide treatment in the 5xFAD mouse model of AD.....	59
3.2.1	Effect of inhaler Budesonide treatment on behavior in the 5xFAD mouse model of AD.....	59
3.2.2	Effect of inhaled Budesonide on amyloid pathology in the 5xFAD mouse model of AD.....	62
3.2.3	Effect of inhalation Budesonide treatment on neurodegeneration in the 5xFAD mouse model of AD.....	65
3.2.4	Effect of inhalation Budesonide treatment on neuroinflammation in the 5xFAD mouse model of AD.....	74
4.	Discussion.....	82
4.1	Budesonide delivery methods: intranasal vs. inhaler.....	82
4.2	Sex difference in the response of 5xFAD mouse model to Budesonide treatment.....	83
4.3	Impact of Budesonide treatment on disease pathology in 5xFAD mice.....	84
4.4	Future directions for preclinical research and translating preclinical findings to explore a synergistic approach in AD Treatment.....	93
4.5	Inhaled Budesonide treatment as a prospective clinical approach for AD patients	94
5.	Abstract	96
6.	List of figures	97
7.	List of tables.....	99
8.	Reference	102
9.	Acknowledgments	124
10.	Publications.....	126

List of abbreviations

+	plus or positive
°C	degree Celsius
μ	micro (10e-6)
5xFAD	five times familial Alzheimer's disease
6E10	n-terminal antibody against Aβ
aa	amino acids
AAIC	Alzheimer's Association International Conference
Ac	acetylation
AD	Alzheimer's disease
ANOVA	analysis of variance
AP-1	activator protein-1
apoE	apolipoprotein E
APP	amyloid precursor protein
ARIA-E	amyloid-related imaging abnormalities – edema
ARIA-H	amyloid-related imaging abnormalities – hemorrhages
ARIAs	amyloid-related imaging abnormalities
Aβ	β-amyloid peptide
BBB	blood–brain barrier
BBB	blood-brain barrier
bp	base pair
Bud	Budesonide
C1q	Complement component 1q
C3	Complement component 3
CA1	Cornu Ammonis 1
CA1so	Cornu Ammonis 1 stratum oriens
CA1sr	Cornu Ammonis 1 stratum radiatum
CAA	cerebral amyloid angiopathy
CBP	cAMP response element binding protein
CCP	classical complement pathway
CNS	central nervous system
COPD	chronic obstructive pulmonary disease
CSF	cerebrospinal fluid
Ctrl	control
CXCR3	C-X-C motif chemokine receptor 3
Cyp40	cyclophilin 40

DABCO	1,4-Diazabicyclo[2.2.2]octan
DAPI	4',6-diamidino-2-phenylindole
ddH ₂ O	double-distilled water
DG	dentate gyrus
DNA	desoxyribonuclein acid
DZNE	German Center for Neurodegenerative Diseases
EDTA	ethylenediaminetetraacetic acid
ENT	entorhinal cortex
et al.	et alii (Latin = and others)
FACS	fluorescence-activated cell Sorting
FAD	familial Alzheimer's disease
FCS	fetal calf serum
FDA	Food and Drug Administration
FDG-PET	fluorodeoxyglucose positron emission tomography
FKBP52	FK506 Binding Protein 52
g	gram
GCs	glucocorticoids
GFAP	glial fibrillary acidic protein
GR	glucocorticoid receptor
HPA	hypothalamic-pituitary-adrenal
Hsp	heat shock protein
Iba1	ionized calcium-binding adapter molecule 1
IDE	insulin-degrading enzyme
IFN	interferon
IL-6	Interleukin 6
Inh	inhaler
iNOS	nitric oxide synthase
Int	intranasal
JNK	Jun N-terminal kinase
L	liter
LAMP1	lysosomal associated membrane protein 1
Lck	lymphocyte-specific protein-tyrosine kinase
LSM	laser scanning microscope
LTP	long-term potentiation
MBP	myelin basic protein
MerTK	Mer tyrosine kinase
MHC	major histocompatibility complex

mo	months
MRI	magnetic resonance imaging
MRs	mineralocorticoid receptors
MS	multiple sclerosis
n	number of biological replicates
N	number of analyzed samples of one biological replicate
Na ₂ HPO ₄	di-sodium hydrogen phosphate dihydrate
NaCl	sodium chloride
NaH ₂ PO ₄	sodium dihydrogen phosphate dihydrate
NeuN	Neuronal Nuclei
NfL	neurofilament light chain
NFTs	neurofibrillary tangles
NFκB	nuclear factor-κB
NLRP3	NLR family pyrin domain containing 3
NOR	novel object recognition
NPTX2	neuronal pentraxin 2
OB	olfactory bulb
Olig2	oligodendrocyte lineage transcription factor 2
ON	over night
P	Phosphorylation
PAS	periodic acid-Schiff
PBS	phosphate buffered saline
PET	positron emission tomography
PFA	paraformaldehyde
PFC	prefrontal cortex
pH	potential hydrogen
Pol	RNA polymerase
PSD95	postsynaptic density protein 95
pTau	phosphorylated Tau
pThr	phosphorylated threonine
RA	rheumatoid arthritis
RNA	ribonucleic acid
ROI	region of interest
rpm	revolutions per minute
RT	room temperature
SEM	standard error of the mean
SV2A	synaptic vesicle protein 2A

TBS	tris buffered saline
TCR	T cell receptor
Th	T helper
ThioS	Thioflavin S
TLR	toll-like receptors
TNF- α	tumor necrosis factor alpha
TREM2	triggering receptor expressed on myeloid cells 2
Tris-HCl	tris(hydroxymethyl)aminomethane-hydroxyl chloride
v/v	volume per volume
VLA	very late antigen
w/v	weight per volume
WHO	World Health Organization
wt	wildtype

1. Introduction

1.1 Alzheimer's disease (AD)

Alzheimer's disease (AD) is recognized by the World Health Organization as a global public health priority ([World Health Organization, 2022](#)). Alois Alzheimer first described AD in 1907. Clinically, AD is characterized by cognitive impairment, most prominently, by progressive memory. Currently, AD is the most common cause of dementia and the fifth leading cause of death in adults older than 65 years ([Wong, 2020](#)). Despite extensive research spanning decades, options for approved treatments with confirmed disease-modifying effects have been limited. However, advancements have been made recently, with the Food and Drug Administration (FDA) granting accelerated approval to aducanumab on June 21, 2021, followed by now full approval for lecanemab and donenemab. These drugs have been shown to slow the progression of Alzheimer's disease in clinical studies. ([Van Dyck CH, 2023](#)) ([Lilly E, 2023](#))

1.1.1 Symptoms and diagnosis of AD

The most common early clinical signs of AD are cognitive symptoms, most prominently memory loss, and neuropsychiatric symptoms such as depression and apathy. Middle-stage and later symptoms include disorientation, confusion, behavioral changes, and problems with language ([Dulewicz M, 2022](#)). The neurobiological basis of these symptoms is developing for decades before symptom onset. Disease pathology can be detected based on the assessment of fluid and imaging markers reflecting pathological changes decades before disease onset ([Delaby C, 2022](#)). Based on the degree of cognitive impairment, AD is often divided into three stages: the preclinical stage, characterized by normal cognitive ability; the prodromal stage, characterized by mild cognitive impairment; and the dementia stage, characterized by functional impairment ([Vermunt L, 2019](#)).

Previously, Alzheimer's disease was diagnosed through structural MRI (Magnetic Resonance Imaging), combined with the analysis of cerebrospinal fluid (CSF) acquired through an invasive lumbar puncture, or via FDG-PET (Fluorodeoxyglucose Positron Emission Tomography) or amyloid PET scan ([Reitz and Mayeux, 2014](#)). Changes in CSF amyloid-beta species occur approximately 20 years before the onset of cognitive symptoms and increase in parallel with increasing amyloid deposition in autosomal dominant AD ([Barthélemy, N. R., 2020](#); [Suárez-Calvet. M, 2020](#)).

In recent years, significant advancements have been made with blood tests using new generations of biomarkers for diagnosing AD. One such advancement is the detection of the plasma A β 42/A β 40 ratio, which can indicate the preferential deposition of A β 42 monomer into plaques ([Li Y, 2022](#)). Elevated levels of plasma pThr181, pThr217, and pThr231 tau species are also used to differentiate individuals who are amyloid PET-positive from those who are amyloid PET-negative. Moreover, biomarkers related to neuroinflammation, such as glial fibrillary acidic protein (GFAP), and neurodegeneration, such as neurofilament light chain (NfL) are being developed. GFAP is expressed by astrocytes and increases in conjunction with amyloid positivity, although it is not specific to AD ([Chatterjee P, 2022](#)).

At the 2024 Alzheimer's Association International Conference (AAIC), revised diagnostic guidelines for AD were introduced, highlighting the integration of blood-based biomarkers (BBM). Key biomarkers such as phosphorylated tau (p-tau181, p-tau217, p-tau231) and A β 42/40 ratios are now considered sufficient to establish an early biological diagnosis of AD and to inform clinical decision making throughout the disease continuum. These biomarkers detect amyloid beta and tau pathologies, which are central to AD neuropathologic changes. This shift to blood-based biomarkers, which were traditionally detected through cerebrospinal fluid (CSF) analysis or amyloid PET, provides a more accessible, less invasive, and cost-effective diagnostic tool. These developments are particularly beneficial for early detection in underserved and rural populations, as they make diag-

nosis more widely available, bridging the gap between research advancements and clinical care. ([Jack, 2024](#))

1.1.2 Pathology of AD

Amyloid

The major pathological hallmarks of AD are accumulations of insoluble deposits of amyloid β -peptide ($A\beta$) (**Figure 1.1**), which is derived by sequential proteolytic processing from a large type I transmembrane protein, the β -amyloid precursor protein (APP). The proteolytic enzymes involved in its processing are named secretases. β - and γ -secretase sequentially process $A\beta$ peptides of varying lengths (37–43 amino acids), with longer $A\beta$ peptides (namely, $A\beta_{42}$ and $A\beta_{43}$) being more prone to deposit into insoluble amyloid fibrils that form neuritic plaques. In contrast, α -secretase prevents its generation by cleaving within the middle of the amyloid domain ([Haass C, 2012](#)). $A\beta$ fibrils can increase oxidative stress, trigger inflammatory cascades, and activate caspases and may be upstream tau protein hyperphosphorylation and aggregation into neurofibrillary tangles (NFTs), which ultimately results in neuronal damage ([Iliyasu MO, 2023](#)). Familial AD mutations in the APP gene and components of the γ -secretase complex, presenilin 1 and 2, either increase the ratio of amyloidogenic $A\beta$ peptides produced by APP processing or lead to forms of $A\beta$ that are more prone to aggregate ([Nilsberth C, 2001](#)).

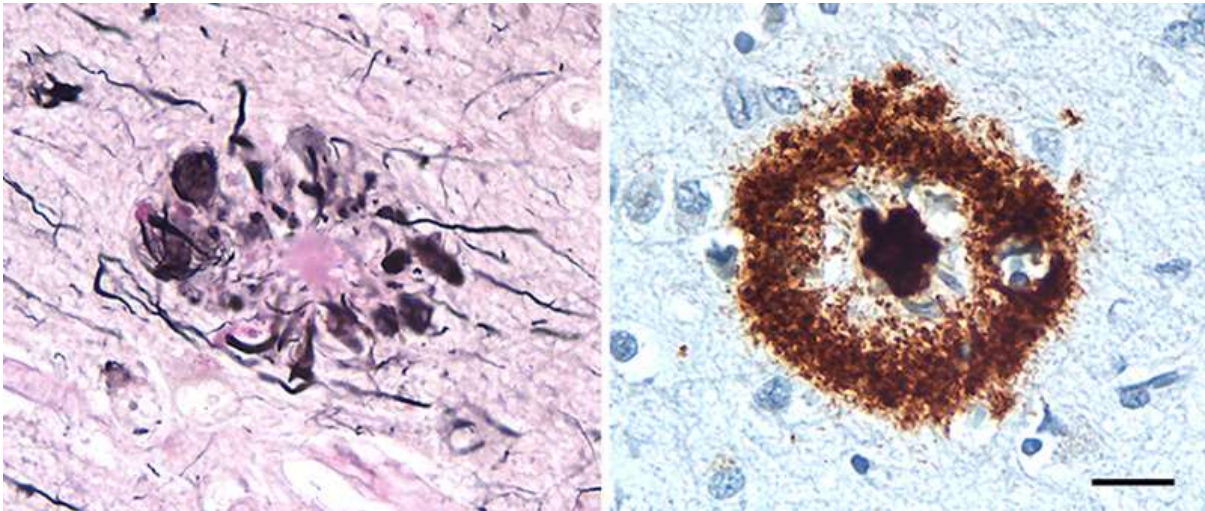


Figure 1.1: A β plaques in the cortex of individuals with Alzheimer's disease (AD)

On the left, a plaque is stained with the Naoumenko-Feigin silver method and periodic acid-Schiff (PAS) counterstain, revealing an amyloid core (dark pink) surrounded by a profusion of abnormal neurites (black). On the right, a plaque is immunostained with antibody 4G8 to the A β protein (brown), combined with a Nissl counterstain (blue). Glial nuclei are visible both between the plaque core and the outer corona, and within and surrounding the corona. The scale bar is 20 μ m for both panels. ([Walker L C, 2020](#))

The anatomic distribution of A β plaques is variable, but in general, the neocortex is more vulnerable and/or affected earlier than the primary motor and sensory areas ([Cupidi C, 2010](#)). According to Thal and colleagues, the progression of A β plaque distribution occurs in five phases. In the first phase, diffuse A β plaques appear in the neocortex. In the second phase, the allocortex, hippocampal formation, and amygdala are affected. In the third phase, plaques arise in the basal ganglia and diencephalon. In the fourth phase, they appear in the midbrain and medulla oblongata. Finally, in the fifth phase, the pons and cerebellum are affected. (**Figure 1.2**) ([Walker L C, 2020](#))

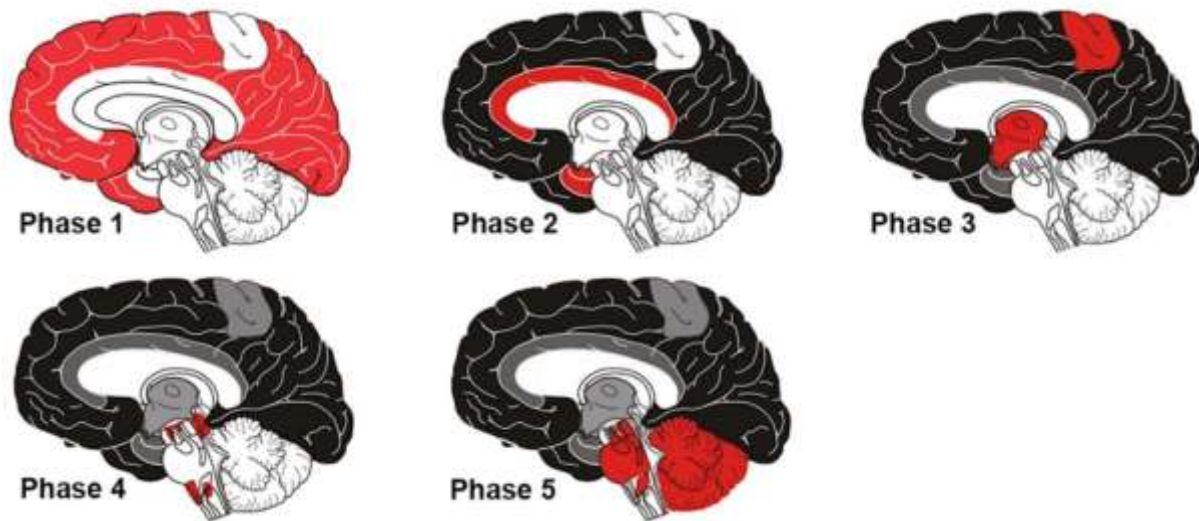


Figure 1.2: Schematic representation of the expansion of A β plaques (A β phases)
For A β plaque deposition newly involved brain regions are marked in red, already affected areas are painted in black. Illustration courtesy of Dietmar Thal, KU Leuven.

A β plaques are categorized as dense-core and diffuse plaques ([Wisniewski, 1973](#)). Dense-core plaques feature a central core of aggregated fibrillary amyloid, surrounded by loose A β -peptides and gliosis. β -sheet binding dyes like Congo Red, Methoxy-XO4, or ThioflavinS (ThioS) reveal these cores. Diffuse plaques lack a central core, having a more amorphous structure ([Selkoe, DJ, 2001](#)). Recent studies have suggested that dense-core plaques, which are formed by microglia, might be less harmful because they sequester toxic oligomers, potentially preventing these oligomers from diffusing into the brain environment ([Huang Y, 2021](#)); though this is debated.

Neurofibrillary tangles

Neurofibrillary tangles (NFTs) are pathological, insoluble aggregates of hyperphosphorylated tau proteins, observed within the neurons of AD patients. In healthy neurons, tau normally binds to and stabilizes microtubules. In Alzheimer's disease, however, abnormal chemical changes cause tau to detach from microtubules and adhere to other tau molecules, forming threads that eventually join to create tangles inside neurons. (**Figure 1.3**) ([DeTure, 2019](#))

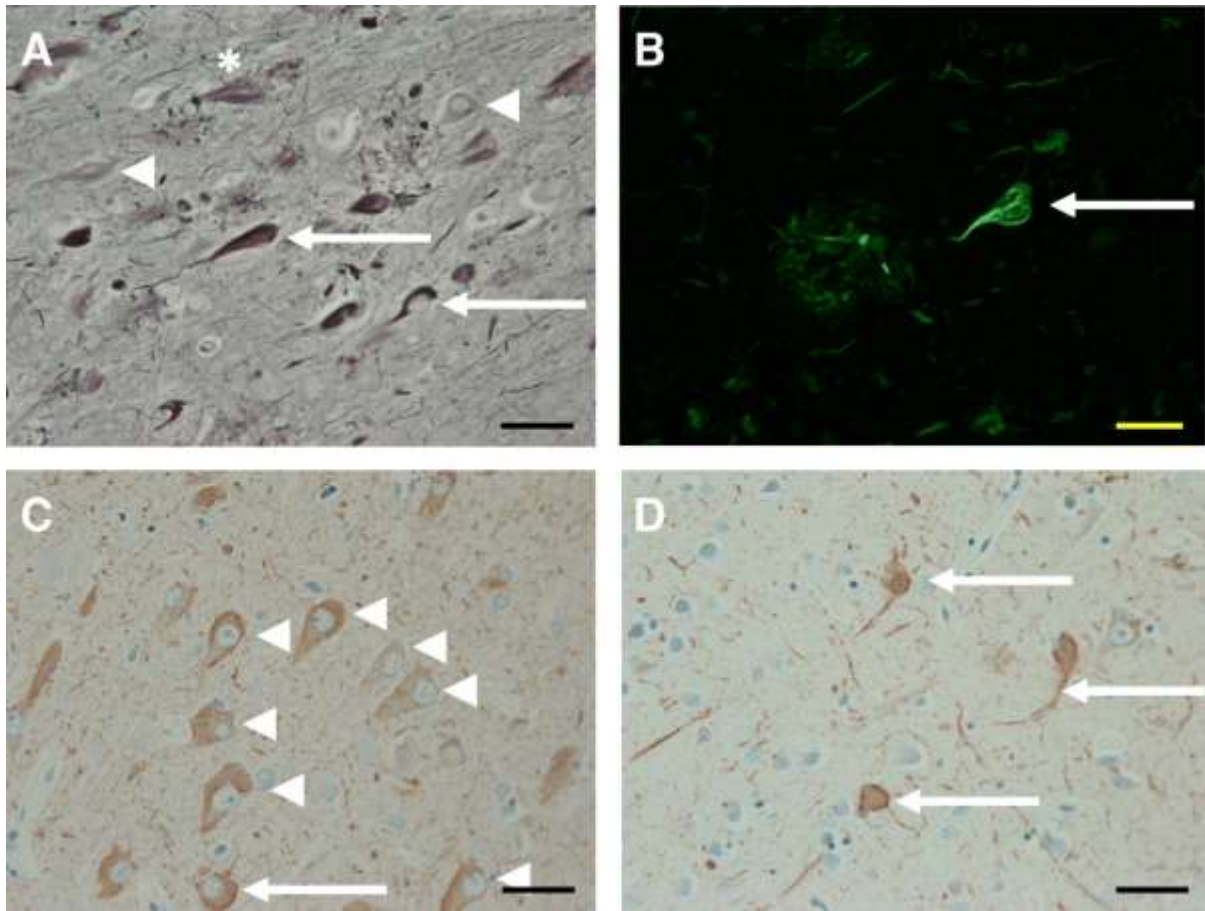


Figure 1.3: Neurofibrillary tangles in AD patient. (A) Silver staining and (B) Thioflavin S staining highlight numerous mature tangles (arrows) and some pre-tangles (arrow-heads) along with amyloid plaques and tau neuropil threads. The progression of NFTs from pre-tangles is clearly observed using tau immunohistochemistry (C, D). Scale bars are 40 µm. (DeTure, 2019)

Neurofibrillary tangles (NFTs) in Alzheimer's disease contribute to neuronal death through several interconnected mechanisms. Hyperphosphorylated tau, the main component of NFTs, destabilizes microtubules, disrupting axonal transport and impairing synaptic function, which leads to a reduction in the trafficking of essential nutrients and organelles, causing synaptic dysfunction and eventual neuronal atrophy ([Iqbal, 2010](#); [Wang and Mandelkow, 2016](#)). NFTs also induce cellular stress responses such as the unfolded protein response and autophagy, which, when overwhelmed, trigger apoptosis

([Lee, 2001](#)). Misfolded tau can impair mitochondrial transport along axons, reduce mitochondrial ATP production, and increase the production of reactive oxygen species (ROS). The accumulation of ROS induces oxidative stress, damaging cellular proteins, lipids, and DNA, further exacerbating neuronal injury and promoting cell death ([Spires, 2014](#); [Wang, 2009](#)). Furthermore, NFTs create a pro-inflammatory environment by activating microglia, which release pro-inflammatory cytokines, exacerbating neuronal damage ([Heneka, 2015](#)). Together, these mechanisms form a vicious cycle of neurodegeneration and inflammation, driving the progressive cognitive decline observed in AD ([Selkoe, 2002](#); [Bloom, 2014](#)).

Advanced imaging shows that abnormal tau accumulates in specific brain regions related to memory. As amyloid-beta levels rise and reach a tipping point, tau pathology spreads rapidly throughout the brain. Unlike A β , the stage of tau pathology correlates well with the progression of cognitive impairment ([Nelson, 2012](#)). The Braak staging system describes this tau pathology progression ([Braak H, 1991](#)):

Stages I and II: Neurofibrillary tangles (NFTs) are initially found in the transentorhinal region. Individuals at this stage are typically asymptomatic.

Stages III and IV: NFTs spread to the hippocampus and begin to affect the limbic system. Memory-related symptoms often start to appear.

Stages V and VI: NFTs become widespread throughout the neocortex, correlating with severe cognitive decline and dementia.

Neurodegeneration

Neurodegeneration is a hallmark of Alzheimer's disease, linked to progressive cognitive decline and memory loss ([Scheltens P, 2016](#)). A prominent hypothesis explaining AD development is the amyloid cascade theory, which posits that A β accumulation is an early and crucial event. These peptides aggregate to form amyloid plaques, believed to disrupt cellular function and initiate downstream effects, including tau hyperphosphorylation and

NFT formation, leading to neuronal damage and cognitive decline ([Hardy, 1992](#); [Hardy, 2002](#)).

A critical component of this pathological process involves the interplay between amyloid-beta ($A\beta$) and tau proteins, along with neuroinflammation. $A\beta$ aggregates disrupt synaptic communication and activate immune cells, leading to an inflammatory response. This inflammation is marked by the release of cytokines and other inflammatory mediators that exacerbate neuronal damage ([Selkoe, 2008](#)). Hyperphosphorylated tau loses its ability to stabilize microtubules, leading to their disintegration and the collapse of the neuronal cytoskeleton. This destabilization impairs axonal transport, which is vital for neuron survival and synaptic function. The aggregation of tau into neurofibrillary tangles further disrupts cellular processes, leading to cell death ([Iqbal, 2010](#); [Wang, 2016](#)).

Chronic inflammation can lead to the phagocytosis of synapses by microglia, known as synaptic pruning. While beneficial during development, excessive synaptic pruning in the adult brain results in significant synapse loss, contributing to the cognitive deficits seen in AD ([Hong, 2016](#)). Additionally, astrocytes, which typically support neuronal function, can become reactive and further contribute to the inflammatory milieu, exacerbating damage to neurons and synapses ([Liddelow, 2017](#)).

The pathogenesis of AD also involves the disruption of neural network connectivity. Studies using functional MRI have shown altered activity in the default mode network (DMN), a set of brain regions that show higher activity during rest and are involved in memory and self-referential thought processes. This network disruption is thought to underlie the early memory deficits observed in AD. ([Greicius MD, 2004](#))

Excitatory and inhibitory (E/I) balance is fundamental to normal brain function, and its disruption has been implicated in AD. The loss of inhibitory interneurons and the concomitant aberrant increase in glutamate-mediated excitatory signaling can lead to excitotoxicity. This imbalance contributes to neuronal dysfunction and death, further exacer-

bating the neurodegenerative process. (Palop JJ, 2012)

Ultimately, the pathological cascade in AD results in widespread neuronal loss, especially in the hippocampus and cortex, correlates with cognitive deficits (Terry RD, 1991). This neuronal loss affects critical cognitive networks, leading to impairments in attention, working memory, executive function, and episodic memory. The progressive nature of these pathological changes mirrors the gradual but relentless cognitive decline characteristic of AD, culminating in the extensive functional impairment seen in the disease's later stages.

Brain atrophy, characterized by a decrease in neuronal density and resulting in tissue loss, exhibits both spatial and temporal correlations with the progression of amyloid plaques and tau neurofibrillary tangles. This process manifests as sulci widening and gyri shrinkage, alongside significant reductions in brain weight. Notably, brain atrophy initiates in the medial temporal lobes and fusiform gyrus at least three years prior to an AD diagnosis, subsequently spreading to the posterior temporal and parietal lobes, and ultimately affecting the frontal lobes. Moreover, the rates of atrophy intensify as individual's transition from a cognitively normal state to an AD diagnosis. (Whitwell JL, 2010)

In summary, the interplay between amyloid-beta accumulation, tau pathology, and neuroinflammation drives the synaptic and neuronal loss observed in Alzheimer's disease. This multifaceted process involves direct synaptic disruption by A β plaques, tau-induced cytoskeletal instability, and chronic neuroinflammation, all contributing to the progressive cognitive decline characteristic of the disease.

Neuroinflammation

In recent years, an increasing number of studies have shown that AD pathogenesis is strongly intertwined with immunological mechanisms in the brain. Innate immune responses are triggered when misfolded and aggregated proteins bind to pattern recogni-

tion receptors on microglia and astrocyte.

Microglia Upon activation, microglia abandon their typical roles of tissue surveillance and synaptic remodeling to launch an acute inflammatory response. This shift aids in the clearance of amyloid deposits and aims to restore tissue homeostasis. However, this change is a double-edged sword. While initially protective, prolonged exposure to pro-inflammatory cytokines and the subsequent withdrawal of microglial processes can lead to functional impairments that contribute to a toxic environment, potentially causing neuronal damage (Heneka M T, 2015)

In AD, microglia interact with soluble amyloid- β (A β) oligomers and fibrils through a variety of receptors, including class A scavenger receptor A1, CD36, CD14, α 6 β 1 integrin, CD47, and toll-like receptors (TLR2, TLR4, TLR6, and TLR9). These interactions not only prompt microglia to produce pro-inflammatory cytokines and chemokines, which can be detrimental (Bamberger ME, 2003; Paresce DM, 1996; Stewart CR, 2010; Liu Y, 2005), but also lead to the phagocytosis of A β fibrils and trafficking via the endosomal/lysosomal pathway. Despite the resilience of fibrillary A β to enzymatic breakdown, soluble forms of A β can be more readily degraded by extracellular proteases like neprilysin and the insulin-degrading enzyme (IDE), pointing towards a nuanced interplay between microglial activation, amyloid pathology, and neuronal health (Lee CYD, 2010).

In sporadic AD cases, inefficient phagocytic clearance of A β , leading to increased cytokine levels, has been identified as a major pathogenic pathway. (Mawuenyega KG, 2010) Moreover, a rare mutation in the extracellular domain of TREM2 increases the risk of AD similarly to apoE ϵ 4. TREM2 is highly expressed by microglia and mediates the phagocytic clearance of neuronal debris and the downregulation of the inflammatory response. TREM2 expression is typically upregulated under pathological conditions in vivo and increased levels of TREM2 have been observed in AD patients. (Lue L F, 2015)

Astrocyte Astrocytes regulate synaptic communication and are essential for proper brain

functioning. In AD pathology, astrocytes become reactive and are closely associated with A β deposition. They show increased expression of glial fibrillary acidic protein (GFAP) and, similarly to microglia, release cytokines, interleukins, nitric oxide, and other potentially cytotoxic molecules upon exposure to A β , thereby exacerbating the neuroinflammatory response. Astrocytes also play a potential role in internalizing and degrading A β in vivo. Astrocyte-mediated clearance of A β requires ApoE, and astrocyte-dependent lipidation of ApoE enhances the ability of microglia to clear A β . (Terwel D, 2011) Reactive astrocytes modulate synaptic communication and neuronal network function, potentially contributing to cognitive decline in AD. (Smit T, 2021)

Complement system Synapse loss in AD correlates with cognitive decline. The complement system is a major component of the innate immune system, involved in chronic neuroinflammation characterized by gliosis, elevated levels of pro-inflammatory cytokines, and synapse loss. Classical complement pathway (CCP) factors are abnormally elevated in the brains and cerebrospinal fluid (CSF) of AD patients and are associated with A β deposits (Wu T, 2019). C1q, the initiating protein of the classical complement cascade, is increased and associated with synapses before overt plaque deposition. Subsequent activation of the CCP results in the proteolytic cleavage of the complement factor C3, leading to opsonization and microglial phagocytosis of complement-tagged synapses. Additionally, astrocytes contact and eliminate synapses in a C1q-dependent manner, contributing to pathological synapse loss. Specifically, astrocytes are more associated with the elimination of excitatory synapses, while microglia are more involved in inhibitory synapse elimination. (Dejanovic, 2022)

Caspases Caspases are a family of intracellular proteases that play key roles in apoptosis and inflammation. The inflammasome is a multiprotein complex that can activate inflammatory caspases. The NLRP3 inflammasome assembles within microglia upon activation, leading to increased cleavage and activity of caspase-1 and subsequent IL-1 β release. (Heneka MT, 2018) Elevated levels of active caspases have been detected in

the brains of AD patients. ([Burguillos MA, 2011](#))

As mentioned in the previous section, cytokines contribute to nearly every aspect of neuroinflammation, bystander neuronal injury, and the microglial response to A β deposits. Pro-inflammatory cytokines, including TNF- α , IL-6, and IL-1 α , are increased in AD. Chemokines are also suggested to regulate microglial migration to areas of neuroinflammation, thereby enhancing local inflammation in AD. In addition to cytokines and chemokines, inducible nitric oxide synthase (iNOS) and reactive oxygen species are also involved in AD pathology.

1.1.3 Therapy

Disease modifying treatments

Anti-Amyloid directed therapies

In the past 20 years, several anti-A β passive immunizations have progressed to phase 2 and phase 3 clinical trials. As depicted in **Table 1.1** ([Self WK, 2023](#)), most antibodies have demonstrated the ability to remove amyloid, with the exceptions of solanezumab and crenezumab, which may be attributed to their targeting of soluble A β species. Notable drugs in this category include Aducanumab (Aduhelm), Lecanemab (Leqembi), and Donanemab. Aducanumab gained FDA accelerated approval in June 2021, although its clinical benefit remains debated. Lecanemab initially received accelerated approval in January 2023 and was later converted to traditional approval in July 2023, demonstrating significant reduction in cognitive decline and amyloid plaques ([FDA, 2023](#)). Donanemab, marketed as Kisunla, was approved by the FDA on July 2, 2024, for the treatment of early symptomatic Alzheimer's disease, including mild cognitive impairment (MCI) and mild dementia ([Mullard, 2024](#)). While these drugs target amyloid plaques, safety concerns, particularly ARIA-related complications, warrant vigilant monitoring during treatment to mitigate potential adverse effects and restrict application. Safety concerns are due to the

side effect of hemorrhage (ARIA-H) and edema (ARIA-E) (amyloid-related imaging abnormalities (ARIAs)). ARIA could result from inflammatory reactions and endothelial cell damage from A β and or abeta immune complexes deposition in the small- to medium-sized blood vessels or their vicinity of the brain and leptomeninges. ([Antolini L, 2021](#)) To mitigate these side effects, there is ongoing discussion about using anti-inflammatory drugs. ([Alzforum, 2023](#))

Table 1.1: Summary of large-scale clinical trials of anti-amyloid passive immunization([Self WK, 2023](#)).

Monoclonal antibody (RCT)	Trial endpoint (weeks)	Number of trial participants	Amyloid negative in treatment group at end (%)	Dose	Cognitive benefit compared to placebo	ARIA-E (% treatment greater than placebo)	ARIA-H (% treatment greater than placebo)	A β target
Solanezumab (Expedition 1,2)	80	2052	-	400mg	No	0.5	-0.7	Soluble monomer
Crenezumab (CREAD 1,2)	102	1619	-	60mg/kg	No	0.1	0.5	Soluble oligomers
Gantenerumab (Graduate 1,2)	116	1965	27	1020mg	No	-	-	Insoluble fibrils
Aducanumab (EMERGE)	78	1638	48	10mg/kg	Yes	33.0	13.0	Insoluble fibrils
Aducanumab (ENGAGE)	78	1647	31	10mg/kg	No	33.0	13.0	Insoluble fibrils
Donanemab (TRAILBLAZER-ALZ 2)	76	1736	76	700mg	Yes	21.9	17.8	Plaque-associated A β
Lecanemab (Clarity AD)	78	1734	81	10mg/kg	Yes	10.9	6.3	Protofibrils

Anti-Tau therapies

In recent years, significant advancements have also been made in developing anti-tau therapies for Alzheimer's disease (AD). Monoclonal antibodies have been at the forefront of these developments. Therapies like gosuranemab (BIIB092) and semorinemab (RO7105705) aim to bind extracellular tau and prevent its spread between neurons. Despite initial promise, gosuranemab did not show significant efficacy in clinical trials for progressive supranuclear palsy (PSP) and AD. ([Shulman, 2023](#)) Semorinemab also demonstrated safety in trials but failed to meet primary efficacy endpoints in reducing cognitive decline. ([Teng, 2022](#)) Tilavonemab (ABBV-8E12) targets the mid-region of the tau protein and, similar to gosuranemab and semorinemab, did not show clinical benefits in PSP and AD trials. ([Höglinger, 2021](#)) Other monoclonal antibodies, such as bepranemab (UCB0107) and E2814, are in various stages of clinical testing and have shown potential in reducing tau levels and impacting disease biomarkers. ([Barton, 2021](#); [Rawal, 2023](#))

Active immunotherapies, including vaccines, are another promising approach. AADvac1 is designed to elicit an immune response against pathological tau, promoting its clearance from the brain. Early clinical trials have shown promising results regarding safety and immunogenicity. ([Novak, 2021](#))

Small molecules like TRx0237 (LMTX) and methylene blue have also been explored for their ability to inhibit tau aggregation and promote the disassembly of tau filaments but clinical studies have failed so far. ([TauRx, 2023](#))

Another anti-tau directed therapy that has emerged as promising involves antisense oligonucleotides (ASOs). ASOs work by targeting the tau mRNA, reducing the production of the tau protein before it can accumulate and form toxic aggregates in the brain. This approach offers a more upstream mechanism of action compared to monoclonal antibodies, which typically target extracellular tau. Recent preclinical and early clinical studies have

demonstrated the potential of anti-tau ASOs in lowering tau levels and slowing the progression of Alzheimer's disease (AD). ([Mummery, 2023](#))

Overall, these tau-targeting therapies represent a multifaceted approach to treating Alzheimer's disease, focusing on reducing tau pathology to protect neuronal function. Continued research and clinical trials are essential to validate these treatments' efficacy and safety, with the ultimate goal of providing effective therapies for patients with AD.

Neuroinflammation

Currently, numerous AD clinical trials are targeting neuroinflammation ([Cummings J, 2022](#)). One of the key targets in this area is TREM2, a receptor expressed on microglia that plays a critical role in regulating the brain's immune response. TREM2 agonism is being studied for its ability to enhance microglial function, such as promoting phagocytosis and amyloid plaque clearance. ([Schlepckow, 2020](#)) However, there is also concern that activating TREM2 could drive microglia into a reactive state, exacerbating neuroinflammation and potentially contributing to neuronal loss in AD ([Wang S, 2020](#)). This dual potential makes TREM2 a complex but promising target for ongoing clinical trials aimed at modulating neuroinflammation in AD.

In addition to targeting TREM2, efforts are also being directed toward inflammasome inhibitors, which aim to suppress the activation of inflammasomes—protein complexes that drive inflammatory responses within the brain. By inhibiting these pathways, researchers hope to reduce the chronic inflammation that contributes to the progression of neurodegeneration in AD. These approaches are part of a broader effort to modulate the brain's immune response to alleviate AD pathology and slow disease progression. ([Xu, 2023](#))

Symptomatic treatment approaches

In addition, there are also treatments focus on alleviating symptoms without modulating

the underlying disease pathology. These symptomatic treatments include acetylcholinesterase inhibitors and memantine, along with combination therapies. Acetylcholinesterase inhibitors, such as donepezil, rivastigmine, and galantamine, work by increasing acetylcholine levels in the brain, a neurotransmitter crucial for memory and learning that is typically diminished in Alzheimer's patients. These drugs have been shown to offer modest improvements in cognitive function, behavioral symptoms, and daily activities (Birks0, 2016; Raina, 2008).

Memantine, an NMDA receptor antagonist, regulates glutamate activity. Excess glutamate can lead to neuronal damage, and memantine helps protect neurons from this excitotoxicity, thereby slowing symptom progression in moderate to severe AD. Studies have demonstrated memantine's benefits in improving cognitive function and daily activities, as well as reducing caregiver burden (Reisberg, 2003; Tariot, 2004).

In addition, combination therapy involving donepezil and memantine is approved outside the EU and marketed as Namzaric. This therapy combines the benefits of both acetylcholinesterase inhibition and NMDA receptor antagonism, aiming to provide a more comprehensive approach to managing symptoms in moderate to severe AD. Research indicates that this combination can enhance cognitive function and overall patient outcomes more effectively than either drug alone (van Dyck, 2007). These medications form the foundation of pharmacological treatment for Alzheimer's disease, focusing on stabilizing cognitive decline and improving patient outcomes.

Furthermore, several other targets are under investigation, including promoting the efferocytosis pathway (S Morioka, 2022) and modulating gut bacteria (Chandra S, 2023), among others.

1.2 Glucocorticoids

1.2.1 Glucocorticoid biology

Glucocorticoids (GCs) are steroid hormones involved in several physiological processes, including metabolism, water and electrolyte balance, immune response, growth, cardiovascular function, mood and cognitive functions, reproduction, and development. They are primarily synthesized in the cortex of the adrenal gland, and also extra-adrenally in the thymus, vasculature, brain, and epithelial barriers. ([Timmermans S, 2019](#)) The production of adrenal GC is regulated by the hypothalamic-pituitary-adrenal (HPA) axis, which becomes activated and increased upon physiological (activated immune response) and emotional stress. ([Spiga F, 2011](#))

Due to their lipophilic nature, free GCs diffuse through the cell membrane to exert their function. They can either interact with a membrane-bound glucocorticoid receptor (GR), as described for human monocytes and B cells, or they can passively penetrate into the cytosol. Once inside the cytosol, GCs bind to GRs, causing their release from a heat-shock protein complex composed of Hsp70, Hsp90, Hsp40, the co-chaperone p23, and the immunophilins FKBP52 and Cyp40. This release allows for the interaction of GRs with cytosolic signaling proteins such as phosphoinositide 3-kinase, and in most cases, their translocation into the nucleus followed by the modulation of transcription. GCs also bind to mineralocorticoid receptors (MRs) with high affinity. In macrophages and the brain, GCs are major ligands of MRs. By contrast, in tissues such as the kidney and colon, MR activation by GCs is largely prevented by the enzyme 11 β -hydroxysteroid dehydrogenase type II, which converts active cortisol into its inactive metabolite cortisone (**Figure 1.4**). Within the nucleus, both GRs and MRs can bind to palindromic DNA sequence elements in the promoter and enhancer regions of GC-responsive genes, followed by their transactivation. Additionally, GRs can also interact with other transcription factors such as activator protein (AP)-1 and nuclear factor (NF)- κ B without direct DNA contact.

(Schweingruber N, 2012)

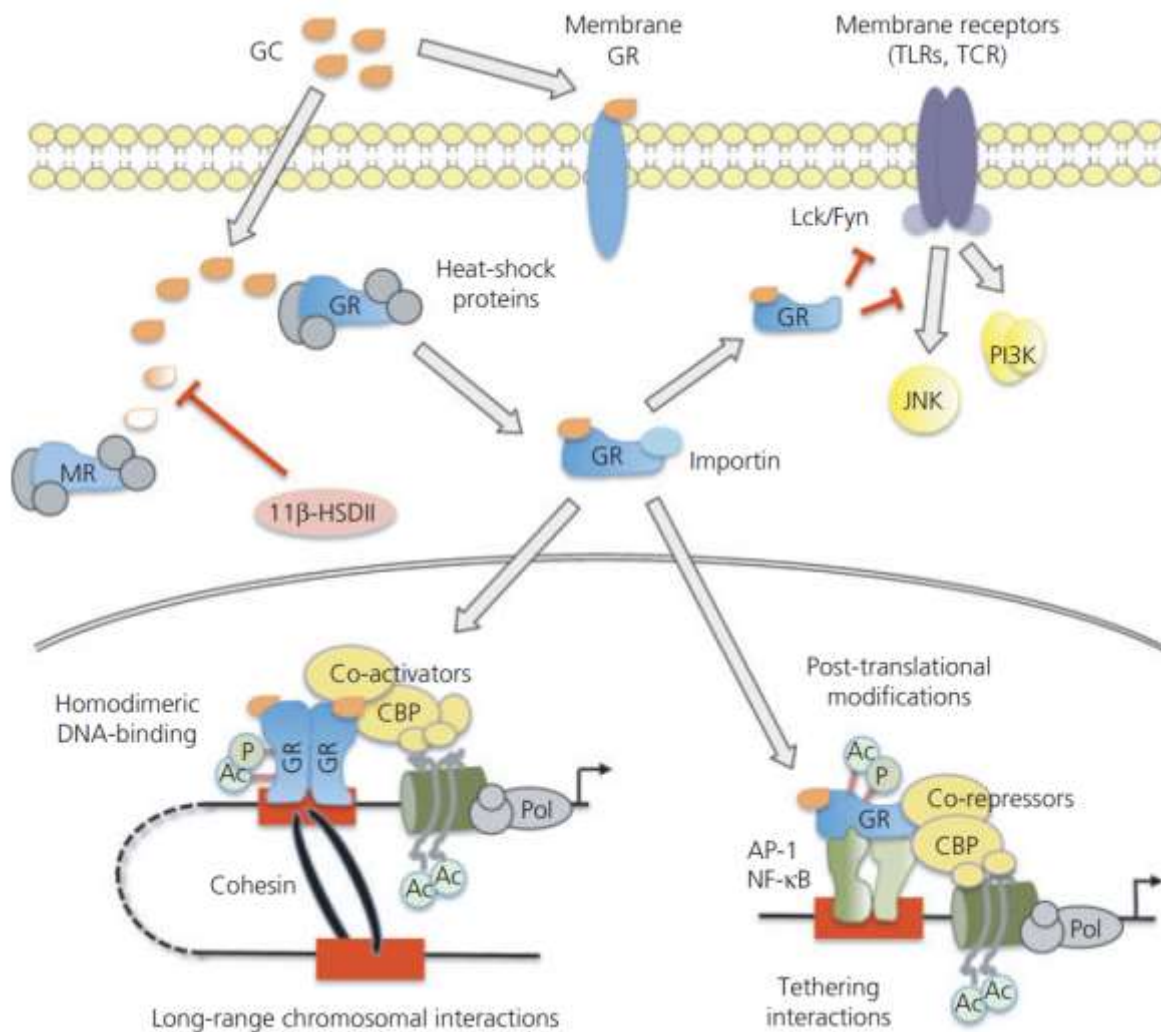


Figure 1.4: Cellular activity of glucocorticoids (GCs). Ac, acetylation; AP-1, activator protein-1; CBP, cAMP response element binding protein; Fyn, a Src family tyrosine-protein kinase; JNK, Jun N-terminal kinase; Lck, lymphocyte-specific protein-tyrosine kinase; NF-κB, nuclear factor-κB; P, phosphorylation; Pol, RNA polymerase II; TCR, T cell receptor; TLR, Toll-like receptor. (Figure adopted from [Schweingruber N, 2012](#))

1.2.2 Hormetic function of GCs

Glucocorticoids at low concentrations confer several benefits, including anti-inflammatory actions, immune system modulation to deter overactivity, and assistance in stress adap-

tation. GCs also modulate blood pressure and electrolyte balance and high doses of glucocorticoids are associated with a spectrum of adverse effects. These include reduced insulin sensitivity leading to hyperglycemia, suppression of the hypothalamic-pituitary-adrenal (HPA) axis, obesity, muscle loss, cardiovascular complications, such as hypertension. Moreover, they can weaken the immune response, increasing susceptibility to infections, contribute to a decline in bone density, and disturb hormonal homeostasis (Noetlin S, 2022; Fardet L, 2007).

In the central nervous system (CNS), glucocorticoids (GCs) play a crucial role in modulating glutamatergic synapses, particularly in the hippocampus and prefrontal cortex, by binding to mineralocorticoid and glucocorticoid receptors on synaptic membranes and within the cytosol of neurons. (Gulyaeva, 2023) Through this binding, GCs influence both presynaptic and postsynaptic compartments, regulating vesicular transport, glutamate release, and the properties of NMDA and AMPA receptors, which are key to synaptic plasticity and behavioral adaptation. By modulating these receptors, GCs enhance the brain's capacity for learning, memory consolidation, and stress adaptation. During stress, GCs initiate signal transduction pathways that affect neurotransmitter release and ion channel activity, particularly impacting ionotropic glutamate receptors crucial for long-term potentiation (LTP), a process central to memory and learning. However, chronic or excessive GC exposure can disrupt these pathways, impairing synaptic plasticity and contributing to cognitive decline. This hormone-mediated regulation ensures the brain remains adaptable to environmental changes, but overexposure can lead to synaptic dysregulation (Gulyaeva, 2021) When present in optimal amounts, GCs assist in stress adaptation, enhance learning, and support memory consolidation, crucial for restoring equilibrium after stress (Choi GE, 2021).

However, the therapeutic effects of GCs are contingent upon their concentration, adhering to a hormetic curve where too little or too much can be equally detrimental. **(Figure 1.5)** Low to moderate levels of GCs are beneficial, conferring resilience to the brain, but

chronic exposure to high levels may precipitate adverse outcomes like neuronal injury and cognitive decline. This is particularly evident in conditions of sustained high endogenous cortisol levels, which can disrupt neuronal excitability and plasticity, diminish long-term potentiation (LTP), and reduce hippocampal volume, leading to memory and cognitive issues ([De Kloet CS, 2006](#); [Diamond DM, 2007](#); [Lupien SJ, 1998](#)).

The implications of prolonged exposure to elevated GC levels are substantial, with links to the onset of neuropsychiatric disorders such as depression and anxiety, as well as an acceleration of neurodegenerative diseases like Alzheimer's. ([Knezevic, 2023](#)) This is due to GC-induced neuronal atrophy, especially in memory-critical regions like the hippocampus, and the exacerbation of neurotoxic protein accumulation ([Choi GE, 2021](#)).

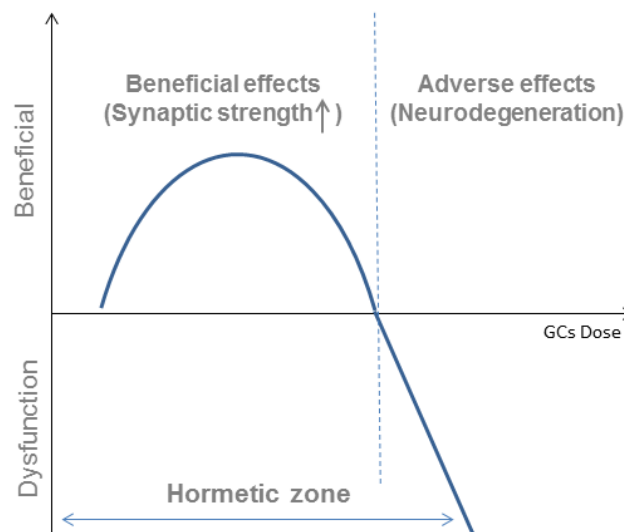


Figure 1.5: Biphasic effects of glucocorticoids following inverted U-shape curve Glucocorticoids assist cells in maintaining equilibrium and foster the repair and appropriate allocation of essential cellular components under normal to mild stress conditions, which aids in maintaining synaptic strength. However, persistent high levels can disrupt these processes, leading to cellular dysfunction and heightened neurodegeneration due to the breakdown of cellular quality control mechanisms. ([Choi GE, 2021](#))

Furthermore, GCs exert rapid non-genomic effects that adjust cellular signaling pathways instead of directly interacting with DNA. These can influence neurotransmitter release and receptor sensitivity, thereby affecting mood and behavior swiftly ([Gray JD, 2017](#)). GCs also affect glial cells, such as astrocytes and microglia, modulating brain inflammation. Their impact is even linked to circadian rhythms, modifying how neurons respond to stress ([Shimba A, 2020](#)). While targeting GC pathways might offer therapeutic benefits for neurodegenerative disorders, maintaining hormonal balance is essential, as deviations can disrupt neural function. In essence, GCs equip the brain to handle acute stress but can be damaging under chronic stress, emphasizing the importance of precise hormonal regulation.

1.2.3 Clinical application of GCs

The first time GC was used in treatment was in 1948 by Philip Hench, who administered cortisone to patients with rheumatoid arthritis (RA). ([Hench P, 1950](#)) Currently, due to their anti-inflammatory and immunosuppressive actions, GCs and their synthetic derivatives are still commonly used for the treatment of autoimmune, inflammatory, and allergic disorders, including rheumatoid arthritis ([Hua C, 2020](#)), lupus erythematosus ([Mejia-Vilet JM, 2021](#)), inflammatory bowel disease, multiple sclerosis ([Fischer HJ, 2019](#)), inflammatory dermatologic conditions, chronic obstructive pulmonary disease (COPD) ([Umoh VA, 2013](#)), transplant rejection, and asthma ([Timmermans S, 2019](#)).

Commonly used glucocorticoids include prednisone, prednisolone, triamcinolone, methylprednisolone, dexamethasone, and others. They are modified in the chemical structures of the cortisone (hydrocortisone) backbone to enhance their anti-inflammatory effects. The chemical modifications include the introduction of a 6 α -fluoro substitution, and reduction of binding to the mineralocorticoid receptor by inserting a C=C double bond at C1, C2, or replacing a lipophilic substituent such as 21 α -esters attached to the D-ring to increase binding to glucocorticoid receptors. Numerous genes are regulated by glu-

cocorticoids, and **Figure 1.6** demonstrates the broad physiological effects of glucocorticoids on the nervous (behavior, anxiety, vision), cardiovascular, immune, respiratory, reproductive, and musculoskeletal systems, as well as on metabolism. ([Yang R, 2021](#))





		Regulation	Gene function	Differential gene
	Respiratory system	Up	COVID-19-binding receptor	ACE2
		Down	Inflammatory in COVID-19	IL6
	Osteoarticular system	Up	Inflammation and oxidative stress	KLF9, MKP-1, MKP-2, TLR2, FOXO3
		Up	Regulation of osteoblast function	GPM6B
		Up	Cartilage development	ZBTB16
		Down	Inflammation and oxidative stress	TNFSF15, CCL2, FGFR3, COX-2, IL6, IL11
		Down	Pain	NGF
	Liver	Up	Regulation of gluconeogenesis	G6PC, PC, HNF4A, KLF15, FOXO1
		Down		PCK1
	Nervous system	Up	Alzheimer's disease-amyloid secretase pathway	PRKCH, MAPK13, PCSK7
		Down		PCSK6, APP, MAPKAPK3
	Stress reaction	Up	Activate stress responses	PPG
	Cancer	Down	Tumor growth	IL6, VEGF
	Inflammatory	Down	Inflammatory	IL-2, IL-5, IL-6, TNF α , GM-CSF, CCL1
	Immune system	Up	Regulation of systemic lupus	CD28,CD40LG
		Down	erythematosus	HLA-DQA1, FCGR3A, C2, CD86

Figure 1.6: The genes regulated by glucocorticoids. The genes regulated by glucocorticoids in respiratory system, osteoarticular system, liver, nervous system, stress reaction, cancers, inflammation, Alzheimer disease and systemic lupus erythematosus, et al. (Figure adopted from [Yang R, 2021](#))

1.2.4 GCs in neuroinflammation

The CNS is a prominent target of GCs, as GRs are ubiquitously expressed in neurons, glial cells (such as astrocytes, oligodendrocytes, and microglia), and brain vasculature. ([Williams S, 2020](#)) Furthermore, glucocorticoid receptors (GRs) are differentially expressed in human cortical regions, including the basolateral amygdala, CA1 hippocampus, and dentate gyrus. The effects of glucocorticoids (GCs) on behavior, cognition, and mood are influenced by factors such as gender, age, hormone concentrations, and the

timing and duration of exposure to stress. (Scheimann JR, 2018) At the cellular level, GCs are necessary for neuronal growth and differentiation, impacting several neuronal functions, including cell survival, integrity, and synaptic plasticity (Viho EMG, 2019). Additionally, GCs play a crucial role in regulating the immune system and mediating metabolism in the brain. For example, microglia, which abundantly express glucocorticoid receptors, may experience ameliorated neuroinflammation upon GC treatment (ERos-Bernal, 2011). Microglia, typically exist in a “resting” state in a healthy adult brain. However, upon tissue injury, disease, or aging, microglia rapidly transform into an activated state, releasing cytokines to coordinate the response of both innate and adaptive immunity, control infection, remove cell debris, and promote tissue repair (Neumann H, 2009). GCs can also influence the interaction between neurons and microglia. For example, during hippocampal neurogenesis, cell debris from apoptotic newborn cells and stress-induced glucocorticoid secretion promote microglial activation and transcriptional induction of the phagocytic receptor MerTK, regulating new neuron production to maintain homeostasis in the adult hippocampal neurogenic niche. (**Figure 1.7**)

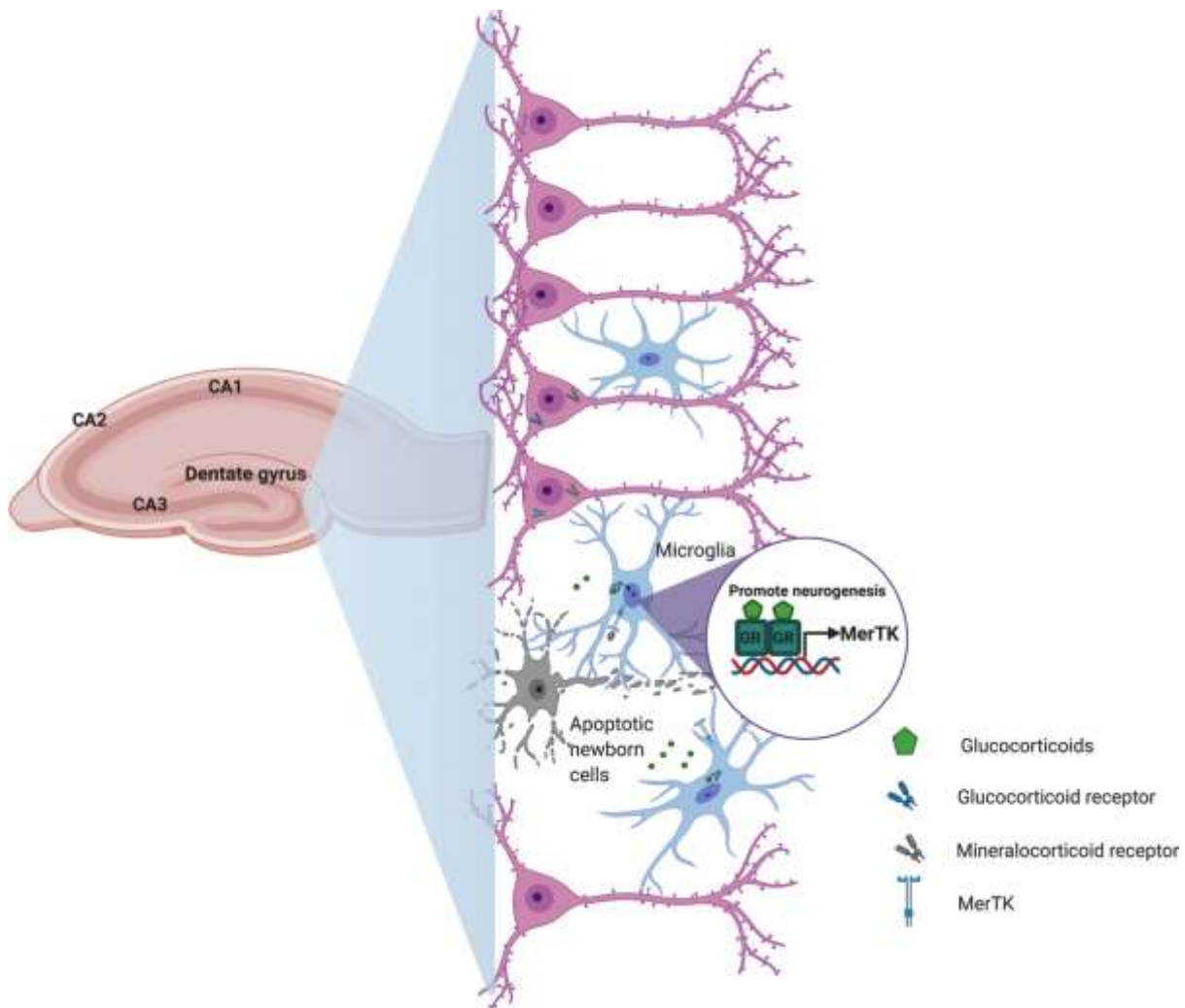


Figure 1.7: Schematic representation of how glucocorticoids could contribute to central nervous system homeostasis. Figure adapted from (D Diaz-Jimenez, 2021).

In the murine CNS, GCs inhibit the production of pro-inflammatory cytokines by T helper (Th)1 cells, such as interferon (IFN)- γ , and down-regulate the expression of cell adhesion molecules, such as very late antigen (VLA)-4, and chemokine receptors, e.g., CXCR3. Conversely, GCs increase the secretion of anti-inflammatory cytokines by Th2 cells and exert a suppressive effect on Th1 cells. They also induce T cell apoptosis and cause the expansion of myeloid-derived suppressor cells (MDSCs), negatively impacting T cell activity. GCs can restore the integrity of the blood-brain barrier (BBB) by down-regulating matrix metalloproteinases (MMPs). They repress nitric oxide (NO) production by myeloid cells such as macrophages through the inhibition of inducible NO synthase (iNOS) and

down-regulation of major histocompatibility complex (MHC) II molecules, interfering with T cell activation. Furthermore, GCs positively influence the secretion of the anti-inflammatory cytokine IL-10 by myeloid cells. ([Schweingruber N, 2012](#))

1.2.5 GCs are associated with reduced dementia risk

A recent study based on health claims data from the AOK (German health insurance) demonstrated that inhaled and intranasal applications of glucocorticosteroids (GCC) are associated with a significantly reduced risk of dementia compared to controls. (**Figure 1.8**) ([Nerius M, 2020](#)). The protective effect is most evident for inhaled GCCs, followed by nasal and oral forms.

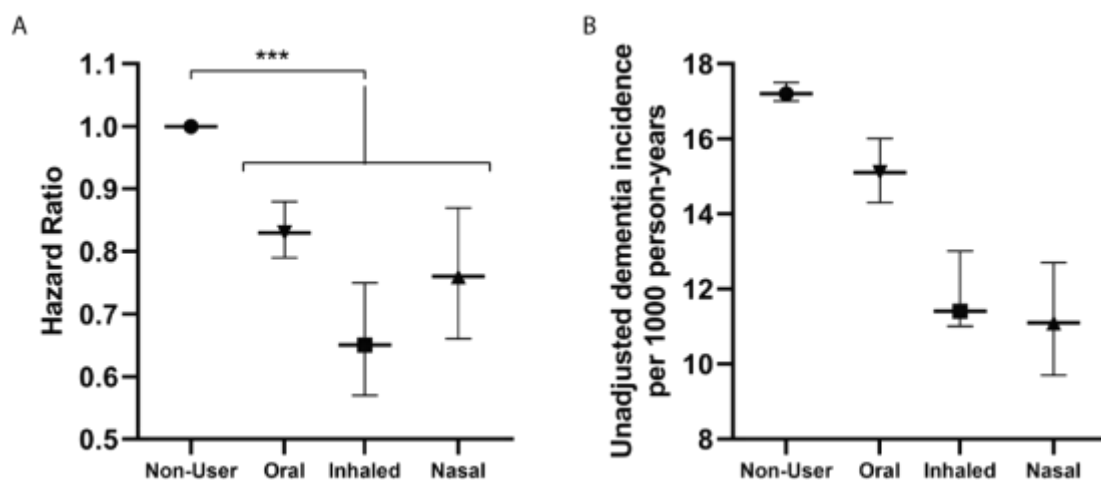


Figure 1.8: Topical glucocorticoids are associated with a lower risk of dementia. (Data adapted from [Nerius M, 2020](#)). (A) Hazard ratio (HR) from Cox-proportional hazard models for use of GCs and route of application. Mean HR \pm 95% confidence interval, ***p<0.001. (B) Unadjusted dementia incidence per 1000 person-years exposed. Mean incidence \pm 95% confidence interval.

The potential mechanisms behind these findings are unknown but may involve the anti-inflammatory properties of GCs. GCs can reduce neuroinflammation by modulating the activity of glial cells, such as astrocytes and microglia, which play key roles in the inflammatory response in the brain. By binding to glucocorticoid receptors, GCs can inhibit

the expression of pro-inflammatory genes and activate anti-inflammatory pathways. This dual action could help to maintain cellular homeostasis and reduce the neuroinflammatory processes that contribute to neurodegeneration and cognitive decline in AD ([Vandevyver, 2013](#); [Labzin, 2018](#)).

This notion is supported by a study utilizing the inhaled GC drug Budesonide in a chronic asthma mouse model which demonstrated that Budesonide can inhibit asthma-induced neuroinflammation and attenuate neuron loss. ([Xia M X, 2014](#))

Elevated concentrations of glucocorticoids, in particular endogenous GC levels, have been associated with brain atrophy and cognitive dysfunction ([Shorey2023](#); [Ouanes S, 2019](#)); however, reduced dosages and localized delivery methods may confer protective effects. Based on these observations, we hypothesize that glucocorticosteroids (GCCs) administered via inhalation or intranasal routes could directly target the brain, mitigating neuroinflammation while minimizing the potential for adverse systemic side effects.

1.3 Project plan

1.3.1 Aim of project

Health claim data indicate an association between glucocorticoid use and a reduced risk of dementia, especially when administered intranasally or via inhalation. As an anti-inflammatory drug, GCs bear the potential of attenuating neuroinflammation, which plays a crucial role in AD pathogenesis. Our project aimed to administer Budesonide, a GC which is widely used for the treatment of asthma and allergic rhinitis, to the 5xFAD mouse model of Alzheimer's disease. Budesonide was given intranasally or through inhalation, with treatment start either before or after plaque deposition. With our study designed we aimed to determine whether Budesonide reaches the brain, exerts anti-inflammatory effects, ameliorates amyloid and amyloid-associated pathology and symptoms. Assessments included behavioral analysis, immunohistochemistry for plaque

deposition, quantification of neuron and synapse loss, cytokine level measurements, microglial RNA sequencing analysis, single nuclei sequencing, and plasma biomarker analysis.

1.3.2 Experimental plan

1.3.2.1 5xFAD mouse model of Alzheimer's diseases

The animal model we used in our project was the 5xFAD transgenic mouse, a widely used model for amyloid pathology. The genetic modifications in this model include five familial Alzheimer's disease mutations within two human transgenes: APP and PSEN1, APP with the familial Swedish, Florida (I716V) and London mutations, together with mutant PS1 (M14 6L, L28 6V) under the control of the murine Thy-1 promoter. These mutations are known to enhance the production of amyloid-beta 42, leading to early and aggressive amyloid plaque formation, detectable as early as two months of age in the brain of these mice ([Oakley H, 2006](#)).

Notably, by four months of age, there is significant neuronal loss in areas crucial for cognition, including the subiculum and cortical layers 5 and 6, with concomitant synaptic degeneration and gliosis ([Jawhar S, 2012](#)). Behavioral assessments have revealed cognitive impairments in spatial memory and learning in 5xFAD mice at early time points, providing a functional readout for therapeutic interventions ([O'Leary TP, 2009](#)). The 5xFAD mouse model is particularly suited to this approach due to its rapid progression of Alzheimer's-like pathology. This model provides an opportunity to assess not only the amyloid pathology but also the synaptic loss and cognitive decline over a reasonable time frame for a preclinical study, paralleling the human condition and allowing for the exploration of the disease's multifactorial nature ([Sasaguri H, 2017](#)).

1.3.2.2 Intranasal treatment

In this project, we administered Budesonide intranasally to animals of both sexes after

briefly anesthetizing them with isoflurane. We treated both 5xFAD and wt mice as controls. As shown in **Figure 1.9**, the treatment started when the mice were 1.5 months old, aligning with the onset of amyloid pathology in 5xFAD mice. The treatment continued until the mice reached 6 months of age, at which point a series of behavioral tests was conducted. Subsequently, the mice were sacrificed, and their tissues were collected for further analysis. (Data is shown in supplement.)

Preclinical treatment

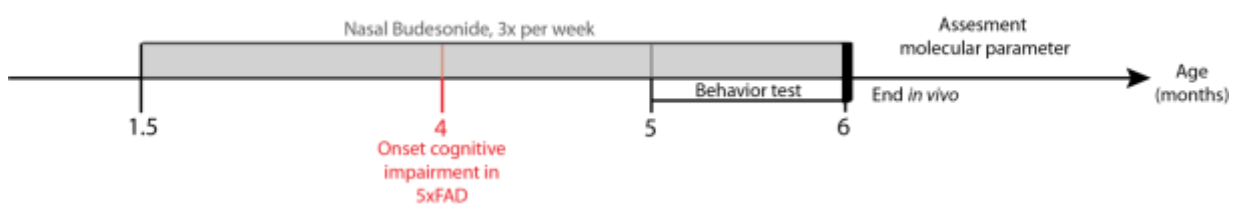


Figure 1.9: Intranasal Budesonide treatment timeline.

1.3.2.3 Inhalation treatment

Since intranasal treatment required repetitive isoflurane narcosis which on its own interferes with cognition and inflammation ([Wang, 2018](#)), inhaler treatment was employed in the second phase of this project. To better reflect clinical conditions, treatment commenced at 4 months, aligning with the onset of cognitive impairment in 5xFAD mice. Since male 5xFAD mice did not exhibit impairment in behavioral tests at that time point, only female animals were included in the experimental design. As illustrated in **Figure 1.10**, treatment continued until the end of month 6. Behavior tests were conducted during month 6. The mice were sacrificed at the end of month 6, and their tissues were utilized for further analysis.

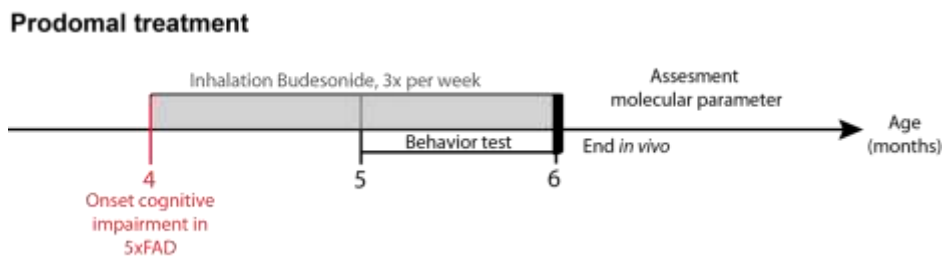


Figure 1.10: Inhalation Budesonide treatment timeline.

1.3.2.4 Behavior test plan

To evaluate the impact of Budesonide treatment on memory performance, various types of spatial memory were assessed. (**Figure 1.11**)

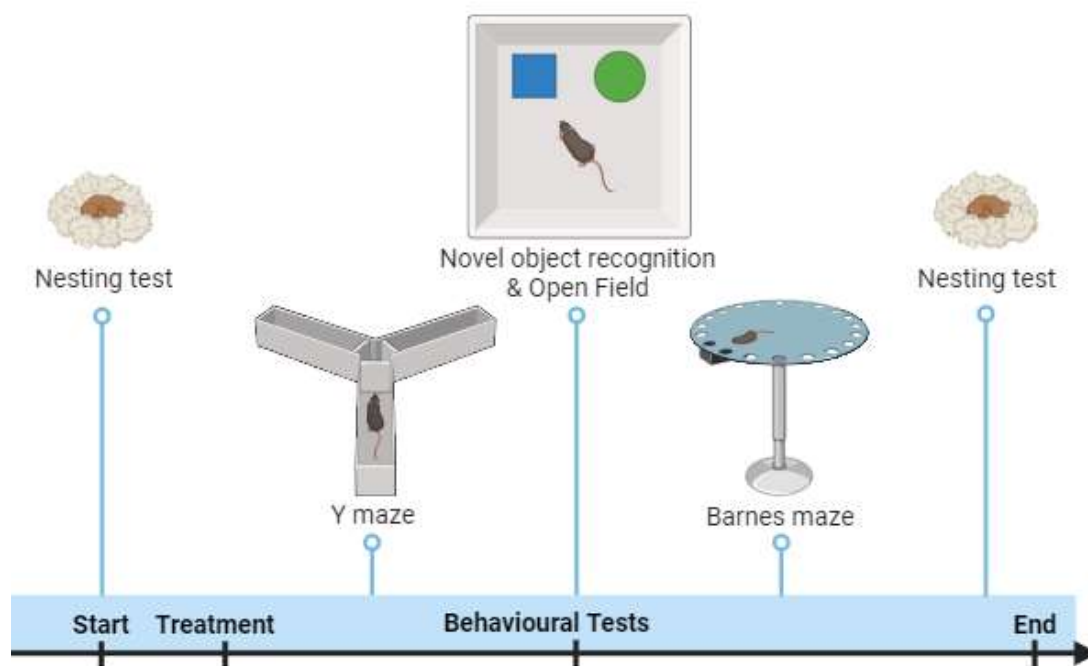


Figure 1.11 Behavior test plan for intranasal and inhaler treated mice batch.

Spatial hippocampus-dependent memory impairment is often observed early in AD patients, and GC receptors are highly expressed in hippocampal regions. Recognition memory was evaluated using the novel object recognition test, which examines the functions of several brain regions, including the hippocampus, perirhinal cortex, prefrontal

cortex, amygdala, and entorhinal cortex. (EC Warburton, 2015) Additionally, the potential effects of Budesonide treatment on anxiety-like behavior were analyzed using an open field test, which was conducted concurrently with the novel object recognition task. (Mitra R, 2008) Spatial reference memory was assessed using the Barnes maze, following a 6-day protocol. The primary aim of the Barnes maze is to examine the functioning of the hippocampus, particularly its role in spatial learning and memory. This test challenges an animal's ability to use spatial cues to navigate a maze, offering insights into hippocampal integrity and its connection to spatial memory deficits commonly seen in AD.

Another behavior test applied in this project is the nest building test. This test was applied before the initiation of treatment and after the completion of treatment. In the nest building test, mice were provided with material to build a nest, a task that requires coordinated motor skills, cognitive planning, and decision-making – abilities that are often impaired in AD.

2. Materials and methods

2.1 Materials

2.1.1 Compounds, consumables

Chemicals were purchased from Merck Millipore (Darmstadt, Germany), Roth (Karlsruhe, Germany) or Sigma-Aldrich (München, Germany). All plastic consumables were purchased from BD Falcon (BD Biosciences, Le Pont de Claix, France), Greiner bio-One GmbH (Frickenhausen, Germany), Starlab GmbH (Hamburg, Germany), or Eppendorf AG (Hamburg, Germany). Dissection tools were purchased from Fine Science tools (FST, Foster City, USA). Mouse inhaler InExpose® was purchased from Scireq/Emka technologies (Canada). Plasma collection tube Microvette was purchased from Sarstedt (Nümbrecht, Germany). Detail of consumables and compounds see **table 2.1**.

Table 2.1: List of consumables and compounds.

Reagent	Manufacturer/Catalog number
Bovine Serum albumin (BSA), reagent grade	Hiss Diagnostics (1900-0016)
DABCO	SIGMA-ALDRICH (290734-100ML)
Glycerol	MP Biomedicals (151194)
Hydrogen Peroxide (30%)	Merck Millipore (1.072.10.0250)
Immersol 518 F	Zeiss (10539438)
Isoflurane (Vetflurane® 1000 mg/g)	Pharmacy (PZN 4001404)
Mowiol 4-88	AppliChem (A9011,0250)
Na ₂ HPO ₄ / di-Sodium hydrogen phosphate dihydrate	Roth (4984.1)
NaH ₂ PO ₄ /Sodium dihydrogen phosphate dihydrate	Roth (t879.2)
NaOH Sodium hydroxide Beads	AppliChem (A4224,1000)
O.C.T. compound embedding medium	VWR (361603E)
Paraformaldehyde	AppliChem(A3813,0500)
Pentobarbital-natrium (Release ad us. Vet. 300 mg/ml)	Wirtschaftsgenossenschaft deutscher Tierärzte (PZN 21217)
Sucrose	Merck Millipore (1076511000)
SuperFrost Plus slides	Thermo Fisher Scientific (10149870)
Surgical disposable blades (sterile)	B. Braun (BA211)
Thioflavine S	Sigma-Aldrich (T1892-25G)
Tris (BASE)	Roth (4855.2)
Triton X-100	Sigma-Aldrich (X100-100ML)

2.1.2 Buffers and solutions

All chemicals were purchased from AppliChem GmbH (Darmstadt, Germany), Merck (Darmstadt, Germany), VWR (Darmstadt, Germany) or Roth (Karlsruhe, Germany). All solutions were prepared with sterile ddH₂O and stored at room temperature (RT) unless described otherwise. Detail of buffer preparation see in **table 2.2**.

Table 2.2: Summary of general buffers and solutions.

Buffer/Solution	Composition
100 % blocking solution (for IHC)	2.5 [v/v] fetal bovine serum (FBS) 2.5 [v/v] BSA 2.5 [v/v] fish gelatin In 1x PBS pH 7.4 Stored at -20° C
30 % sucrose	30 % [w/v] Sucrose in 1x PBS at 4° C
4 % paraformaldehyde (PFA)	4 % [w/v] PFA 400 ml ddH ₂ O heat up to 55° C 600 ml 0.2 M Phosphate buffer Stored at -20 °C
Cryoprotective medium:	25% [v/v] Glycerol 25% [v/v] Ethyleneglycol 1x PBS
Mowiol mounting media	13.3 % Mowiol 33.3 % Glycerol 133 mM Tris-HCl pH 8.5 24mg/ml DABCO Stored at -20 °C
TBST	0.1 % [v/v] Triton-X-100 in TBS
tris-buffered saline (TBS)	0.05 M TRISMA Base 0.15 M NaCl adjust pH to 7.6 with HCl

2.1.3 Antibodies

Primary antibodies used in this project, their application and the correspondent concentrations are listed in **Table 2.3**. A summary of all secondary antibodies with their respective conjugates that were used in this thesis are shown in **Table 2.4**.

Table 2.3: List of primary antibodies

Antibody	Host species	Company	Catalog number	Working dilution (Application)
6E10	mouse	Covance	SIG-39300	1:2000 (IHC)
A β 42	rabbit	Invitrogen / Thermo Fisher	44-344	1:1000 (IHC)
C1q	rabbit	Abcam	ab182451	1:500 (IHC)
CD68	rat	BD / Thermo Fisher	NC 9471873	1:500 (IHC)
GFAP	guinea pig	Synaptic Systems	173004	1:500 (IHC)
Homer1	chicken	Synaptic Systems	160003	1:500 (IHC)
Iba1	rabbit	WAKO	019-19741 / NC9288364	1:2000 (IHC)
Iba1	goat	Abcam	ab5076	1:1000 (IHC)
LAMP1 (CD107a)	rat	BD	553792	1:500 (IHC)
MBP	chicken	Invitrogen	PA110008	1:500 (IHC)
NeuN	mouse	Millipore	MAB377	1:500 (IHC)
Olig2	rabbit	Millipore	AB9610	1:500 (IHC)
PSD95	mouse	Millipore	MAB1596	1:500 (IHC)
Synapsin1/2	guinea pig	Synaptic Systems	106 004	1:500 (IHC)

Table 2.4: List of secondary antibodies

Antibody	Host	Conjugate	Company	Catalog number	Working dilution (Application)
Anti-ginea pig	goat	Alexa555	Invitrogen	1900250	1:300 (IHC)
Anti-goat	donkey	Alexa555	Thermo Fisher	A21432	1:300 (IHC)
Anti-mouse	rabbit	Alexa488	Invitrogen	A11008	1:300 (IHC)
Anti-mouse	goat	Cy3	Dianova	115-165-146	1:300 (IHC)
Anti-mouse	donkey	Alexa647	Thermo Fisher	A31571	1:300 (IHC)
Anti-rabbit	goat	Alexa488	Invitrogen	A11008	1:300 (IHC)
Anti-rabbit	goat	Cy3	Dianova	111-165-144	1:300 (IHC)
Anti-rabbit	donkey	Alexa647	Invitrogen	1964354	1:300 (IHC)
Anti-rat	donkey	Alexa488	Thermo Fisher	A21208	1:300 (IHC)
Anti-rat	goat	Cy3	Invitrogen	1842804	1:300 (IHC)

2.1.4 Software

All softwares used for imaging and data analysis are shown in **table 2.5**.

Table 2.5: Overview of used software.

Software	Application	Source
Adobe Illustrator 25.4	Illustration of figures	Adobe Systems Inc
bioRender	Schemes for figures	BioRender.com
Fiji (Imagej.net)	Image processing and analysis	https://imagej.net/software/fiji/
GraphPad Prism® 9.1	Data and statistical analysis	GraphPad Software Inc.
Imaris 9.7.1	Image analysis	Oxford Instruments
MS Office Excel 2016	Data analysis	Microsoft
MS Office Word 2016	Writing and editing	Microsoft
Photoshop 22.4.3	Image processing	Adobe Systems Inc
Zen blue 2.3 lite	Image processing	Zeiss

2.1.5 Equipment

All equipments used in this project are shown in **table 2.6**.

Table 2.6: Overview of used equipment.

Equipment	Company
300 series laboratory tube pumps D/E	Watson-Marlow, Germany
Cryostate 3050S	Leica Microsystems, Nussloch, Germany
LSM 980 microscopy	Zeiss, Germany
LSM upright 700 microscopy	Zeiss, Germany
Magnetic hotplate stirrer	IKA/Fisher scientific, Germany
Mouse inhaler InExpose	Scireq/Emka technologies, Canada
Platform shakers	Heidolph, Germany
Thermo scientific Fresco 17 microcentrifuge	Fisher scientific, Germany
Vortex-Genie 2 mixer	Scientific industries, Germany

2.2 Methods

2.2.1 Generation of 5xFAD mouse line

In this project, heterozygous B6SJL-tg(APP^{Sw}FILon,PSEN1^{M146L}*L286V)⁶⁷⁹⁹Vas (5xFAD) mice were crossed with wt B6SJL F1 to generate B6SJL-F2 5xFAD and B6SJL-F2 wt litter mates. This background is heterozygous for the retinal degeneration mutation Pde6brd1, which causes blindness in Pde6b^{rd1} homozygous mice; we therefore excluded offspring homozygous for Pde6b^{rd1} from this study. 5xFAD and wt mice of both sexes were included in this study to investigate effects of nasal and inhaled Budesonide on AD pathology and behavior. All mice born within two weeks were merged into one cohort. All experimental procedures were in accordance with guidelines established by the DZNE and were approved by Local Animal Care Commission of North-Rhine-Westphalia (81-02.04.2019.A150).

2.2.2 Drug delivery of Budesonide

Intranasal treatment

The intranasal treatment was conducted under brief inhalational anesthesia with 2% isoflurane, lasting for 1-2 minutes. The anesthetized animal was taken out of the box and held by the neck grip, hanging vertically. The respective solution (Budesonide 350 µg/kg body weight or control solution) was quickly pipetted onto the nostrils of the animals using a pipette. The control solution was prepared according to the solvent of Budesonide, containing Polysorbate 80 (125 µg/ml), NaCl (8.5 mg/ml), EDTA (50 µg/ml), Sodium Citrate Dihydrate (0.624 mg/ml), Citric Acid (0.188 mg/ml), and Water for Injection q.s. to 0.5 ml. The animal was then held vertically in the neck grip until the drops were inhaled. Care was taken to ensure the anesthesia did not wear off too much, as this would cause the animals to shake their heads instead of absorbing the pipetted drops. The animal was then placed back in the cage and observed until the anesthesia wore off.

Inhalation treatment

The inhalation treatment was performed with mouse inhaler InExpose®, a device designed to deliver aerosolized compounds (such as drugs, nanoparticles, or gases) to laboratory animals, primarily rodents, in a controlled and precise manner. This system ensures that the test subjects receive consistent and uniform exposure to the substance being studied.

The instrument comprises the following components (**Figure 2.1**):

Aerosol Generator: Produces the aerosolized form of the test compound. Different types of generators may be used depending on the nature of the substance (liquid, solid, etc.).

Exposure Chamber: Where the animals are placed. The aerosolized compound is delivered into this chamber for the animals to inhale. The exposure chamber is designed to

ensure uniform distribution of the aerosol.

Control System: Includes the necessary software and hardware to control and monitor the entire process, ensuring that the conditions are stable and that the dose delivered is accurate.

Exhaust System: After exposure, the air from the chamber is safely removed and filtered to ensure that no potentially hazardous compounds are released into the environment.

Animals were first placed into SCIREQ's SoftRestraints, a soft metal net that prevents mice from retreating and exposes the mouse's nose to the nose-only exposure chamber. As shown in **Figure 2.2**, Budesonide was first loaded into the aerosol generator, and the system calibrated to deliver the precise dosage required. Then Budesonide was converted into an aerosol, which was then passed into the exposure chamber. The animals were placed in the exposure chamber and received Budesonide aerosol. Once the exposure was complete, the animals were removed from the chamber, and the aerosol in the chamber was safely exhausted and filtered.



Figure 2.1: InExpose inhalation exposure system. Upper: Images of placement of mice in SCIREQ's SoftRestraint with nose-only inhalation exposure. Lower: Instrument setup of InExpose inhalation exposure chamber.

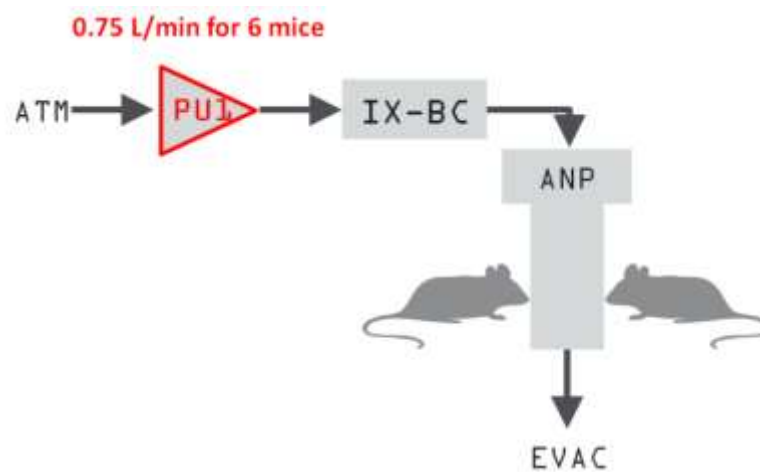


Figure 2.2 InExpose inhalation exposure system tubing layout. PU: Pump unit; IX-BC:

Buffer chamber; ANP: Aeronec nebulizer unit; EVAC: Evacuation into fume hood.

Treatment time was calculated according to the average animal lung capacity. A detailed calculation is show below:

(1) Bias flow requirements:

$$V_{bias} = S \times N_{sub} \times V_T \times RR$$

$$V_{bias} = S \times N_{sub} \times V_T \times RR$$

S = Safety Factor (typically 2)

Nsub = Number of subjects

V_T = Tidal volume

RR = Respiration rate

In our experiment, bias flow was set to 550 mL/min.

(2) Aerosol output concentration:

$$C_{dose} = \frac{(r_{neb} \cdot D_{\%}) \times C_{sol'n}}{\dot{V}_{bias}}$$

r_{neb} = Output of nebulizer head Fine Mist = 0.25 ml/min

$D_{\%}$ = Duty cycle

$C_{sol'n}$ = Concentration of compound in solution

\dot{V}_{bias} = Bias flow

$cDose = ((0.25\text{ml/min} \times 1) \times 500\text{ug/ml})/550\text{ml/min} = 0.227\text{ug/ml}$

(3) Estimated delivered dose

$$D_{del} = C_{dose} \times V_T \times RR$$

C_{dose} = Aerosol output concentration

V_T = Tidal volume

RR = Respiration rate

V_T was calculated from the lung capacity based on the body weight (W_{body}) of mice:

$$V_T = 0.1\text{ml} \times W_{body} / 10\text{g}$$

$$D_{del} = 0.227\text{ug/ml} \times (0.1\text{ml} \times W_{body} / 10\text{g}) \times 200 \text{ breath/min} = 454 \times W_{body} \text{ ug/min}$$

Drug deliver does is 350 $\mu\text{g/kg}$ body weight: $D=350 \mu\text{g/kg} \times W_{body}$

$$\text{Treatment time} = D / D_{del} = 350/454 = 0.77\text{min} = 46.2\text{s}$$

For our inhalation treatment, we treated six mice simultaneously; the treatment time was 46 seconds.

2.2.3 Tissue preparation

Depending on the subsequent analysis, the tissue was prepared and stored differently. Mice received an intraperitoneal injection of a lethal dose of pentobarbital (600 mg/kg). Once the mice were sufficiently anesthetized, as confirmed by the absence of pedal reflex, their chests were opened. The ascending aorta of the heart was then punctured using a 26G needle. With a small scissor, a cut was made for a right side cardiac puncture, leading to blood flush out. Blood was then collected by a Microvette capillary blood collection tube. Afterwards the mice were perfused with PBS for 5 minutes at a flow rate of 10 rpm/min using 300 series laboratory tube pumps D/E from Watson-Marlow. Following this, the brains were excised, and half of the brain subjected to post-fixation in 4% PFA for 72 hours, and then cryoprotected in 30% sucrose for a minimum of 48 hours and stored at -80 °C before cutting. Coronal brain sections of 30 µm were prepared using a Cryostate 3050S and preserved at -20°C in Walters antifreeze solution. The other half of the brain, after a quick wash in ice-cold PBS, was dried and snap-frozen on dry ice. The tissue was stored at -80° C until dissection. For plasma samples, Microvette capillary blood collection tube were spun at 1,300g for 3 min at room temperature, and the plasma supernatant was aliquoted and stored at -80 °C. Liver and lung were also collected for investigation of drug distribution, organ tissue was snap-frozen on dry ice then stored at -80° C until mass spectrometry. To validate their genotype, ear and tail tissue was also collected for final genotyping.

2.2.4 Immunohistochemically staining

Free floating sections were rinsed with TBS containing 0.1% Triton X-100 in a 24-well plate. Permeabilization was performed in TBS containing 0.1% Triton X-100 and 0.6% H₂O₂ with 1h incubation time, followed by three times washing with TBS for 5 mins each time. Sections were then incubated in 10% blocking solution (2.5% FBS, 2.5% BSA and 2.5% fish gelatin in PBS at pH 7.4) for 1 h at room temperature. After the blocking pro-

cess, sections were incubated overnight at 4 °C in primary antibody solutions, containing 2% blocking solution. On the following day, after washing the sections three times with TBS for 10 min, sections were incubated with secondary antibodies, diluted in 2% blocking solution, for 1 h at room temperature. The sections were then washed with TBS three times and mounted using mounting media (13.3% Mowiol, 33.3% Glycerol, 24 mg/ml DABCO and 133 mM Tris-HCl at pH8.5) on HistoBond adhesive microscope slide.

2.2.5 Microscopy and imaging processing.

For imaging, microscopes (LSM700, LSM900, LSM980) within the Light Microscopy Facility of the DZNE in Bonn were used. Images were analyzed by Imaris 9.7.1.

A β 42 / ThioS co-staining analysis

To evaluate plaque number and morphology in cortex, four coronal brain sections stained with A β 42 and ThioS at approx. Bregma 1.18 mm, -0.82 mm, -1.82 mm and -2.80 mm were selected. For subiculum plaque analysis only one slice at Bregma -2.80 mm was chosen from each animal. Imaging was done by LSM700 microscope (Carl Zeiss). The cortex and subiculum regions from both hemispheres were imaged with a 20x objective by a depth of 9 μ m and 1 μ m Z-stacks. In cortex, three horizontal tiles were stitched together to gain a broader view. Images were analyzed by Imaris with “surface” function for A β 42 (absolute intensity threshold above 16800, number of voxels above 10) and ThioS (absolute intensity threshold above 42100, number of voxels above 10) volume analysis.

NeuN staining analysis

To evaluate neuronal number in subiculum, one slice at Bregma approx. -2.80 mm stained by NeuN was chosen from each animal. Imaging was done by LSM700 microscope (Carl Zeiss). Subiculum regions from both hemispheres were imaged with a 20x objective by a depth of 9 μ m and 1 μ m Z-stacks. In cortex two horizontal and two vertical tiles were stitched together to gain a broader view. Images were analyzed by Imaris with

“Spot” function for neuronal number (estimated XY diameter 10 μm , “quality” threshold above 10 with background subtraction) quantification.

PSD95 / Synapsin1/2 co-staining analysis

To evaluate the number of synapses in the CA1 region, a slice at Bregma approximately -1.8 mm stained with PSD95 and Synapsin1/2 was selected from each animal. High-magnification imaging was performed using 63x oil objectives in combination with Immersol 518 F. The imaging was carried out with an LSM980 microscope. Both the CA1 stratum oriens (so) and CA1 stratum radiatum (sr) regions from both hemispheres were imaged to a depth of 6.5 μm with 0.5 μm Z-stacks.

The images were analyzed using Imaris with the “Spot” function. PSD95 puncta were identified using a “quality” threshold above 7.35 with background subtraction. Synapsin1/2 puncta were identified using a “quality” threshold above 7.5 with background subtraction. Parameters were also inspected manually and modified if false signals were detected to ensure accuracy. Co-localization of the spots was quantified by measuring the spot distance within 0.5 μm .

PSD95 / C1q co-staining analysis

To evaluate complement opsonization of synapses in CA1, one slice at Bregma approx. -1.8 mm stained by PSD95 and C1q was chosen from each animal. To image with high magnification, 63x oil objectives were used in combination with Immersol 518 F. Imaging was done by LSM980 microscope. CA1so and CA1sr regions from both hemispheres were imaged by a depth of 6.5 μm and 0.5 μm Z-stacks. Images were analyzed by Imaris with “Spot” function for PSD95 puncta (“quality” threshold above 2.5 with background subtraction), C1q puncta (“quality” threshold above 2.25 with background subtraction) and co-localization (spot distance within 0.5 μm) quantification. Parameters were also inspected manually and modified if false signals were detected to ensure accuracy.

Homer1 / GFAP/ Iba1 co-staining analysis

To investigate synaptic proteins in microglial or astrocytic cells in CA1, one slice at Bregma approx. -1.8 mm stained by Homer1 GFAP and Iba1 was chosen from each animal. To image with high magnification 63x oil objectives were used in combination with Immersol 518 F. Imaging was done by LSM980 microscope. CA1so and CA1sr regions from both hemispheres were imaged by a depth of 7 μm and 0.5 μm Z-stacks. Images were analyzed by Imaris with “Surface” function for GFAP (surface grain size 0.082 μm , “quality” threshold above 252, number of voxels above 20) and Iba1 (surface grain size 0.082 μm , “quality” threshold above 112, number of voxels above 20) volume quantification; Homer1 puncta number and intracellular localisation was analysis by “Spot” function (“quality” threshold above 2.87 with background subtraction).

2.2.6 Behavior experiments

Nest building

The nest-building behavior assessment in this study was based on the scoring system detailed by Deacon from Nature Protocols ([Deacon, 2006](#)). Mice were separated at the end of the light phase (5 pm) and left with one block of cotton material (2.0mg - 3.0mg). Precise weight of cotton material was measured right before separation. On the next morning at the beginning of the light phase (8am) nests were scored and untorn nest material was weighted. Mice were group-housed again. This method employs a 5-point rating scale to evaluate the quality of nests built by mice. The scoring system is as follows:

Score 1: The Nestlet is not noticeably touched, with more than 90% of the material remaining intact.

Score 2: The Nestlet is partially torn, with 50-90% of the material remaining intact.

Score 3: The Nestlet is mostly shredded, but no identifiable nest site is present. Less than 50% of the Nestlet remains intact, and less than 90% of the shredded material is within a

quarter of the cage floor area.

Score 4: An identifiable but flat nest is formed. More than 90% of the Nestlet is torn, and the material is gathered into a nest within a quarter of the cage floor area, but the nest walls are higher than the mouse's body height for less than 50% of its circumference.

Score 5: A near-perfect nest is created. More than 90% of the Nestlet is torn, and the nest forms a crater with walls higher than the mouse's body height for more than 50% of its circumference.

Nest building performance was measured 2d before start of the treatment at 4 months of age and 2d before animals were sacrificed at 6 months of age.

Alternating Y Maze

Spontaneous alternation rate was tested in a Y shaped arena with 30cm arm length and 10cm arm diameter. Animals were always placed in the southern arm facing the central area of the maze. They were free to explore the maze for 8 mins. Arm entry was counted manually when all four paws of the animal were in the new arm. Alternation rate was calculated as follows:

$$\text{Alternation rate [\%]} = \frac{\text{Number of alternations [n]}}{\text{Total arm entries [n]} - 2} \times 100[\%]$$

Novel Object Recognition (NOR)

Animals were trained and tested individually in a 50cm x 50cm squared polyacrylamide box with 50cm high walls. First, each animal was habituated to the box for 6 mins where it could freely explore the arena without objects. This session was analyzed for open field behavior. After habituation, animals were put back to the home cage for 3 mins and then placed again to the arena for 6 mins with two of the same objects located in the center zone. Duration of object exploration was counted manually when the nose was directed to the object with maximal 2cm distance and when the animal was touching the objects with its nose and or front paws. Training session was repeated 3 times in total, each with 6 mins duration and 3 mins inter-trial break in home cage.

Animals were tested 24h after training. One object was replaced by a new placed at the same location. Animals were free to explore both objects for 6 mins and exploration was scored as previously described. After each session, arena and objects were cleaned with 70% ethanol. Novel object exploration during the test session was calculated as follows:

$$\text{Novel object recognition [\%]} = \frac{\text{Exploration time new object [s]}}{\text{Exploration time new object [s]} + \text{Exploration time old object [s]}} \times 100\%$$

Barnes Maze

A round table with 90cm diameter and 20 evenly placed holes at the edge was used as Barnes maze arena. Below one hole an escape box was placed. The arena was split in four evenly sized zones (target, left, right opposite) with the escape hole located in the middle of the target zone. Animals were always placed in the center of the table in a non-transparent beaker for 30s before start of a trial. Mice were habituated on day 1 for 3 mins on the table in low light intensity condition (lux). After 3 mins animals were guided to the escape box and box entry was closed. The animal was left in the dark escape box for 2 mins before being put back to the home cage. After 15 mins habituation was repeated. From day 2-5 animals were trained to learn the location of the escape box with 4 trials per day. Animals were given 60s exploration to find the escape box. If they could not find the box in the given time, they were guided by the experimenter to the hole with the box. When the animal stepped into the box, the entry was closed and they were kept in the dark box for 30s before returning to their home cage. The escape box was removed for the probe trial on day 6, here the animal was free to explore the arena for 90s. If they remembered the location of the box correctly, they spent more time in the target zone. Automated center point detection from Ethovision 13 was used to obtain time spent in zone [%].

Alternating Y Maze, Novel Object Recognition and Barnes Maze were done by Dr. Kristin Oberländer. Nesting was done by me together with Dr. Kristin Oberländer.

2.2.7 Statistical analysis

All results were statistically evaluated using GraphPad Prism 9.1. Comparison of means between two groups was analyzed with an unpaired two-tailed t-test. Multiple groups were compared with the one-way ANOVA followed by Sidak's multiple comparisons test, comparison pairs are "wt control versus wt Budesonide", "wt control versus FAD control" and "FAD control versus FAD Budesonide". All data was represented with the standard error of the mean (SEM) as error bars. All p-values under 0.05 were considered statistically significant and are marked as following: * $p < 0.05$ ** $p < 0.01$ *** $p < 0.001$ **** $p < 0.0001$. The number of biological samples is indicated by n.

3. Results

3.1 Organ distribution of Budesonide

To validate bioavailability, investigate the distribution of the drug in the body, and compare the effects of the two treatment methods, mass spectrometry was used to examine the distribution of Budesonide in different tissues. For intranasal treatment, 6 month old B6.SJL mice were treated after brief isoflurane anesthesia, followed by administration of 5 times volume of standard Budesonide treatment. Standard treatment was calculated according to animal body weight (350 µg/kg). After nasal administration, Budesonide was detected in liver homogenate, lung homogenate, plasma, and most importantly in different regions of the brain. Following the treatment, the animals were perfused, and the brains were harvested, stored at -80°C, and subsequently transferred to Dr. Matthias Vogel's lab at BfArM for mass spectrometry analysis. For inhalation treatment, mice were treated 5 times longer (230 seconds) compared to standard treatment (standard treatment time was 46 seconds).

Mass spectrometry data (analyzed by Dr. Matthias Vogel) showed that mice which received intranasal treatment had a significantly higher concentration of Budesonide compared to those that received inhaler treatment (**Figure 3.1**). As expected, lung tissue was shown to contain highest concentration of Budesonide in comparison to other tissue because of the direct delivery route by respiratory tract. In the mouse liver and plasma, Budesonide was also detected 5 and 15 mins after treatment. Tissue from mice that received only isoflurane anesthesia and no treatment served as control group. In these controls, no Budesonide was detected. Budesonide distribution was also analyzed in different brain regions (subsequent coronal sections) (**Figure 3.2**)

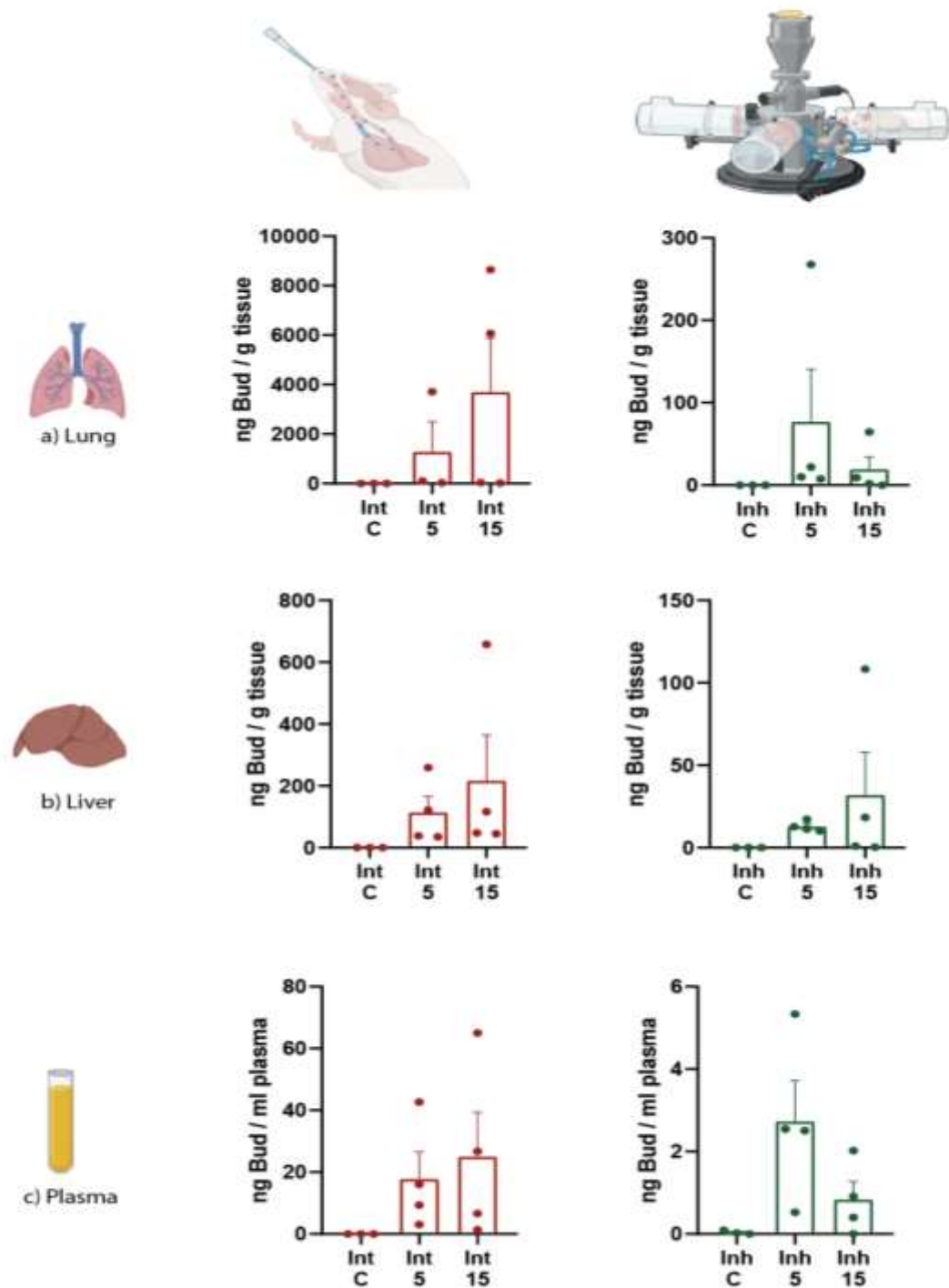


Figure 3.1: Budesonide distribution in mice organs after intranasal and inhaler treatment measured by mass spectrometry. Lung (a), liver (b) and plasma (c) were collected from mice perfused 5 mins (Int 5/ Inh 5) and 15 mins (Int 15/ Inh 15) after received intranasal or inhaler treatment and as control group mice without treatment (Int C/

Inh C). Each data point represents one animal included in this experiment.

To investigate the spatial distribution of Budesonide upon intranasal application in the brain, the mice were subjected to coronal sectioning, resulting in four distinct anatomical brain regions designated as B1, B2, B3, and B4. The B1 segment encompassed the olfactory bulb (OB) and the prefrontal cortex, B2 comprised the dorsal hippocampus, B3 included the ventral hippocampus, and B4 represented the cerebellum. Additionally, each treatment setting included a control group without treatment to serve as a background control.

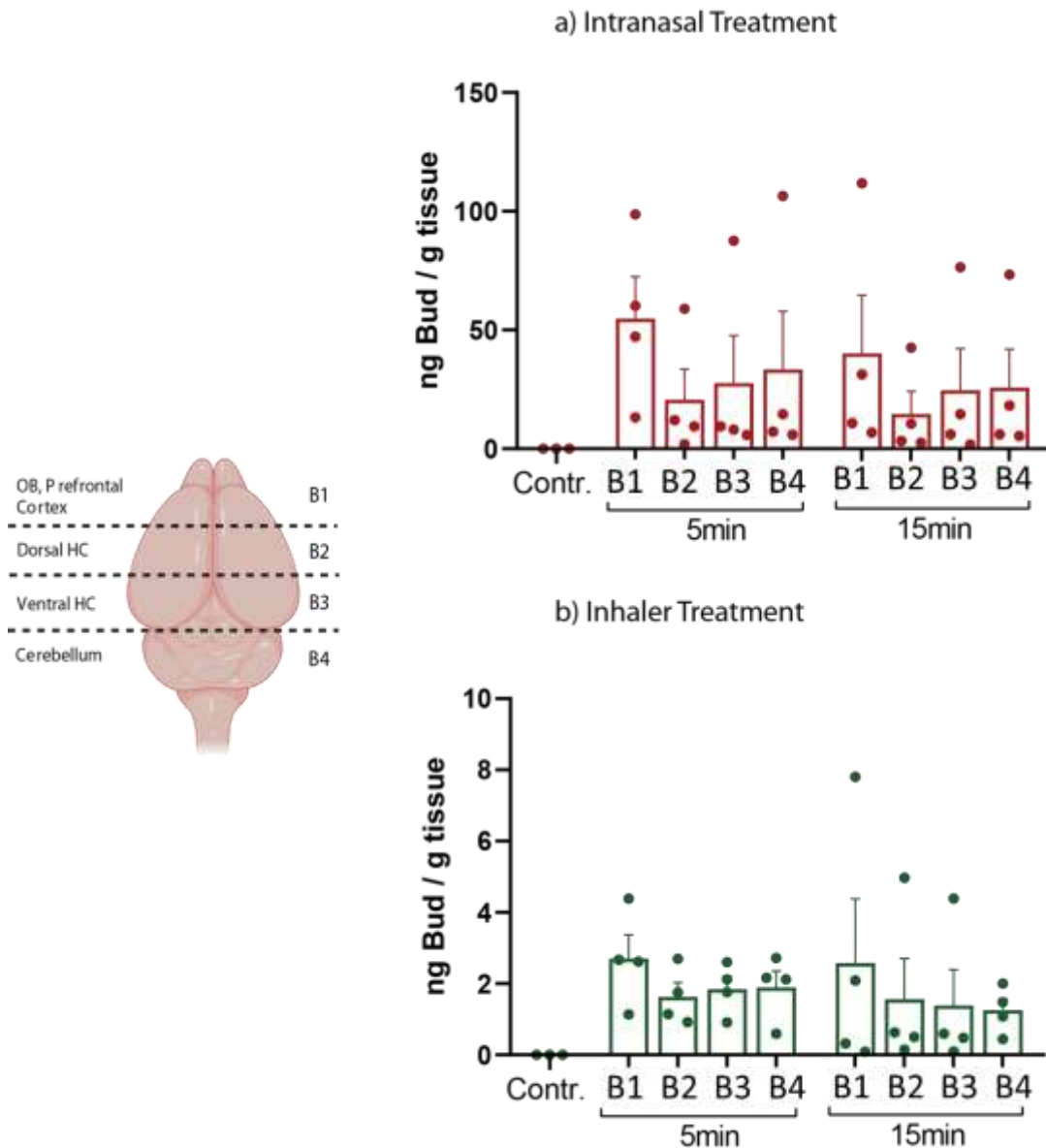


Figure 3.2: Budesonide distribution in different regions of mice brain after intranasal and inhaler treatment measured by mass spectrometry. Subregion map of mouse brain is shown in the left panel. (a) Budesonide distribution in intranasally treated mice. (b) Budesonide distribution in Inhaler treated mice. Each data point represents one animal included in this experiment.

In comparison to inhaler treatment, intranasally treated animals showed higher concentration of Budesonide in all four brain regions. Under both treatment methods, we observed a concentration gradient from anterior to posterior brain segments.

In summary, the mass spectrometry data showed that intranasal and inhaled Budesonide reach the brain tissue.

3.2 Effects of inhaler Budesonide treatment in the 5xFAD mouse model of AD.

3.2.1 Effect of inhaler Budesonide treatment on behavior in the 5xFAD mouse model of AD

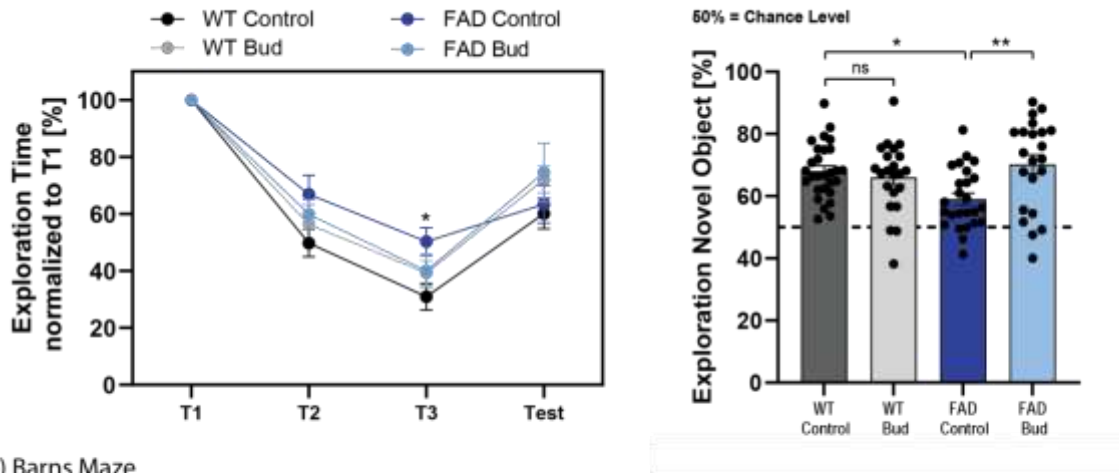
To test treatment effects at a disease stage corresponding to the time of onset of cognitive impairment, we chose a treatment paradigm of inhaled Budesonide from 4 months on, followed by behavior tests (done by Dr. Kristin Oberländer) at 6 months of age (**Figure 3.3**).

In the novel object recognition (NOR) test (**Fig 3.3a**) 6 month old female 5xFAD mice exhibited significantly slower learning with the familiar object during the first three trials and shorter exploration time with the novel object during the test trial in comparison to wt mice, indicating impaired cognitive function. Budesonide treated 5xFAD mice demonstrated faster learning with the familiar object in the initial trials and significantly longer exploration time with the novel object in the test trial in comparison to the 5xFAD control mice, indicating better cognitive performance. Similarly, in the Barnes maze test (**Fig 3.3b**), untreated 5xFAD mice spent less time in the target zone compared to wt controls, indicating spatial memory deficits. In contrast, Budesonide treated 5xFAD mice spent

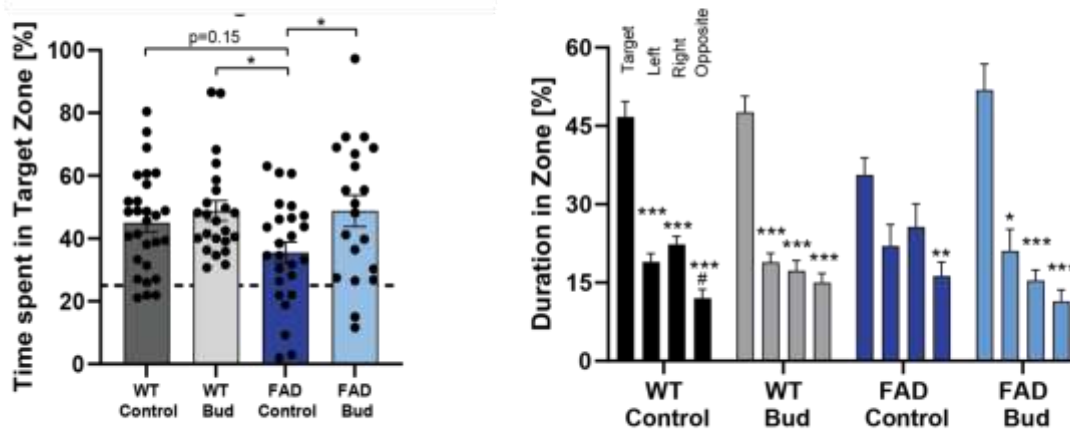
significantly longer time in the target zone than untreated 5xFAD mice, suggesting better spatial memory. Additionally, further analysis of time spent in four zones (target, left, right, and opposite zones) revealed that Budesonide-treated 5xFAD mice spent significantly longer time in the target zone compared to the other zones, demonstrating better learning and memory retention than untreated 5xFAD controls.

In the nest building test, according to the nesting protocol from Deacon ([Deacon, 2006](#)), as depicted in **Figure 3.3c**, at 4 months of age, displayed distinct nesting behaviors. Wild-type mice demonstrated an average nesting score of 4, whereas 5xFAD mice exhibited a slightly lower average score of 3.5. The reduced nesting performance in 5xFAD mice suggests the onset of cognitive impairment at this age, consistent with early-stage deficits in this Alzheimer's disease model. By 6 months, the wt control mice maintained an average nesting score of 4, while the 5xFAD mice showed a significant decline, scoring only an average of 2 and leaving a considerable amount of nesting material unused. Following Budesonide inhalation treatment, the 5xFAD mice demonstrated nesting behavior with average scores above 3. The comparison of nesting scores before and after treatment indicates that Budesonide inhalation may effectively halt or mitigate cognitive impairments in 5xFAD mice, highlighting its potential as a therapeutic intervention for Alzheimer's disease.

a) Novel object recognition



b) Barnes Maze



c) Nesting

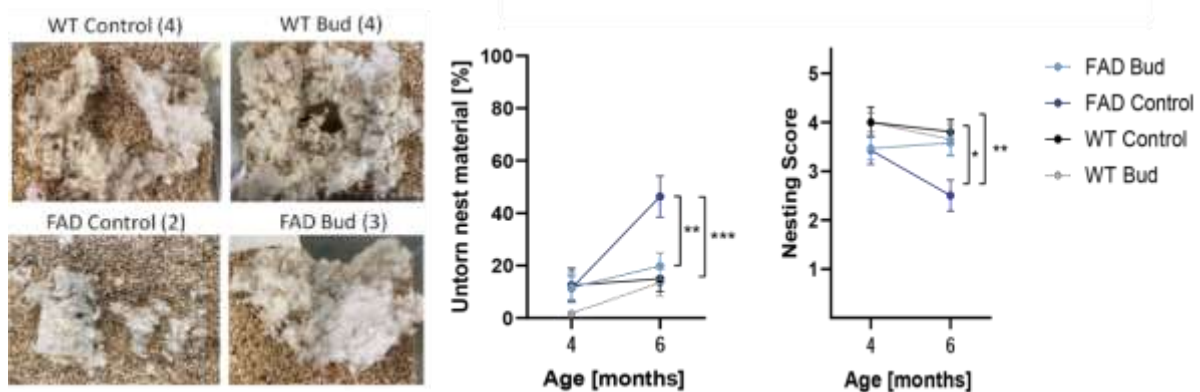


Figure 3.3: Behavior experiment results summary of 6-month short term inhalation treated female mice. a) Novel Object Recognition Test. Left: Percentage of exploration time normalized to Trail day1 (T1) across four groups: WT Control, WT Bud, FAD Control, and FAD Bud, measured at trail day1 (T1), trail day2 (T2), trail day3 (T3) and test trail (test). Right: Percentage of time spent exploring the novel object. b) Barnes Maze Test.

Left: Percentage of time spent in the target zone during the test trial, comparing WT Control, WT Bud, FAD Control, and FAD Bud groups. Right: Distribution of time spent in target, left, right, and opposite zones in the test trail. c) Nesting Behavior. Left: Representative images of nests from WT Control, WT Bud, FAD Control, and FAD Bud groups at 6-month-old. Middle: Quantification of nesting scores at 4 and 6 months. Right: Further analysis of the time spent in four zones (target, left, right, opposite). Data is presented as mean \pm SEM; ordinary one-way ANOVA followed by Sidak's multiple comparisons test, * $p \leq 0.05$, ** $p \leq 0.01$, *** $p \leq 0.001$. (Behavior test data analysis done by Dr. Kristin Oberländer)

3.2.2 Effect of inhaled Budesonide on amyloid pathology in the 5xFAD mouse model of AD

Next we investigated the effect of inhaled Budesonide on amyloid pathology by immunohistochemistry staining of A β 42 and ThioflavinS (ThioS) to label the dense core A β -plaques. First, we examined the cortex region from coronal brain slices at Bregma 1.18mm (**Figure 3.4b, g, k**), -0.82mm (**Figure 3.4c, h, l**), -1.82mm (**Figure 3.4d, i, m**) and -2.80mm (**Figure 3.4e, j, n**). Image analysis showed Budesonide treated 5xFAD animal have significant smaller ThioS dense core volume in Bregma -0.82mm (s1, k) and Bregma -1.82mm (s3, m), also a similar trend was seen in other two position (s2, l and s4, n). However A β 42 volume analysis didn't show significant change upon inhaler Budesonide treatment.

We further analyzed the total number of ThioS-labeled dense core plaques across the same coronal sections (s1, s2, s3, s4) (**Figure 3.4o**). Budesonide treated 5xFAD mice exhibited a significantly lower number of ThioS-positive dense core plaques compared to the untreated 5xFAD control group. This reduction in both the volume and total number of ThioS-labeled dense core plaques suggests that Budesonide may have a therapeutic effect on amyloid pathology, specifically by reducing the size and quantity of dense core plaques in this Alzheimer's disease model.

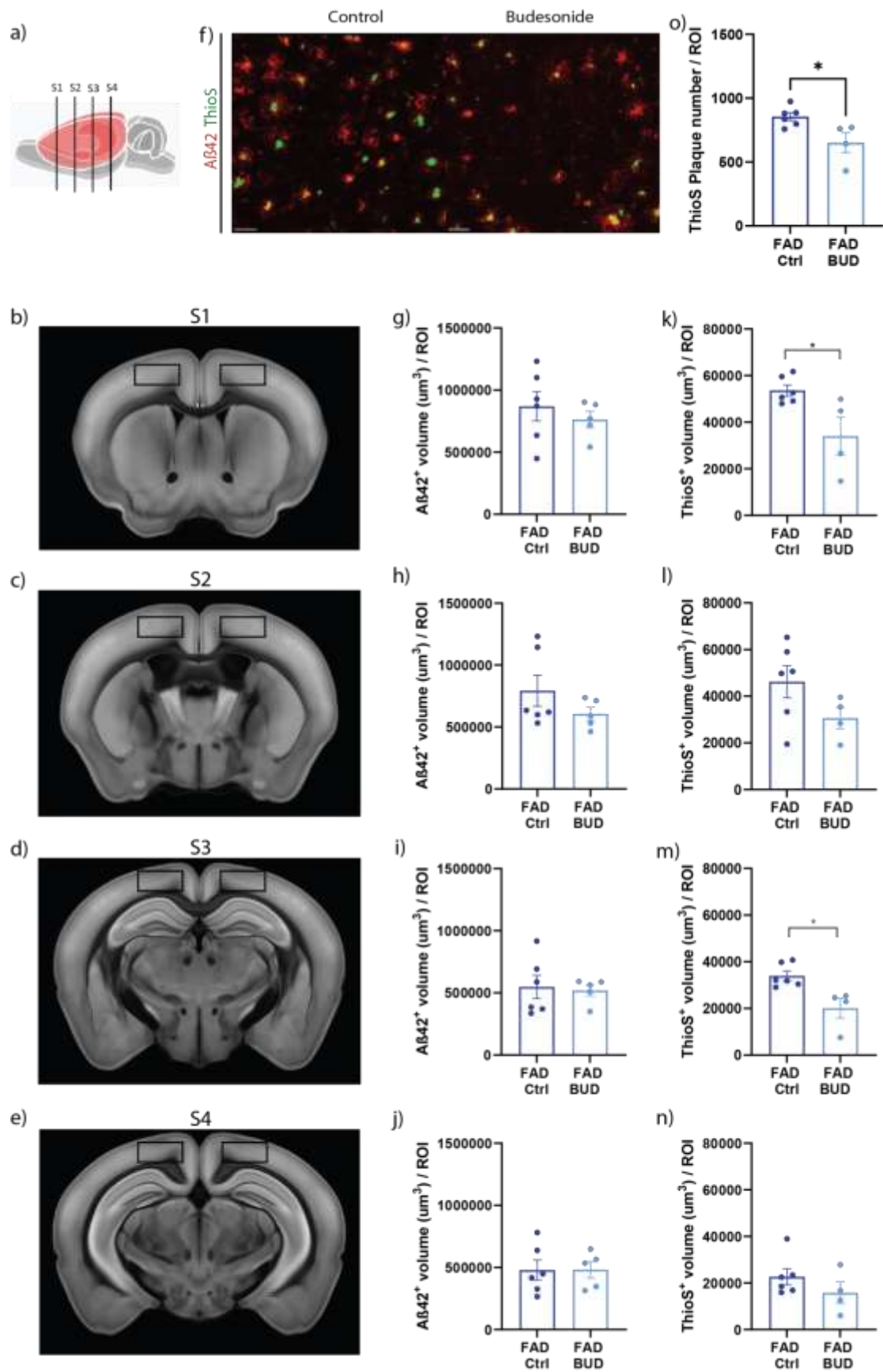


Figure 3.4: Quantification of A β plaque volume in the cortex of 5xFAD mice upon inhalation Budesonide treatment. Dense core volume of A β -plaques in cortex was altered upon inhaler Budesonide treatment at 6 month old 5xFAD female mice. a) Schematic map of coronal level of brain slices quantified for A β plaque pathology analysis, detail coronal level is shown in b) s1: Bregma 1.18mm, c) s2: Bregma -0.82mm, d) s3: Bregma -1.82mm and e) s4: Bregma -2.80mm. Imaging regions are labeled in black box. f) Representative images of histological staining for ThioS (green), A β 42 (red) in 6 month old 5xFAD untreated (left) and Budesonide treated (right) animals. Images were taken within cortex layer V-VI using a confocal microscope with 20x objective. Here representative maximum projections of z-stacks are shown. Scale bar: 50 μ m. g-j) The average A β 42 volume in ROI of cortex from s1 (b), s2 (c), s3 (d) and s4 (e) are shown in g, h, i and j. k-n) The average ThioS volume in ROI of cortex from s1 (b), s2 (c), s3 (d) and s4 (e) are shown in k, l, m and n. Data is presented as mean \pm SEM. Untreated 5xFAD controls are shown in dark blue and Budesonide treated data are displayed in light blue column. Unpaired student's t-test, * $p \leq 0.05$.

The number and volume of amyloid plaques (A β 42) and dense core plaques (thioS) in the subiculum was analyzed to determine the effects of inhaled Budesonide in 6-month-old female 5xFAD mice. The data did not show any significant change between the control and treated groups (**Figure 3.5**).

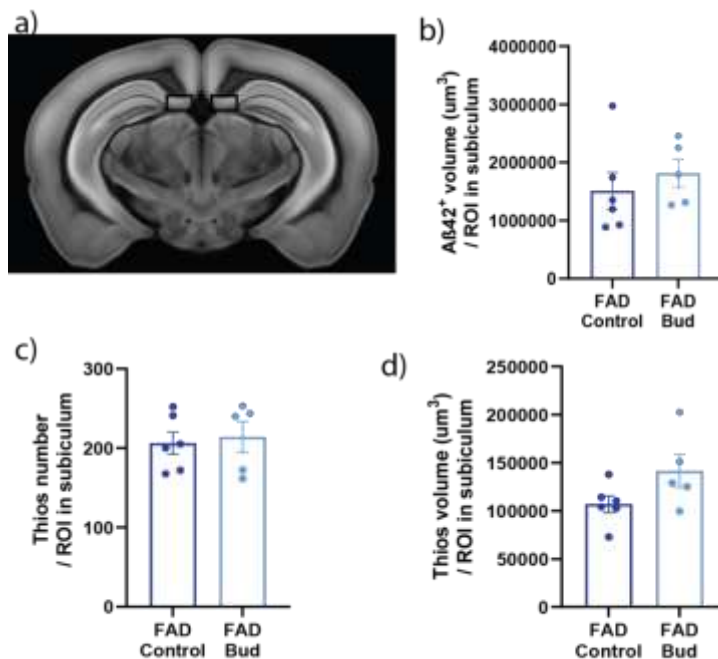


Figure 3.5: Quantification of dense core number and volume of A β plaques, as well as A β 42 volume, in the subiculum upon inhaler Budesonide treatment in

6-month-old female 5xFAD mice. a) Schematic map of coronal level of brain slices quantified for A β plaque in the subiculum. Imaging regions are labeled in black box. (b) A β 42 volume quantification of ROI in the subiculum. (c) ThioS plaque number quantification of ROI in the subiculum. (d) ThioS plaque volume quantification of ROI in the subiculum. Data is presented as mean \pm SEM.

3.2.3 Effect of inhalation Budesonide treatment on neurodegeneration in the 5xFAD mouse model of AD.

Since several behavior tests showed treatment effects in the 5xFAD mouse model, we next studied whether Budesonide treatment would affect neuron loss.

3.2.3.1 Neuronal loss was reduced upon short term inhalation Budesonide treatment

As a hallmark of Alzheimer's disease (AD) and neurodegeneration, neuronal loss was assessed via immunohistochemistry staining with the neuronal marker NeuN. Previous studies indicated that significant neuronal loss in 5xFAD mice is observed by 9 months of age. However, our prior research demonstrated significant neuronal loss in the subiculum of 6 month old 5xFAD mice with an SJL background. Therefore, we quantified the number of NeuN⁺ cells and the average fluorescence signal intensity in the subiculum of 6-month-old female mice (**Figure 3.6**).

At 6 months of age, female 5xFAD mice exhibited approximately 50% neuronal loss in the subiculum compared to wt mice. Upon short term inhalation treatment with Budesonide, treated 5xFAD mice showed significant higher neuronal numbers compared to control mice (**Figure 3.6c**).

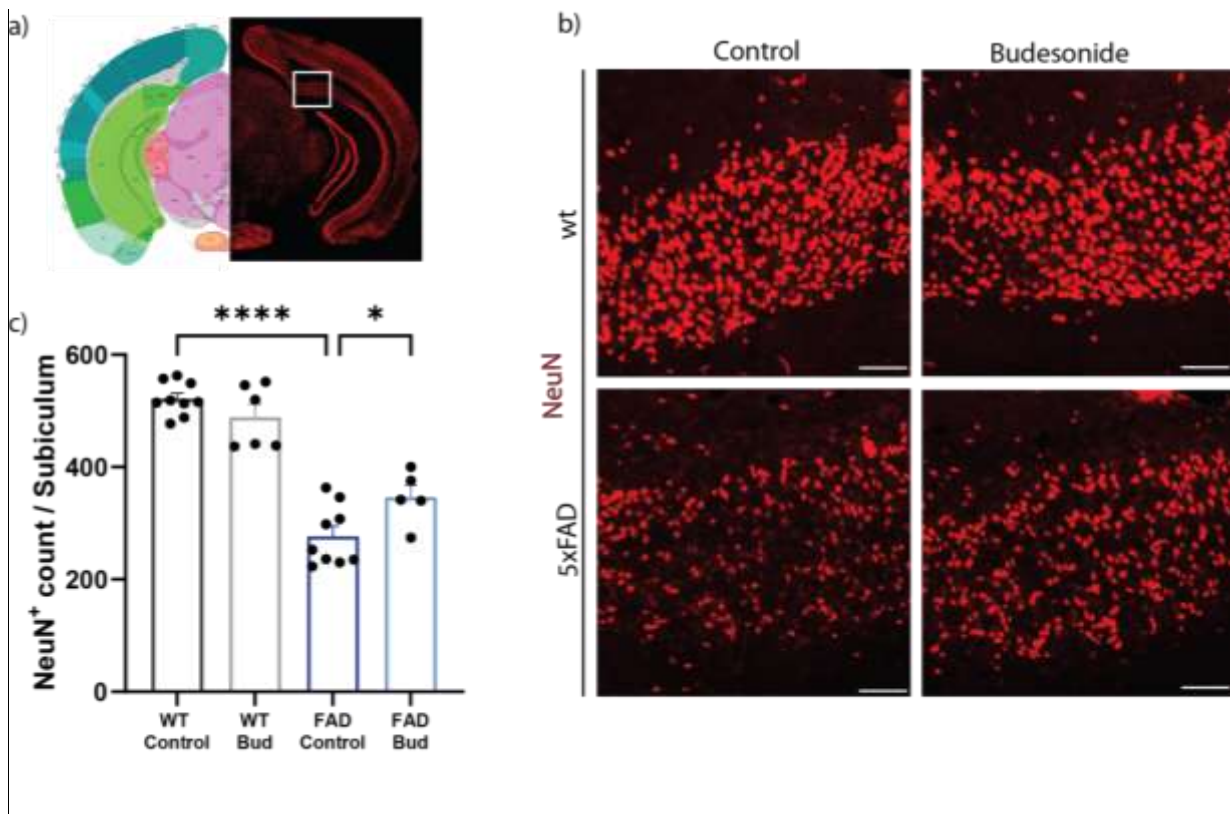


Figure 3.6: Quantification of Neuronal Markers in 6-Month-Old Female wt and 5xFAD Mice Following short term Inhalation Budesonide Treatment a) The schematic map depicts the coronal level of brain slices used for NeuN staining quantification. The imaging region is indicated by a white box. b) Representative images of Immunofluorescence staining for NeuN (red) are shown in 6-month-old untreated (left) and Budesonide-treated (right) wt (upper) and 5xFAD (lower) mice. Images were taken within the subiculum using a confocal microscope with a 20x objective. The presented images are maximum projections of z-stacks. Scale bar: 50 μ m. c) Neuronal loss quantification in the subiculum of 6-month-old female mice. Data is presented as mean \pm SEM. An ordinary one-way ANOVA followed by Sidak's multiple comparisons test was used for statistical analysis. Significance levels are indicated as * $p \leq 0.05$ and **** $p \leq 0.0001$.

3.2.3.2 Blood Neurofilament light chain (NfL) was lower in the 5xFAD mice upon short term inhaler Budesonide treatment

To further analyze the effect of inhaled Budesonide on neuronal injury in the 5xFAD mouse model, NfL (neurofilament light chain) concentration was measured in plasma samples. By 6 months of age, female 5xFAD mice showed a significantly higher (9-fold) concentration of NfL compared to wt mice in the plasma. Female 5xFAD mice that re-

ceived short-term inhaler Budesonide treatment showed a significantly lower NfL concentration, whereas no difference was observed in wt mice that received the same treatment. (**Figure 3.7**)

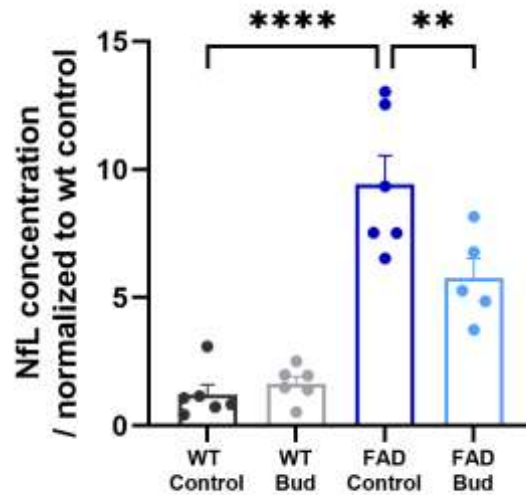


Figure 3.7: Quantification of Neurofilament light chain (Nf-L) concentration in the plasma of wt and 5xFAD mice upon short-term inhalation Budesonide treatment. Neurofilament light chain (NfL) increasing in 5xFAD mice was altered upon short term inhalation Budesonide treatment at 6 month. $N \geq 5$. Data is presented as mean \pm SEM; ordinary one-way ANOVA followed by Sidak's multiple comparisons test, ** $p \leq 0.01$, **** $p \leq 0.0001$. (Sample measured by Pauline Bongard)

3.2.3.3 Effect of inhaled Budesonide on brain atrophy in the 5xFAD mouse model of AD

To investigate the effects of inhaled Budesonide on brain atrophy, we assessed total brain weight and hippocampal volume as measured by MR volumetry in 6-month-old female 5xFAD mice. The 5xFAD mice showed a trend towards lower total brain weight compared to wt controls. Budesonide treated 5xFAD mice exhibited higher brain weights compared to untreated 5xFAD mice, approaching levels observed in wt controls (**Figure 3.8a**).

Additionally, ex vivo T2-weighted MRI revealed a larger hippocampal volume in Budesonide treated 5xFAD mice compared to untreated 5xFAD mice. Specifically, the dorsal and total hippocampal volumes were significantly larger in the Budesonide-treated group (**Figure 3.8b**). The dorsal hippocampus is crucial for spatial memory and navigation, while the total hippocampus plays a broader role in various memory functions. These findings suggest that Budesonide treatment may mitigate brain atrophy, particularly in the hippocampus, in the 5xFAD mouse model of Alzheimer's disease.

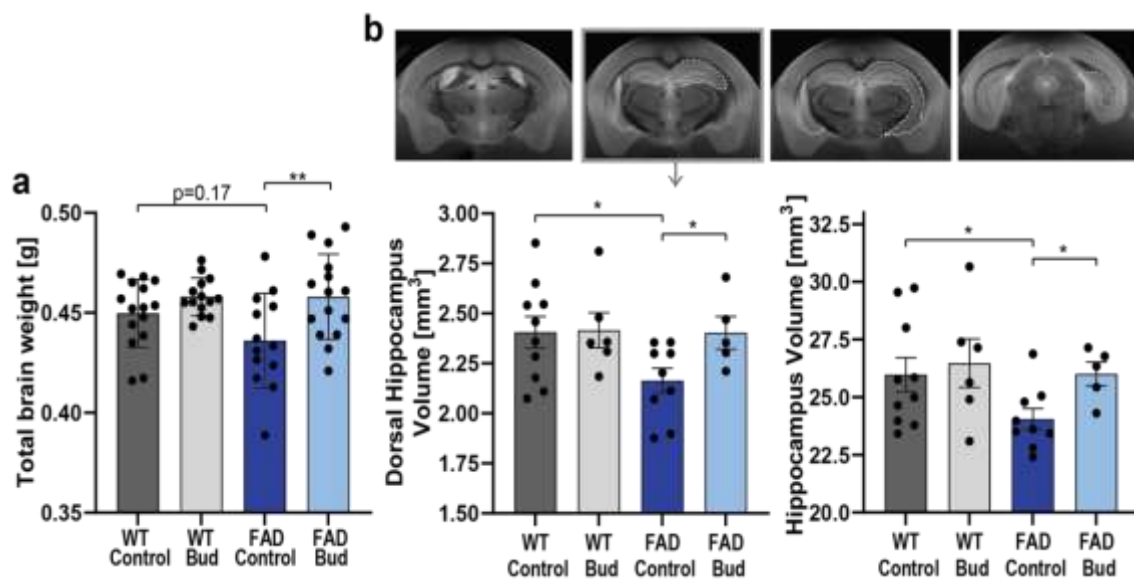


Figure 3.8: Brain atrophy evaluation in 6-month-old female mice. a) Total brain weight evaluation. b) Dorsal and total hippocampal volume assessment via ex vivo MRI. Data is presented as mean±SEM; ordinary one-way ANOVA followed by Sidak's multiple comparisons test, * $p \leq 0.05$, ** $p \leq 0.01$. (MRI images analyzed by Dr. Kristin Oberländer)

3.2.3.4 Synaptic loss was reduced upon short term inhaler Budesonide treatment

Next, we investigated another hallmark of Alzheimer's disease pathology, synaptic loss, and its alteration upon Budesonide treatment. As reported in the literature, 5xFAD mice show synaptic loss in the hippocampus as early as 3 months of age. To determine the degree of synaptic loss and the treatment effect at 6 months old, the CA1 region of female 5xFAD mouse brain slices was analyzed by immunohistochemistry staining for synapsin1/2 (a pre-synaptic marker), PSD95 (a post-synaptic marker), and the

co-localization of synapsin1/2 and PSD95 as a functional synaptic marker.

At 6 months old, female 5xFAD animals showed synaptic loss in the CA1 stratum oriens (CA1so) (**Figure 3.9**) and stratum radiatum (CA1sr) (**Figure 3.10**) compared to wt animals. Upon short term inhaler Budesonide treatment, treated 5xFAD animals showed more pre-synaptic, post-synaptic markers, and co-localization than untreated 5xFAD animals. (Figure 3.9c).

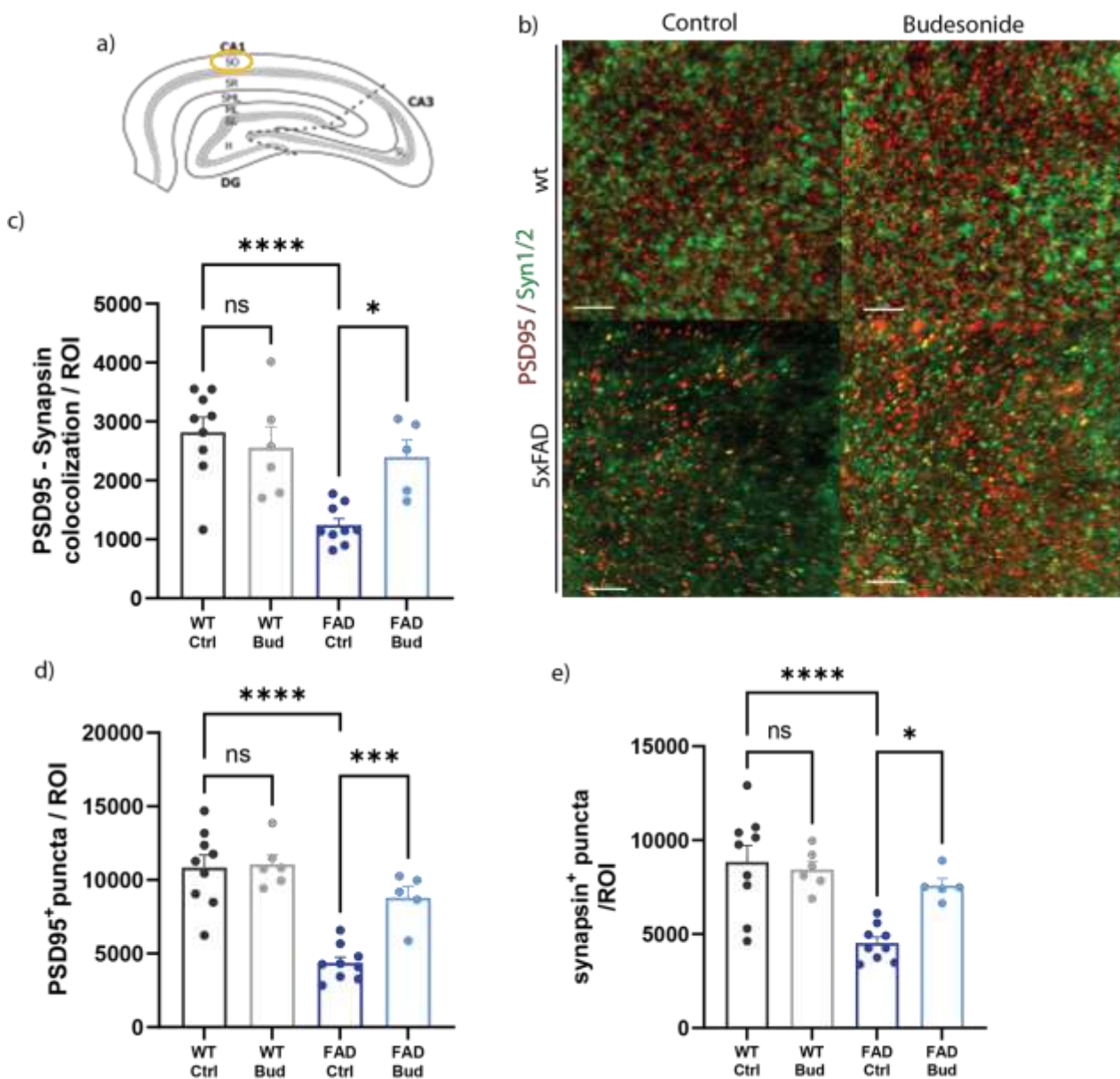


Figure 3.9: Quantification of pre- and post- synaptic marker in the CA1 stratum oriens (CA1so) layer of 6 month old female 5xFAD and wt mice upon inhalational Budesonide treatment. a) Schematic map of CA1 stratum oriens (CA1so) at coronal level of brain slices for synaptic marker staining. Imaging region is marked in orange circle. b) Representative images of histological staining for PSD95 (red) and Synapsin1/2 (green) in 6 month old 5xFAD untreated (left) and Budesonide treated (right) in wt (upper) and 5xFAD (lower) animals. Images were taken within CA1 stratum oriens (CA1so) using a confocal microscope with 63x oil objective. Here representative maximum projections of z-stacks are shown. Scale bar: 20 μ m. c) Functional pre-/post-synaptic marker co-localization puncta pairs quantified in CA1 stratum oriens (CA1so) of 6 month female mice. d) Post-synaptic marker PSD95⁺ puncta quantification. e) Pre-synaptic marker Synapsin1/2⁺ puncta quantification. Data is presented as mean \pm SEM; ordinary one-way ANOVA followed by Sidak's multiple comparisons test, * $p\leq 0.05$, *** $p\leq 0.001$, **** $p\leq 0.0001$.

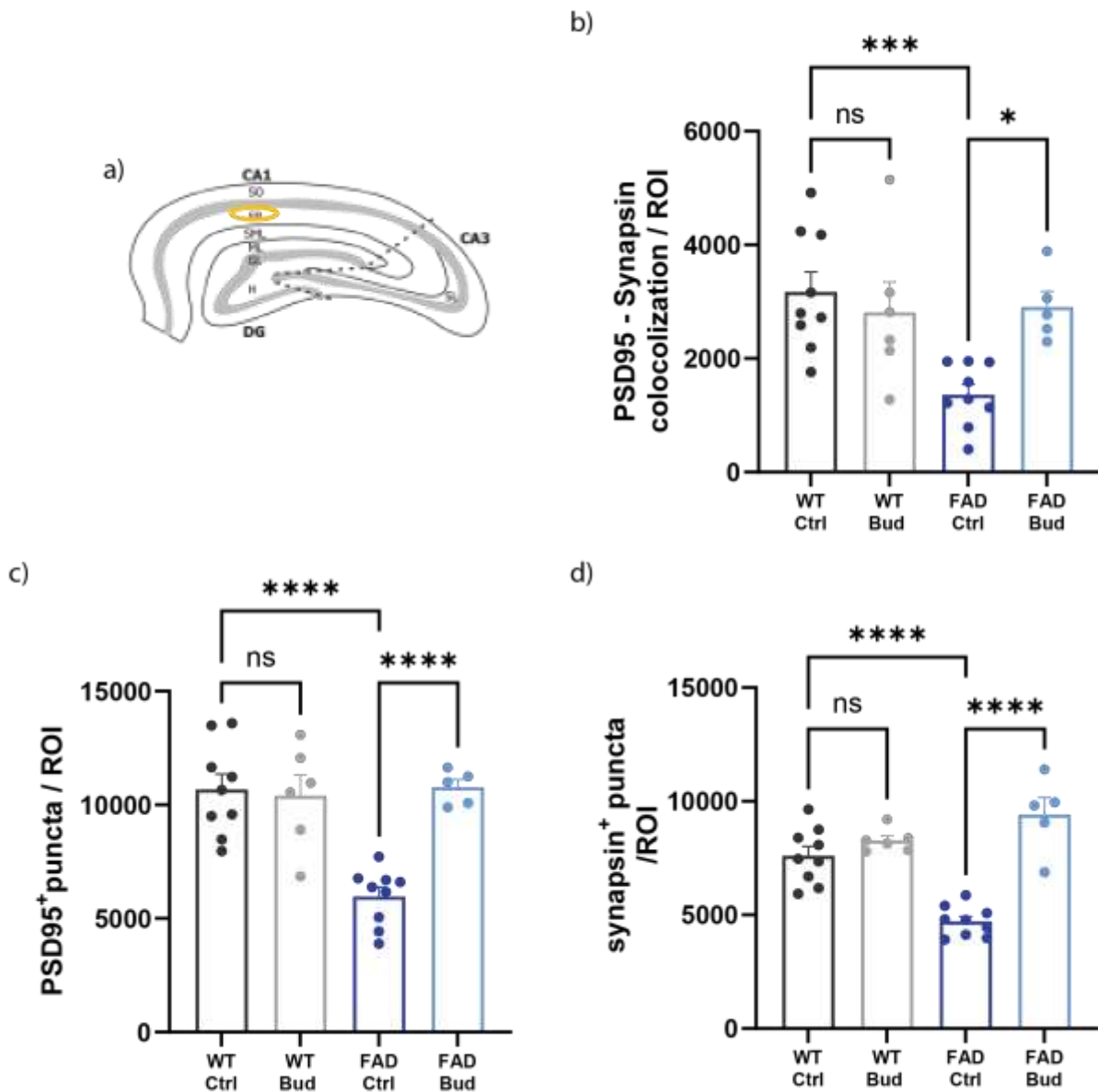


Figure 3.10: Quantification of pre- and post-synaptic marker in the CA1 stratum radiatum (CA1sr) layer of 6 month old female 5xFAD and wt mice upon inhalational Budesonide treatment. Budesonide treatment rescued CA1 stratum radiatum (CA1sr) layer synaptic loss of 6 month old female 5xFAD mice. a) Schematic map of CA1 stratum radiatum (CA1sr) at coronal level of brain slices for synaptic marker staining. Imaging region is marked in orange circle. b) Functional pre-/post-synaptic marker co-localization puncta pairs quantified in CA1 stratum radiatum (CA1sr) of 6 month female mice. c) Post-synaptic marker PSD95⁺ puncta quantification. d) Pre-synaptic marker Synapsin1/2⁺ puncta quantification. Data is presented as mean±SEM; ordinary one-way ANOVA followed by Sidak's multiple comparisons test, *p≤0.5, ***p≤0.01, ****p≤0.001.

In parallel with the findings in the hippocampal region, 6-month-old female 5xFAD animals exhibited a trend to synapse loss in the cortical areas. Analysis of cortical tissue sections (**Figure 3.11**) revealed a reduction in synaptic density in the 5xFAD mice compared to wt controls. Following short term inhaler Budesonide treatment, significantly higher levels of synaptic markers were observed in the 5xFAD animals. This was evidenced by enhanced expression of pre- and post-synaptic markers and increased co-localization in the cortical synapses.

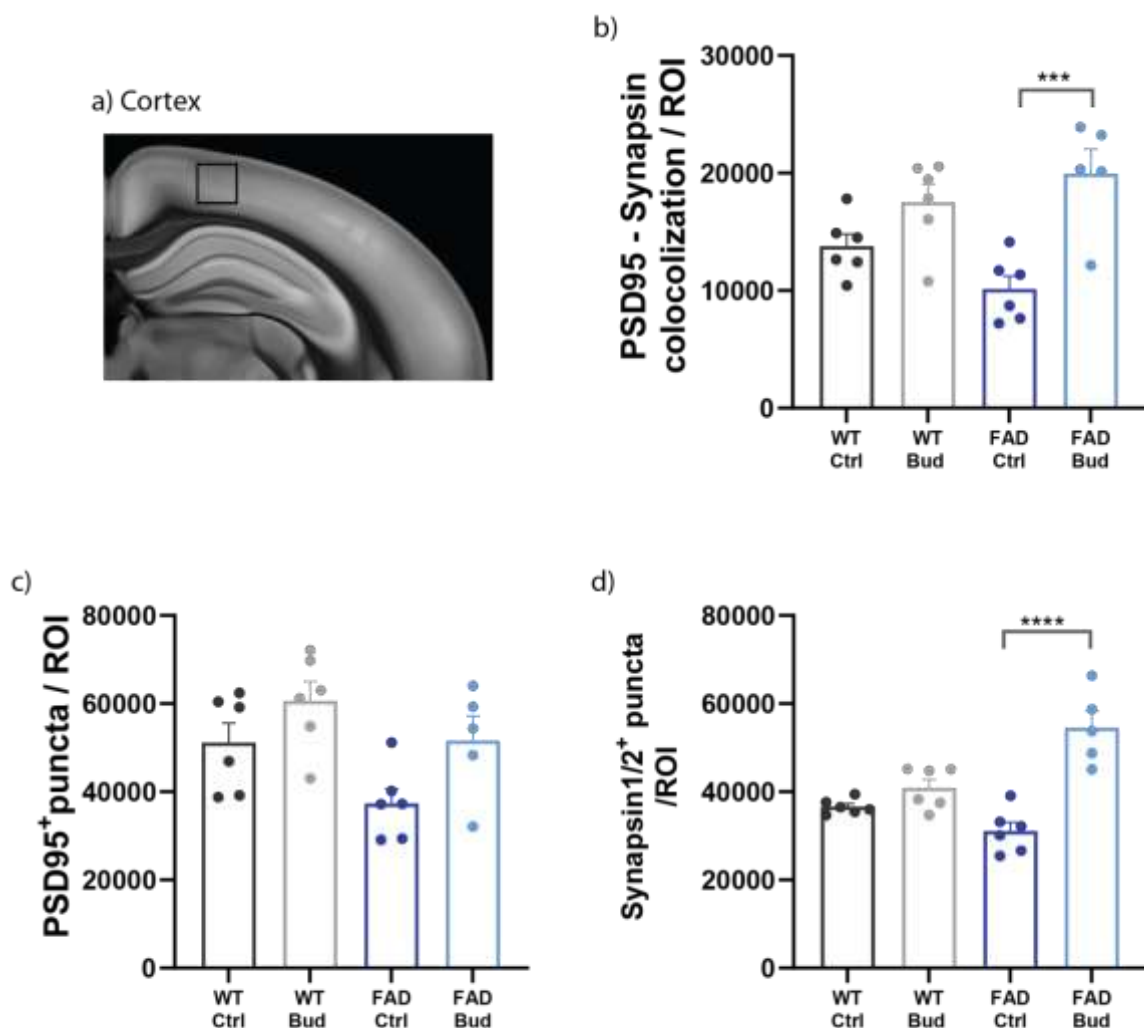


Figure 3.11: Quantification of pre- and post- synaptic marker in the cortex of 6 month old female 5xFAD and wt mice upon inhalational Budesonide treatment.

a) Schematic map of cortex at coronal level of brain slices for synaptic marker staining. Imaging region is marked in black square. b) Functional pre-/post-synaptic marker co-localization quantified in the cortex of 6 month female mice. c) Post-synaptic marker PSD95⁺ puncta quantification. d) Pre-synaptic marker Synapsin1/2⁺ puncta quantification. Data is presented as mean \pm SEM; ordinary one-way ANOVA followed by Sidak's multiple comparisons test, * $p\leq 0.05$, *** $p\leq 0.001$, **** $p\leq 0.0001$.

Furthermore, this effect was also validated by positron emission tomography (PET) scanning. (**Figure 4.2**) PET scanning was done by Prof. Dr. Heike Endepols in Uniklinikum Köln. By targeting SV2A, a synaptic vesicle protein, with the radioligand ([¹⁸F]MNI1126), we aimed to gauge synaptic density. Remarkably, the uptake of [¹⁸F]MNI1126 was significantly reduced in 5xFAD controls when compared to the WT controls, emphasizing the synaptic deficits in the 5xFAD model. However, Budesonide treatment in 5xFAD mice prevented [¹⁸F]MNI1126 uptake deficits compared to untreated 5xFAD controls.

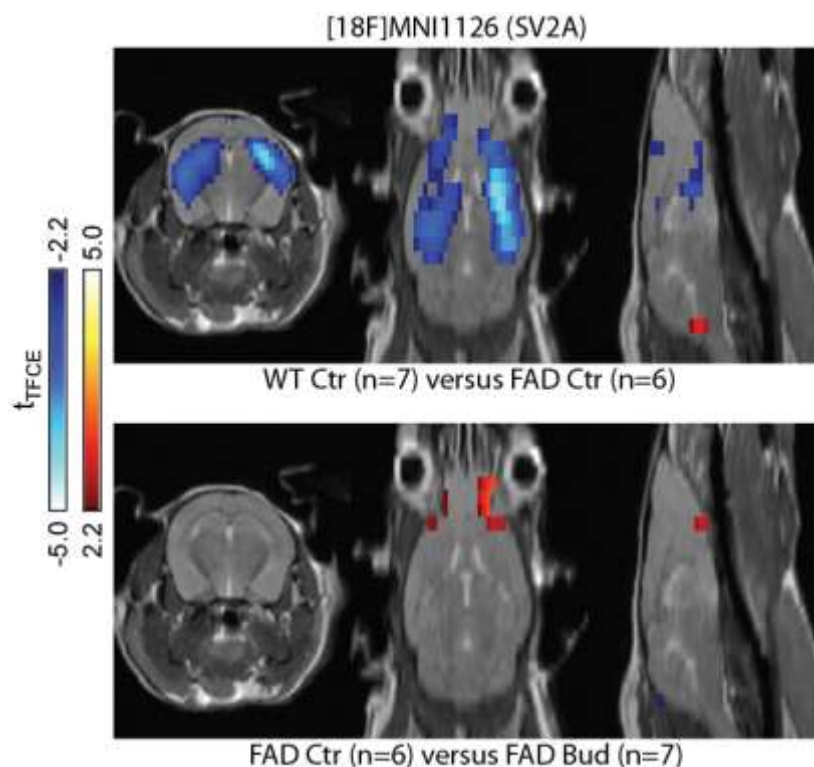


Figure 3.12: Comparative [¹⁸F]MNI1126 PET imaging of synaptic density in wt control, 5xFAD, Budesonide treated 5xFAD mice. Upper: WT control showed signifi-

cant higher SV2A signal in comparison to 5xFAD control animal. (Shown in blue) Lower: FAD control showed significant lower SV2A signal in comparison to Budesonide treated 5xFAD animal. (Data from Prof. Dr. Heike Endepols)

3.2.4 Effect of inhalation Budesonide treatment on neuroinflammation in the 5xFAD mouse model of AD.

3.2.4.1 Assessment of microglial and astrocytic activation in the hippocampus of 5xFAD Mice

Given the well-documented roles of microglia and astrocytes in synaptic pruning and their contribution to the neuroinflammation associated with AD, and considering the observed change in synapse number in Budesonide-treated 5xFAD mice, we next investigated microgliosis, using Iba1 immunostaining. We found, that 5xFAD mice exhibited significant more Iba1⁺ microglia compared to wt controls, indicating increased microglial proliferation. However, there was no significant difference in Iba1 number and signal intensity between treated and untreated 5xFAD mice. Astrocytic activation, assessed by GFAP immunostaining, revealed higher GFAP signal intensity and also higher volume and number of GFAP⁺ astrocytes in 5xFAD mice compared to wt controls, indicating astrocytic activation (**Figure 3.13**).

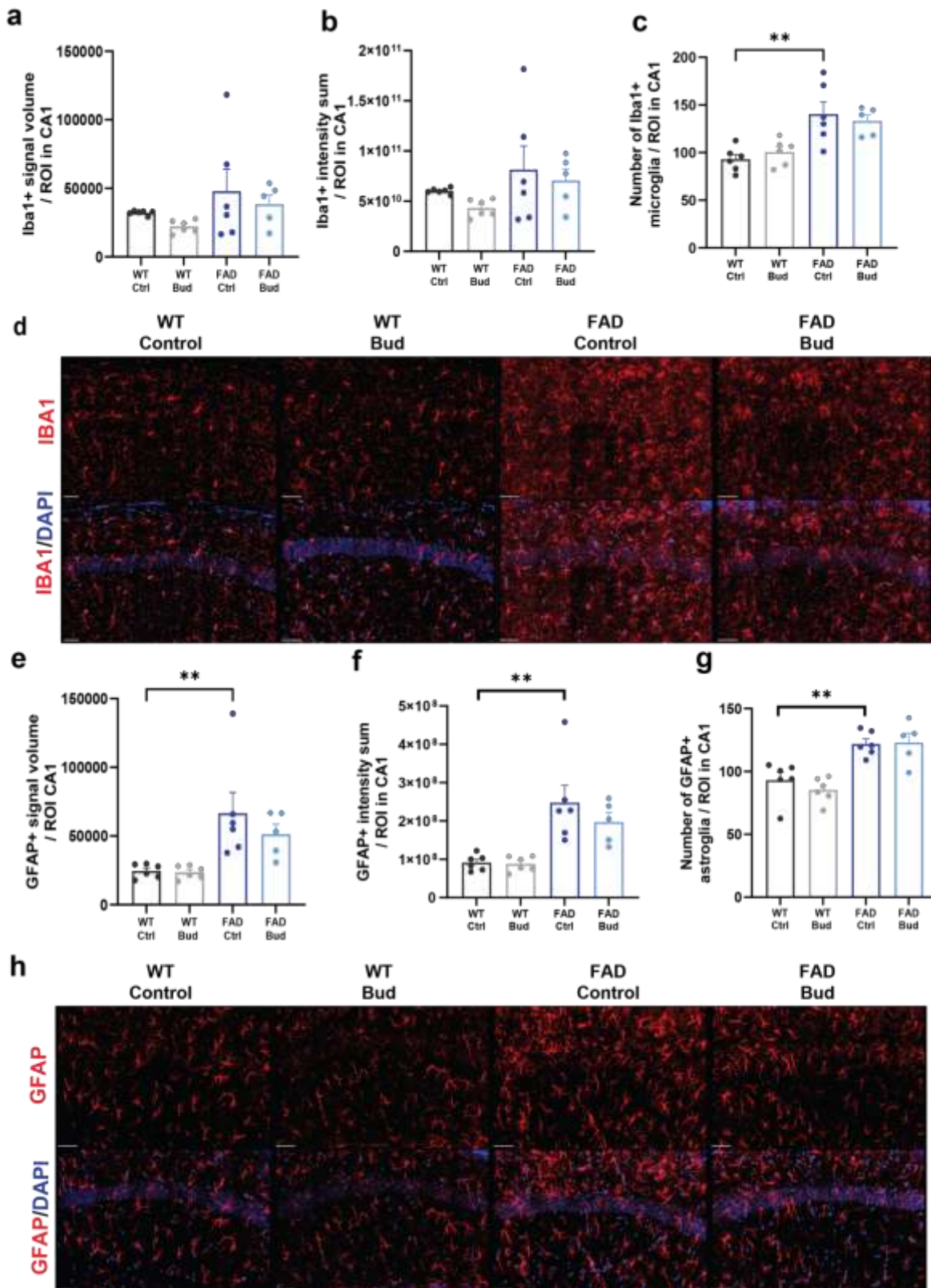


Figure 3.13: Analysis of microglial and astrocytic activation in the hippocampus CA1 region of 6-month-old female 5xFAD mice. Quantification of Iba1 immunohistochem-

istry staining volume (a), total fluorescence signal intensity (b) and iba1 microglia number (c). (d) Representative images of Iba1 (red) and DAPI (blue) staining in the hippocampus CA1 region of 6-month-old wt and 5xFAD Budesonide treated/untreated animals. Scale bar: 20 μ m. Quantification of GFAP immunohistochemistry staining volume (e), total fluorescence signal intensity (f) and GFAP astrocyte number (g). (h) Representative images of GFAP (red) and DAPI (blue) staining in the hippocampus CA1 region of 6-month-old wt and 5xFAD Budesonide treated/untreated animals. Scale bar: 20 μ m. Data is presented as mean \pm SEM. Statistical significance was determined by ANOVA, * $p \leq 0.05$.

3.2.4.2 GFAP plasma levels

Next, we assessed GFAP level in the plasma to evaluate astrocytic activation. Consistent with the hippocampal findings, 5xFAD animals showed a significant increase in GFAP concentration compared to wt controls. Interestingly, upon Budesonide treatment, GFAP levels were significantly lower in the plasma of 5xFAD mice compared to the control-treated 5xFAD mice (**Figure 3.14**).

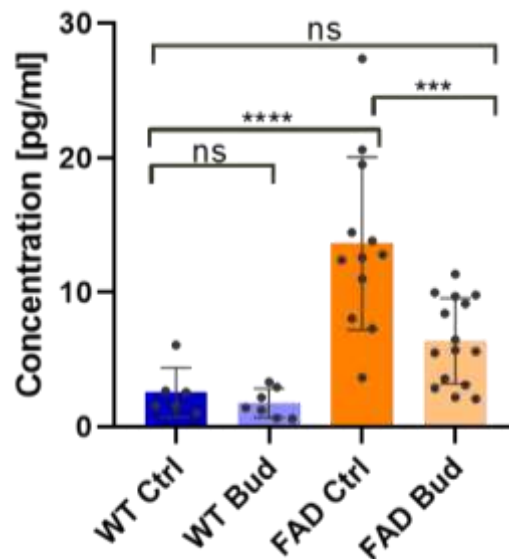


Figure 3.14: GFAP concentration quantification from plasma sample. Data is presented as mean \pm SEM; ordinary one-way ANOVA with Tukey's correction, *** $p \leq 0.001$, **** $p \leq 0.0001$. (Measurement was done by Pauline Bongard.)

3.2.4.3 Complement system alterations upon inhalational Budesonide treatment of female 5xFAD mice

We next aimed at studying gene expression profiles in microglia to investigate potential mechanisms by which Budesonide treatment may mitigate pathology in the 5xFAD mouse model. According to [Keren-Shaul \(2017\)](#), microglia can transition from a homeostatic state (HM) to disease-associated microglia (DAM) in response to AD pathology. This transition includes two stages: DAM1, characterized by upregulation of genes related to immune response and phagocytosis, and DAM2, which involves further upregulation of genes aiding in neuroprotection and debris clearance. We clustered microglia into these defined states, including DAM1, DAM2, and HM, based on their gene expression profiles.

To explore this further, we sorted microglia (CD11b⁺ and CD45^{int}) from one hemisphere via FACS and performed single-cell sequencing (scSeq) using the BD Rhapsody platform. Sequencing was done by Tarek Elmzzahi from Prof. Marc Bayer's group at DZNE Bonn, and data analysis was carried out by Dr. Kristin Oberländer. The scSeq data revealed six microglia clusters (Figure 3.16a), with four clusters corresponding to homeostatic microglia (HM) and two clusters representing disease-associated microglia (DAM). In line with previous findings, we observed that in Budesonide-treated 5xFAD mice, genes associated with the DAM phenotype, including *Apoe*, *Ly86*, and *Ctse*, were significantly downregulated compared to untreated controls (Figure 3.16b, c). This suggests that Budesonide treatment may halt or slow the progression of microglia towards the DAM phenotype, which is often associated with disease pathology.

Additionally, our analysis revealed a significant reduction in complement factor genes, including *C1qb* and *C1qc*, in Budesonide-treated 5xFAD mice compared to controls. These genes are commonly upregulated during DAM progression, and their downregulation in Budesonide-treated mice suggests a potential role for the complement system in

the neuroprotective effects observed with Budesonide. Taken together, these findings suggest that Budesonide treatment may modulate microglial activation and slow the pathological progression of microglia toward the DAM phenotype, possibly contributing to the synaptic preservation observed in treated 5xFAD mice.

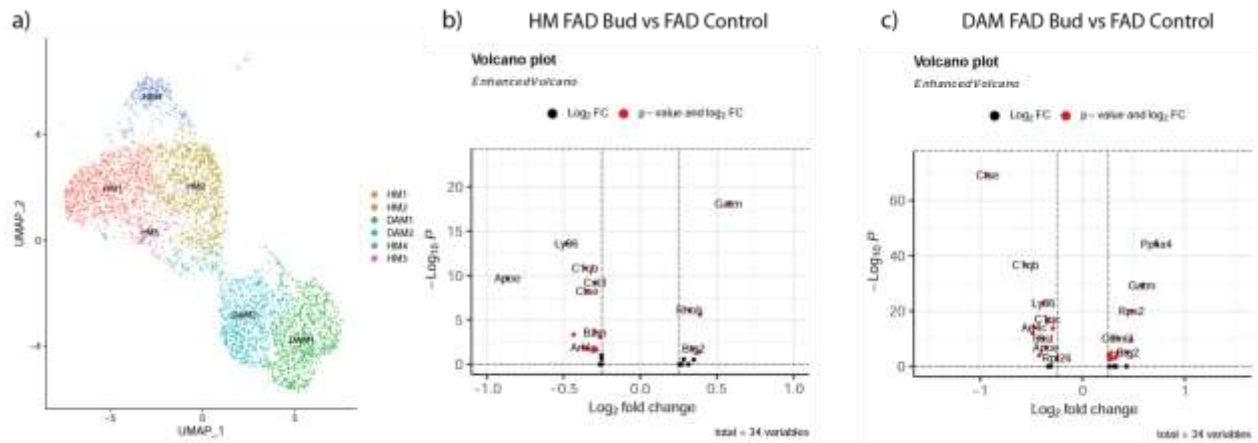


Figure 3.16: Single-cell RNA sequencing analysis of gene expression in homeostatic microglia from Budesonide treated 5xFAD mice compared to untreated 5xFAD controls. The volcano plot shows the log₂ fold change in gene expression (x-axis) against the -log₁₀ p-value (y-axis) for 34 variables. Red dots represent genes that are significantly differentially expressed, while black dots represent genes with no significant change. Key genes include Apoe, Ly86, C1qb, Ctsb, and others involved in microglial function and AD pathology.

Synapse opsonization with C1q has been described, followed by microglial pruning, not only during development, but also in AD ([Hong, 2016](#)). To investigate the number of C1q opsonized synapses in 5xFAD mice with and without Budesonide treatment, we performed immunohistochemistry staining for complement C1q and the post-synaptic protein PSD95. (**Figure 3.17**) Co-localization of C1q and PSD95 was analyzed in the CA1 stratum radiatum (CA1sr) and CA1 stratum oriens (CA1so) layers.

Our results demonstrated that in the CA1sr and so layers, 5xFAD mice had a higher percentage of PSD95 co-localized with C1q compared to wt controls. In the CA1sr layer, Budesonide treatment altered this co-localization in the 5xFAD mice, suggesting an potential effect on complement-mediated synaptic pruning. Budesonide treatment did not

affect this association significantly in the CA1so layer, suggesting that the impact of the treatment on complement-mediated synaptic pruning is specific to the CA1sr region within the hippocampus.

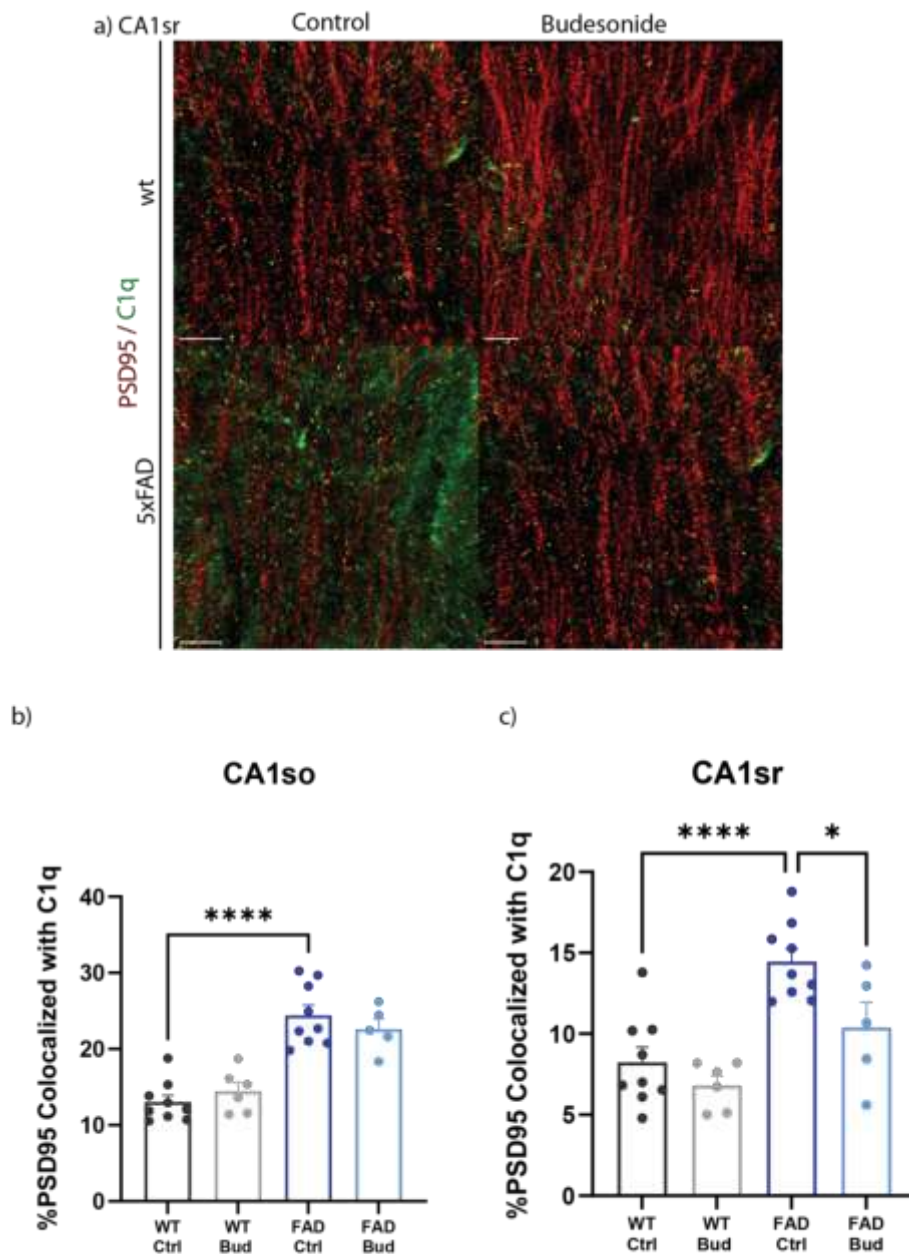


Figure 3.17: Quantification of complement protein C1q association with synapses in 5xFAD and wt mice and treatment effect upon inhalation Budesonide treatment.

a) Representative images of histological staining for PSD95 (red) and c1q (green) in 6 month old 5xFAD untreated (left) and Budesonide treated (right) in wt (upper) and 5xFAD

(lower) animals. Images were taken within CA1 stratum radiatum (CA1sr) using a confocal microscope with 63x oil objective. Here representative maximum projections of z-stacks are shown. Scale bar: 3 μ m. b) C1q and PSD95 co-localization quantified in CA1so layer of 6 month female mice. c) C1q and PSD95 co-localization quantified in CA1sr layer of 6 month female mice. Data is presented as mean \pm SEM; ordinary one-way ANOVA followed by Sidak's multiple comparisons test, *** $p\leq 0.01$.

3.2.4.4 Assessment of synapse markers in hippocampal microglia and astrocytes

We investigated the extent of internalized synaptic material in microglia and astrocytes by analyzing the co-localization of the postsynaptic marker Homer1 with Iba1 and GFAP. Using 3D reconstruction of GFAP and Homer1 fluorescence signals with IMARIS software, we observed an increased amount of Homer1 in astrocytes (**Figure 3.15c**) in the CA1 stratum radiatum layer of female 5xFAD mice compared to wt mice. We additionally found a trend for increased Homer1 co-localization with Iba1 in 5xFAD mice compared to controls. However, Budesonide treatment did not significantly alter the extent of Homer1 colocalization with microglia and astrocytes in 5xFAD mice.

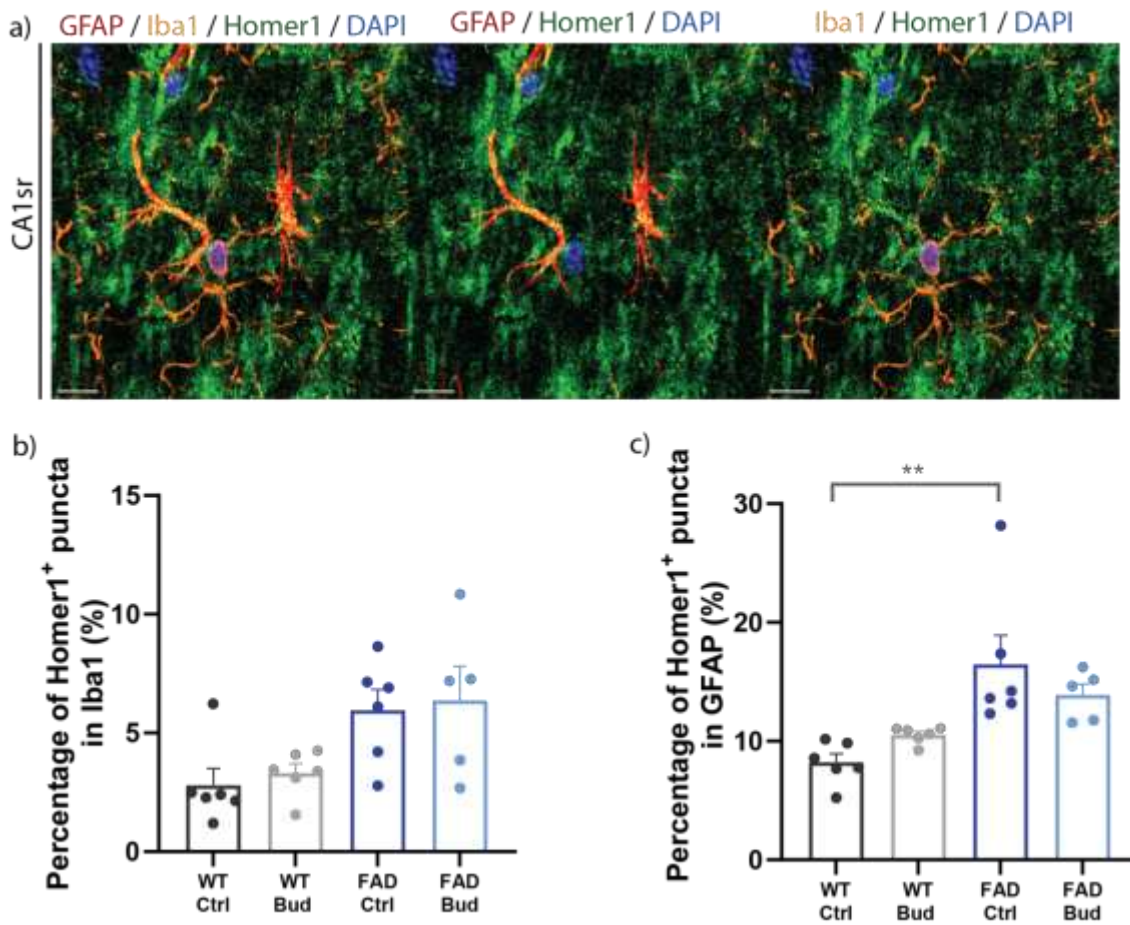


Figure 3.15: Quantification of homer1 in microglia and astrocytes upon inhaled Budesonide treatment in female 5xFAD mice. a) Representative images of histological staining for GFAP (red), Iba1 (orange), homer1 (green) and DAPI (blue) in female 6 month old 5xFAD mice. Synaptic engulfment by astrocyte showed in the middle image, by microglia showed in the right image. Images were taken within CA1 stratum radiatum (CA1sr) using a confocal microscope with 63x oil objective. Here representative maximum projections of z-stacks are shown. Scale bar: 3 μ m. b) Percentage of Homer1 engulfed by microglia quantification. c) Percentage of Homer1 engulfed by astrocyte quantification. Data is presented as mean \pm SEM; ordinary one-way ANOVA followed by Sidak's multiple comparisons test, ** $p \leq 0.01$.

4. Discussion

4.1 Budesonide delivery methods: intranasal vs. inhaler

Budesonide, a glucocorticosteroid with anti-inflammatory properties, has been conventionally used to manage respiratory and allergic conditions. Our recent study suggests that glucocorticoid use is linked to a reduced risk of developing dementia, especially when administered via intranasal and inhalation. Given the blood-brain barrier's restrictive nature, delivering drugs directly to the brain remains a challenge. (Pardridge WM, 2012) Two promising delivery methods which we applied in this project for Budesonide are intranasal and inhaled forms, the latter potentially via the anatomic connection from oro- and nasopharynx. Both application forms may reach the brain via the olfactory system, and come with lower systemic side effects.

Intranasal administration of Budesonide utilizes the unique anatomical connections of the nasal passages to deliver therapeutic agents directly to the CNS. By administering Budesonide through this route, it is possible for the drug to traverse the nasal epithelial cell membranes and subsequently reach the olfactory bulb. This path offers a direct route to the CNS. Such direct delivery could significantly enhance the drug's potential efficacy, particularly for targeting the neuropathological sites implicated in Alzheimer's disease. (Dhuria SV, 2010)

However, the administration of substances intranasally in animal models, particularly mice, often necessitates the use of anesthetics like isoflurane. While isoflurane has been widely used for its rapid induction and recovery phases, there's debate about its potential neurotoxicity and influence on neurophysiological parameters. (Jevtovic-Todorovic V, 2013) Given the potential modulatory effects of isoflurane on blood brain barrier integrity, synaptic transmission, neuroinflammation, and even amyloid-beta dynamics (Xie Z, 2006), its use in our study could inadvertently introduce confounding variables. In addi-

tion, while observing the stress level during treatment, in comparison to recovery from isoflurane anesthesia, mice showed less stress behavior during inhaler treatment.

We therefore chose inhaler treatment for further investigations. Although traditionally associated with pulmonary delivery, there is growing evidence to suggest that inhaled substances can impact neurological processes ([Freiherr J, 2013](#)). Inhaler administration, while potentially delivering lower concentrations of the drug to the brain, offers the advantage of minimizing external interferences like those from anesthesia. This methodological switch provided a cleaner backdrop against which the genuine effects of Budesonide could be studied.

4.2 Sex difference in the response of 5xFAD mouse model to Budesonide treatment

The choice to focus on female mice in this study was not arbitrary but grounded in the observed difference in behavioral impairments between male and female 5xFAD mice. The observation that female 5xFAD mice exhibit cognitive impairment at 6 months of age while their male counterparts do not show such deficits even at 11 months presents a compelling case for sex-dependent resilience in the context of AD-like pathology. This phenomenon could be influenced by several factors, including hormonal differences, variances in disease progression, and divergent responses to inflammatory processes within the central nervous system (CNS).

Testosterone may confer neuroprotective benefits that delay the onset or progression of cognitive deficits. The hormone has been shown to reduce the production of amyloid-beta ($A\beta$), a hallmark of AD pathology, and to support synaptic density and plasticity, which are crucial for cognitive function ([Pike CJ, 2009](#)). In the absence of behavioral impairments in male 5xFAD mice, it is possible that endogenous testosterone levels are providing a protective effect that is not present or is diminished in female mice post-menopause, when estrogen levels decline significantly.

Given the observed sex differences in the timing of cognitive impairment onset, it is crucial to examine how these differences may affect the efficacy of Budesonide treatment. Budesonide, as an anti-inflammatory agent, could have varying effects in male and female mice due to the differential progression of neuroinflammation associated with AD pathology.

In females, where cognitive impairment emerges earlier, Budesonide treatment may need to be initiated sooner to be effective. In contrast, males might benefit from later intervention. Moreover, since inflammation can also be modulated by sex hormones (e.g., estrogens have anti-inflammatory properties) ([CJ Pike, 2017](#)), the window of optimal treatment efficacy could be narrower in females than in males.

A deeper understanding of these sex-specific nuances could not only shed light on the intricate mechanisms of Alzheimer's disease but also guide future therapeutic strategies. Tailoring treatments based on sex might enhance therapeutic efficacy, ensuring that interventions are not just effective but optimized for each individual.

4.3 Impact of Budesonide treatment on disease pathology in 5xFAD mice

In this study, we investigated the effects of Budesonide on Alzheimer's disease (AD) pathology using the 5xFAD mouse model. We focused on key AD hallmarks such as amyloid-beta ($A\beta$) plaque formation, neuronal loss, synaptic integrity, neurofilament light chain (Nf-L) levels, and brain atrophy. Our findings revealed that Budesonide significantly reduced the number and volume of dense-core plaques in the cortex, although it did not significantly alter $A\beta_{42}$ deposition. Additionally, Budesonide preserved neuronal numbers and synaptic density, highlighting its neuroprotective potential.

Regarding synaptic preservation, our results showed fewer C1q-opsonized synapses in Budesonide-treated mice, suggesting reduced complement-mediated synaptic pruning. Although we expected less synaptic engulfment by microglia and astrocytes, this was not

observed. We hypothesize that the reduced percentage of opsonized synapses was due to decreased phagocytosis, although the exact mechanisms remain to be investigated. Further studies are needed to confirm these hypotheses and explore the impact of Budesonide on microglial phagocytic activity and synaptic degradation.

Budesonide's impact on plaque formation

One of the pathological hallmarks of Alzheimer's disease (AD) is the accumulation of extracellular amyloid-beta ($A\beta$) plaques. In our study, we investigated the effect of inhaled Budesonide treatment on amyloid pathology by analyzing immunohistochemistry staining of $A\beta$ 42 and Thioflavin S (ThioS), which labels the dense core of $A\beta$ plaques. We examined the cortex region across coronal brain slices at Bregma 1.18mm, -0.82mm, -1.82mm, and -2.80mm. Image analysis revealed a significant reduction in the number of ThioS stained plaques throughout the examined cortex in Budesonide-treated 5xFAD mice. Furthermore, we observed a reduction in dense core volumes at Bregma -0.82mm and -1.82mm, with a similar trend noted at the other positions. However, $A\beta$ 42 volume in the cortex did not show a significant difference between the treated and control groups, suggesting that Budesonide may have limited impact on overall $A\beta$ 42 deposition in this region.

In our study, we also quantified hippocampal $A\beta$ 40 and $A\beta$ 42 in three different solubility fractions using Meso Scale Discovery (MSD), with experiments done by Dr. Kristin Oberländer. The analysis revealed that Budesonide treatment did not result in a significant reduction in the more insoluble amyloid fractions (SDS and formic acid), which are associated with plaque deposition. However, we observed a significant decrease in soluble $A\beta$ 40 and $A\beta$ 42 in the RIPA fraction. Additionally, when summing the amyloid concentrations from all three fractions, there was a strong trend toward decreased total $A\beta$ 42 in Budesonide-treated 5xFAD mice.

Following the analysis of brain homogenates, we measured $A\beta$ 40 and $A\beta$ 42 levels in the

plasma, both of which were reduced following Budesonide treatment, with A β 40 showing a more pronounced decrease compared to A β 42. While the interpretation of low A β levels in biofluids, particularly in blood or cerebrospinal fluid (CSF), is complex, lower A β 42 levels in CSF are commonly associated with increased disease pathology due to its sequestration into brain plaques. It is possible that the relatively smaller decrease in A β 42 in plasma, compared to A β 40, could reflect that more A β 42 remains in circulation rather than aggregating into plaques in the brain, suggesting a potential positive effect of Budesonide on reducing plaque formation. However, this remains speculative. The unchanged A β 42/40 ratio, often a more reliable biomarker for disease progression, suggests that Budesonide may influence A β metabolism, but may not significantly alter the fundamental mechanisms driving plaque formation. (Data not shown, measurements by Pauline Bongard).

While plaque number is an important metric in evaluating amyloid pathology, plaque morphology and composition also play crucial roles in AD progression. In our study, Budesonide treatment significantly reduced the number and volume of ThioS-stained dense-core plaques in the cortex. However, the toxicity of dense-core plaques compared to diffuse plaques remains a subject of ongoing debate. Therefore, understanding Budesonide's differential effects on various plaque subtypes is critical for assessing its full therapeutic potential in AD management.

Budesonide's impact on neuronal loss in 5xFAD mice

Neuronal loss, a well-documented hallmark of Alzheimer's disease (AD) and other neurodegenerative conditions ([Braak H, 1991](#)), was assessed in our study through NeuN immunohistochemistry staining. Our observations revealed that 6-month-old female 5xFAD mice exhibited approximately 50% neuronal loss in the subiculum compared to wt. Interestingly, short-term Budesonide administration hinted at a protective effect, with treated 5xFAD mice demonstrating significantly higher neuronal numbers compared to untreated 5xFAD mice. This finding is particularly promising, as it suggests that

Budesonide may help mitigate some of the neuronal loss associated with AD pathology. The preservation of neuronal numbers could translate to improved cognitive function and slowed disease progression, making Budesonide a potential therapeutic candidate for AD. Moreover, treated 5xFAD mice displayed a notably higher average NeuN+ cell signal intensity compared to control 5xFAD mice.

Such findings, although preliminary, warrant further investigation. Future studies should focus on elucidating the mechanisms by which Budesonide exerts its neuroprotective effects. Additionally, longitudinal studies would be needed to assess whether the observed neuronal preservation translates to sustained cognitive benefits over time.

Budesonide's impact on neurofilament light chain (Nf-L) levels in 5xFAD mice

Neurofilament Light Chain (Nf-L) is a structural protein of axonal cytoskeletons, leaks into the cerebrospinal fluid (CSF) and subsequently into the bloodstream upon neuronal damage. ([Khalil M, 2018](#)) Elevations of Nf-L in the plasma or serum has recently gained traction as a non-invasive biomarker indicative of neuronal damage, and its levels often correlate with the severity and progression of neurodegenerative diseases. ([Siller, 2019](#)) At the 6 months mark, female 5xFAD mice presented a 9-fold increase in Nf-L levels compared to wt mice. Encouragingly, Budesonide treatment culminated in significant lower blood Nf-L concentrations in the 5xFAD cohort. This data suggests a protective role of Budesonide against neuronal damage in this AD mouse model.

Budesonide's effect on brain atrophy in 5xFAD mice

Our study demonstrated that Budesonide treatment has a significant impact on mitigating brain atrophy in 5xFAD mice. The observed higher in total brain weight and hippocampal volume in Budesonide-treated 5xFAD mice, as confirmed by ex vivo T2-weighted MRI, suggest that Budesonide may play a crucial role in protecting against brain atrophy. Interestingly, while the brain weight showed a significant difference, MRI-based volumetric analysis did not reveal a large effect on overall brain volume. This discrepancy could be

attributed to the fact that the protective effects are localized primarily in the hippocampus, which is particularly vulnerable in AD pathology, while other regions of the brain may not experience the same level of protection. Additionally, brain weight measurements may reflect changes in tissue density or cellular content not captured by volumetric MRI. Further studies are needed to explore the underlying mechanisms driving these differential outcomes.

Budesonide's effect on synaptic loss in 5xFAD mice

Synaptic loss is another hallmark of Alzheimer's disease. Our immunohistochemistry staining and PET imaging data provided strong evidence of Budesonide's potential in mitigating synaptic loss in 5xFAD mice. Specifically, immunohistochemical analysis revealed higher synaptic numbers in the hippocampus CA1 of Budesonide-treated 5xFAD mice compared to untreated controls. Positron Emission Tomography (PET) imaging with the radioligand [18F]MNI1126, which targets the synaptic vesicle protein SV2A, corroborated these findings, suggesting that Budesonide may help preserve or restore synaptic density.

Budesonide's potential mechanisms of action in 5xFAD Mice Reduction in neuro-degeneration

Despite these promising results, further examination was necessary to understand the underlying pathways involved in synaptic preservation. We analyzed synaptic engulfment by microglia and astrocytes using co-localization of the synaptic marker Homer1 with Iba1 and GFAP. Although 5xFAD control mice showed increased Homer 1 signal in astrocytes compared to wt, Budesonide treatment did not significantly alter this, suggesting that the treatment does not impact synaptic integrity through this specific mechanism.

The complement system, particularly C1q, is known to play a critical role in synaptic pruning by tagging synapses for elimination by microglia. Our immunohistochemistry analysis revealed higher co-localization of C1q with PSD95 in the CA1 stratum radiatum

of 5xFAD mice, indicating a potential for increased complement-mediated synaptic pruning. In the CA1sr layer, Budesonide treatment significantly altered this co-localization in the 5xFAD mice, suggesting an effect on complement-mediated synaptic pruning. However, Budesonide treatment did not significantly affect this association in the CA1so layer, suggesting that the impact of the treatment on complement-mediated synaptic pruning is specific to the CA1sr region within the hippocampus.

This region-specific effect is supported by previous studies that show differential synaptic vulnerability to amyloid pathology in various brain regions. For example, synaptic degeneration in the medial prefrontal cortex (mPFC) of 5xFAD mice is more pronounced than in the primary visual cortex (V1). ([Seo, 2021](#)) These observations suggest that local concentrations of amyloid oligomers, neuronal intrinsic factors, or differences in mitochondrial content could contribute to the selective vulnerability of synapses in certain regions. In our study, the greater effect of Budesonide in the CA1sr compared to the CA1so may reflect similar region-specific vulnerabilities within the hippocampus, possibly due to higher levels of amyloid pathology or increased complement-mediated synaptic pruning in the CA1sr.

It is also important to note that we have not yet examined synaptic loss in other regions, such as the cortex, which could provide additional insights into the broader effects of Budesonide on synaptic integrity. Regional selectivity of synaptic loss has been reported in cortical regions, where specific cortical layers exhibit early vulnerability to amyloid-induced damage. The differential impact observed in the hippocampus, and potentially in the cortex, might be related to varying concentrations of amyloid oligomers or intrinsic susceptibilities of neurons in those regions.

Budesonide treatment significantly reduced GFAP concentration in plasma, suggesting a decrease in neuroinflammation. This supports the hypothesis that Budesonide can modulate the inflammatory response, potentially creating a more supportive environment for

neuronal health. However, we found no evidence for microgliosis or astrogliosis in the CA1 region based on Iba1 and GFAP staining. This lack of detectable modulation in the CA1 region may be due to the complexity of neuroinflammatory mechanisms in the brain. Additionally, we did not assess all brain regions, so it is possible that Budesonide's effects on glial activation may be more pronounced in other areas. One explanation could be the differential time course and dynamics of glial cell activation and response to anti-inflammatory treatments. Systemic biomarkers like plasma GFAP might reflect early changes, while localized brain regions could require longer exposure or higher doses for detectable effects. Furthermore, Budesonide may differentially affect subtypes of astrocytes and microglia, which exhibit distinct functional states and responses to the drug. The heterogeneity in glial cell populations and their spatial distribution could also contribute to the apparent lack of significant modulation in the CA1 region.

While our findings indicate that Budesonide-treated 5xFAD mice exhibited less synaptic loss, the exact mechanisms underlying this effect remain unclear. One possible explanation involves the downregulation of complement protein mRNA, particularly C1q, which is known to play a critical role in complement-mediated synaptic pruning. The observed reduction in synaptic loss in Budesonide-treated mice may be partially mediated by this pathway.

However, our study lacks evidence from direct manipulation of the complement system, such as C1q inhibition or genetic knockdown, which could help confirm its involvement in Budesonide's effects. We also did not investigate downstream components of the complement cascade, such as C3 or C4, which play essential roles in complement-mediated synaptic pruning. Understanding whether Budesonide modulates the entire complement cascade or if its effects are limited to C1q downregulation would provide further insight into its therapeutic potential.

Future research should focus on directly manipulating the complement system to test

whether Budesonide's effects are indeed dependent on the complement cascade, especially C1q. This could involve assessing whether C1q inhibition or knockdown eliminates Budesonide's protective effects on synaptic integrity in 5xFAD mice, as well as examining the role of downstream complement components in this process.

Other pathological pathways potentially involved in the treatment effect of Budesonide on 5xFAD mouse model

Phagocytosis pathway: Our microglia scSeq data showed that Budesonide treatment leads to a trend of downregulation of MerTK (Mer Tyrosine Kinase) in microglia in the 5xFAD mouse model. MerTK is part of the TAM receptor tyrosine kinase family and is known to play a role in the regulation of microglial functions, particularly in the phagocytosis of apoptotic cells and debris. ([Jimenez, 2022](#)) In the central nervous system (CNS), efficient clearance of apoptotic cells is crucial to prevent secondary necrosis and to maintain tissue homeostasis. ([Fourgeaud, 2016](#)) During hippocampal neurogenesis, which is a process of producing new neurons throughout life, MerTK helps to regulate the phagocytosis of apoptotic newborn cells by microglia, thereby maintaining a balanced cellular environment that is supportive of neurogenesis. ([Diaz, 2020](#))

Downregulation of MerTK could indicate a reduction in the phagocytic activity of microglia, which may have implications for synaptic pruning. Given the role of microglia in eliminating excess or damaged synapses through phagocytosis, diminished MerTK expression might reduce microglial synapse clearance. This could potentially lead to the preservation of synapses, which could explain the reduced synaptic loss observed in Budesonide-treated 5xFAD mice. In addition, MerTK does not act in isolation and is part of a network of signals and receptors. Its downregulation might affect other pathways related to cell survival, inflammation, and CNS homeostasis.

Infiltrating T Cells: Our FACS sorting data (data not shown) indicated a decrease in CD4 T cell numbers in the brains of Budesonide-treated 5xFAD mice, while the numbers

of CD8 T cells didn't show alternation (N=3). The selective downregulation of CD4+ T cells may point to a potential Budesonide mediated suppression of the Th1 and Th17 subsets, which are known for cytokine secretion, such as IFN- γ and IL-17, that activates microglia and astrocytes, contributing to neurodegeneration. To further validate this FACS data, immunohistochemical CD4+ and CD8+ T cell staining is planned for the follow up study.

APOE: Another finding we gain from scSeq data is a down regulation of APOE upon Budesonide treatment in the microglia of treated 5xFAD mice. Downregulation of APOE in microglia could potentially impact the aggregation and clearance of A β . APOE is known to bind to A β and can influence its deposition and removal in the brain. Alterations in APOE levels might therefore affect the pathological process of A β . ([Huang YWA, 2017](#))

In addition to its role in A β pathology, microglial APOE is a well-established marker of disease-associated microglia (DAM). The downregulation of APOE in Budesonide treated mice may indicate a reduction in microglial inflammatory activation, which is linked to the DAM phenotype. Importantly, research has shown that deletion of microglial APOE reduces amyloid pathology in APP/PS1 mice ([Ulrich, 2018](#)), suggesting that lower APOE levels may contribute to decreased neuroinflammation and amyloid burden. This reduction in APOE expression could therefore represent a shift away from a pro-inflammatory, neurodegenerative state in microglia, providing further insight into Budesonide's potential therapeutic effects.

Blood-Brain Barrier Integrity: Glucocorticoids, like Budesonide, can influence the integrity of the blood-brain barrier (BBB). They have been shown to enhance BBB function by increasing the expression of tight junction proteins such as occludin and claudin-5, which are critical for maintaining barrier strength. ([Salvador. 2014](#)) These effects help reduce vascular permeability and limit the infiltration of immune cells into the CNS, potentially providing protection against neuroinflammatory damage. It is possible that

Budesonide's ability to stabilize the BBB could represent another mechanism through which it mitigates pathology progression. However, further research is required to explore these effects fully.

4.4 Future directions for preclinical research and translating preclinical findings to explore a synergistic approach in AD Treatment

The neuroprotective and anti-neuroinflammatory effects of inhaled Budesonide observed in our study provide a promising avenue for AD treatment. However, further preclinical research is needed to support its therapeutic potential before advancing to clinical trials. In our study, only the 5xFAD mouse model was used, which primarily reflects amyloid pathology. To strengthen the evidence for Budesonide's efficacy, other well-established AD models, including amyloid (APP/PS1) and Tau (P301L or rTg4510) mouse models, could be tested. These models would allow us to explore Budesonide's effect on both amyloid and tau-related pathologies, which are central to AD progression. Testing across multiple models would provide a more comprehensive understanding of its potential therapeutic effects on various aspects of AD pathology, such as tau hyperphosphorylation, neurofibrillary tangle formation, and amyloid plaque deposition.

Moreover, in our study, Budesonide treatment began at 4 months of age, future studies could explore different treatment initiation windows, including later stages of AD, to evaluate Budesonide's potential in treatment of advanced disease. Additionally, testing different treatment durations and the persistence of its effects post-treatment will be essential for determining the optimal therapeutic window and dosage regimen. Longitudinal studies could assess whether Budesonide's protective effects on synaptic density, neuronal survival, and neuroinflammation are sustained over extended periods or whether repeated dosing is necessary to maintain its efficacy.

A Phase 2 clinical trial in mild cognitive impairment (MCI) patients could be the next step to evaluate Budesonide's efficacy. Translatable clinical outcome markers such as neuro-

filament light chain (Nf-L), amyloid-beta ($A\beta$) markers, and MRI scans for structural and functional changes could be employed to assess its therapeutic benefit.

Recent therapeutic strategies in AD have primarily focused on targeting amyloid-beta ($A\beta$) plaques, specifically anti- $A\beta$ monoclonal antibodies. These have demonstrated a potential in ameliorating AD symptoms, however they come with a critical limitation: amyloid-related imaging abnormalities (ARIA). ARIA, characterized by brain edema, microbleed and in severe cases, substantial brain hemorrhages, poses significant safety concerns, with some instances even leading to fatalities in clinical trials and clinical application. Preliminary hypotheses suggest that these adverse effects result from the binding of anti-amyloid antibodies to vascular amyloid, initiating the complement cascade that subsequently damages cerebral vessels, causing fluid leakage and microhemorrhages.

In clinical practice, oral steroids are sometimes administered to ameliorate symptomatic ARIA. Given the neuroprotective and anti-neuroinflammation effects of inhalation GCCs showed from our study and the challenges posed by ARIA in anti- $A\beta$ monoclonal antibody therapies, a synergistic approach incorporating both these therapeutic modalities could appear promising. This may not only diminish the activation of the complement cascade, thereby preventing edema and microhemorrhage, but also possibly enhance the blood-brain barrier (BBB) integrity, further safeguarding against ARIA. However further investigation is needed to understand the exact pathways Budesonide involved and gain further insights into this therapeutic potential or limitations.

4.5 Inhaled Budesonide treatment as a prospective clinical approach for AD patients

Our preclinical data suggest that inhaled Budesonide treatment, starting in prodromal AD/MCI stage may protect against synapse/neuron loss in AD, potentially by its anti-inflammatory effects. This hypothesis finds support in earlier studies on health claims

data from AOK, which have illuminated that inhaled and intranasal glucocorticosteroids are associated with a significantly reduced risk of dementia.

Inhalation therapy has the potential to ensure a more direct drug delivery to the central nervous system, which might enhance the therapeutic impact while minimizing systemic adverse effects. While our study used isoflurane anesthesia for intranasal administration in mice, this step is not required in humans. Thus, intranasal delivery could provide a clinically feasible alternative for CNS-targeted treatments, eliminating the need for anesthesia and avoiding potential side effects. Both inhalation and intranasal routes offer promising methods for delivering treatments like Budesonide effectively to the CNS.

Moreover, when used as an inhalant for respiratory conditions like asthma or allergic rhinitis, has a well-established safety profile. Its long-term use and side effects are well documented. As a repurposing approach, no extensive safety studies have to be taken allowing phase 2 trials. However, dosing, dosing intervals, time of application (morning or evening) are difficult to deduce from animal data (please expand/discuss). Also, to establish those, it would be helpful to establish a target engagement biomarker which allows e.g. dose-finding trials with small patient numbers (please discuss), which can expedite the clinical trial's initial phases, where safety is a primary concern, this offers an added layer of reassurance. Given the dearth of adverse events and its well-established use in other clinical contexts, the transition to studying its effects in Alzheimer's seems both logical and timely.

5. Abstract

This project investigated the therapeutic potential of Budesonide, a glucocorticoid commonly used for asthma therapy, in the treatment of the 5xFAD mouse model of Alzheimer's disease. The findings indicate that inhalation of Budesonide may influence several aspects of AD pathology.

Key results showed that inhalation treatment with Budesonide prevented cognitive decline, impairment of learning, and memory performance in behavioral tests. Additionally, Budesonide treatment was associated with a reduction in brain atrophy without affecting plaque load and amyloid levels. This was paralleled by reduced neuron and synapse loss, and lower blood levels of the neurodegeneration marker NfL. We identified anti-inflammatory changes in microglia of Budesonide treated 5xFAD animals, together with a lower percentage of C1q opsonized synapses as one potential mechanism of Budesonide treatment.

Moreover, we showed that inhaled Budesonide reached the brain regions affected by AD pathology, confirming effective drug delivery.

Further exploration into the molecular mechanisms of Budesonide's effects is essential. Understanding these pathways could lead to optimized treatment protocols that maximize therapeutic benefits while minimizing side effects.

6. List of figures

Figure 1.1: A β plaques in the cortex of individuals with Alzheimer's disease (AD)

Figure 1.2: Schematic representation of the expansion of A β plaques (A β phases)

Figure 1.3: Neurofibrillary tangles in AD patient.

Figure 1.4: Cellular activity of glucocorticoids (GCs)

Figure 1.5: Biphasic effects of glucocorticoids following inverted U-shape curve

Figure 1.6: The genes regulated by glucocorticoids

Figure 1.7: Schematic representation of how glucocorticoids could contribute to central nervous system homeostasis

Figure 1.8: Health claims data from the largest German health insurer AOK

Figure 1.9: Intranasal Budesonide treatment timeline.

Figure 1.10: Inhalation Budesonide treatment timeline.

Figure 1.11: Behavior test plan for intranasal and inhaler treated mice batch

Figure 2.1: InExpose inhalation exposure system

Figure 2.2: InExpose inhalation exposure system tubing layout

Figure 3.1: Budesonide distribution in mice organs after intranasal and inhaler treatment measured by mass spectrometry

Figure 3.2: Budesonide distribution in different regions of mice brain after intranasal and inhaler treatment measured by mass spectrometry.

Figure 3.3: Behavior experiment results summary of 6-month short term inhalation treated female mice.

Figure 3.4: Quantification of A β plaque volume in the cortex of 5xFAD mice upon inhalation Budesonide treatment.

Figure 3.5: Quantification of dense core number and volume of A β plaques, as well as A β 42 volume, in the subiculum upon inhaler Budesonide treatment in 6-month-old female 5xFAD mice.

Figure 3.6: Quantification of Neuronal Markers in 6-Month-Old Female wt and 5xFAD Mice Following short term Inhalation Budesonide Treatment.

Figure 3.7: Quantification of Neurofilament light chain (Nf-L) concentration in the plasma of wt and 5xFAD mice upon short-term inhalation Budesonide treatment.

Figure 3.8: Brain atrophy evaluation in 6-month-old female mice.

Figure 3.9: Quantification of pre- and post- synaptic marker in the CA1 stratum oriens (CA1so) layer of 6 month old female 5xFAD and wt mice upon inhalational Budesonide treatment.

Figure 3.10: Quantification of pre- and post- synaptic marker in the CA1 stratum radiatum (CA1sr) layer of 6 month old female 5xFAD and wt mice upon inhalational Budesonide treatment.

Figure 3.11: Quantification of pre- and post- synaptic marker in the cortex of 6 month old female 5xFAD and wt mice upon inhalational Budesonide treatment.

Figure 3.12: Comparative [18F]MNI1126 PET imaging of synaptic density in wt control, 5xFAD, budesonide treated 5xFAD mice.

Figure 3.13: Analysis of microglial and astrocytic activation in the hippocampus CA1 region of 6-month-old female 5xFAD mice.

Figure 3.14: GFAP concentration quantification from plasma sample.

Figure 3.15: Quantification of homer1 engulfment alternation by microglia and astrocyte upon inhalational Budesonide treatment on female 5xFAD mice.

Figure 3.16: Single-cell RNA sequencing analysis of gene expression in homeostatic microglia from Budesonide treated 5xFAD mice compared to untreated 5xFAD controls.

Figure 3.17: Quantification of complement protein C1q association with synapses in 5xFAD and wt mice and treatment effect upon inhalation Budesonide treatment.

7. List of tables

Table 1.1: Summary of large-scale clinical trials of anti-amyloid passive immunization

Table 2.1: List of consumables and compounds

Table 2.2: Summary of general buffers and solutions

Table 2.3: List of primary antibodies

Table 2.4: List of second antibodies

Table 2.5: Overview of used software

Table 2.6: Overview of used equipment

8. References

Agustí A, De Stefano G, Levi A, et al. Add-on inhaled budesonide in the treatment of hospitalised patients with COVID-19: a randomised clinical trial[J]. *European Respiratory Journal*, 2022, 59(3).

Aksoy-Aksel A, Manahan-Vaughan D. The temporoammonic input to the hippocampal CA1 region displays distinctly different synaptic plasticity compared to the Schaffer collateral input in vivo: significance for synaptic information processing[J]. *Frontiers in synaptic neuroscience*, 2013, 5: 5.

Alzforum. (2023, August 9). Is ARIA an Inflammatory Reaction to Vascular Amyloid? Alzheimer's Association International Conference (AAIC) - 2023. Retrieved from <https://www.alzforum.org/news/conference-coverage/aria-inflammatory-reaction-vascular-amyloid>.

Alzheimer's Association. (2023, July 16). New Alzheimer's diagnostic criteria unveiled at AAIC. Alzheimer's Association International Conference. Retrieved from https://aaic.alz.org/releases_2023/new-alzheimers-diagnostic-criteria-unveiled.asp.

Antolini, L. et al. Spontaneous ARIA-like events in cerebral amyloid angiopathy–related Inflammation: a multicenter prospective longitudinal cohort study. *Neurology* 97, e1809–e1822 (2021).

Bamberger ME, Harris ME, McDonald DR, Husemann J, Landreth GE. A cell surface receptor complex for fibrillar beta-amyloid mediates microglial activation. *J Neurosci*. 2003; 23:2665–74.

Barnes, P. J. (2011). Biochemical basis of asthma therapy. *The Journal of Biological Chemistry*, 286(38), 32899-32905.

Barthélemy, N. R. et al. A soluble phosphorylated tau signature links tau, amyloid and the

evolution of stages of dominantly inherited Alzheimer's disease. *Nat. Med.* 26, 398–407 (2020).

Barton M E, Byrnes W, Mesa I R, et al. Design of a patient-and investigator-blind, randomized, placebo-controlled study to evaluate efficacy, safety, and tolerability of bepranemab, UCB0107, in prodromal to mild Alzheimer's disease: The TOGETHER Study, AH0003[J]. *Alzheimer's & Dementia*, 2021, 17: e057586.

Baruch, K., & Schwartz, M. (2013). CNS-specific T cells shape brain function via the choroid plexus. *Brain, Behavior, and Immunity*, 34, 11-16.

Birks J S, Cochrane Dementia and Cognitive Improvement Group. Cholinesterase inhibitors for Alzheimer's disease[J]. *Cochrane database of systematic reviews*, 1996, 2016(3).

Bloom G S. Amyloid- β and tau: the trigger and bullet in Alzheimer disease pathogenesis[J]. *JAMA neurology*, 2014, 71(4): 505-508.

Braak H, Braak E. Neuropathological staging of Alzheimer-related changes[J]. *Acta neuropathologica*, 1991, 82(4): 239-259.

Braak, H., & Braak, E. (1991). Neuropathological staging of Alzheimer-related changes. *Acta Neuropathologica*, 82(4), 239-259.

Burguillos MA, Deierborg T, Kavanagh E, et al. Caspase signalling controls microglia activation and neurotoxicity. *Nature*. 2011; 472:319–24.

Chan P Y, Silva E A C, De Kouchkovsky D, et al. The TAM family receptor tyrosine kinase TYRO3 is a negative regulator of type 2 immunity[J]. *Science*, 2016, 352(6281): 99-103.

Chandra S, Sisodia S S, Vassar R J. The gut microbiome in Alzheimer's disease: what we know and what remains to be explored[J]. *Molecular neurodegeneration*, 2023, 18(1): 1-21.

Chatterjee P, Vermunt L, Gordon B, et al. Plasma glial fibrillary acidic protein in autosomal dominant Alzheimer's disease: associations with β -amyloid-PET, neurodegeneration and cognition[J]. 2022.

Chen I. A synaptotoxic form of A [beta][J]. *Nature Structural and Molecular Biology*, 2008, 15(8): 785-786.

Choi G E, Han H J. Glucocorticoid impairs mitochondrial quality control in neurons[J]. *Neurobiology of disease*, 2021, 152: 105301.

Cummings J, Lee G, Nahed P, et al. Alzheimer's disease drug development pipeline: 2022[J]. *Alzheimer's & Dementia: Translational Research & Clinical Interventions*, 2022, 8(1): e12295.

Cupidi C, Capobianco R, Goffredo D, et al. Neocortical variation of A β load in fully expressed, pure Alzheimer's disease[J]. *Journal of Alzheimer's Disease*, 2010, 19(1): 57-68.

Da Mesquita S, Papadopoulos Z, Dykstra T, et al. Meningeal lymphatics affect microglia responses and anti-A β immunotherapy[J]. *Nature*, 2021, 593(7858): 255-260.

De Felice E, Gonçalves de Andrade E, Golia M T, et al. Microglial diversity along the hippocampal longitudinal axis impacts synaptic plasticity in adult male mice under homeostatic conditions[J]. *Journal of Neuroinflammation*, 2022, 19(1): 292.

De Kloet C S, Vermetten E, Geuze E, et al. Assessment of HPA-axis function in post-traumatic stress disorder: pharmacological and non-pharmacological challenge tests, a review[J]. *Journal of psychiatric research*, 2006, 40(6): 550-567.

Deacon R M J. Assessing nest building in mice[J]. *Nature protocols*, 2006, 1(3): 1117-1119.

Dejanovic B, Wu T, Tsai M C, et al. Complement C1q-dependent excitatory and inhibitory

synapse elimination by astrocytes and microglia in Alzheimer's disease mouse models[J]. *Nature Aging*, 2022, 2(9): 837-850.

Delaby C, Teunissen C E, Blennow K, et al. Clinical reporting following the quantification of cerebrospinal fluid biomarkers in Alzheimer's disease: An international overview[J]. *Alzheimer's & Dementia*, 2022, 18(10): 1868-1879.

DeTure, M.A., Dickson, D.W. The neuropathological diagnosis of Alzheimer's disease. *Mol Neurodegeneration* 14, 32 (2019). <https://doi.org/10.1186/s13024-019-0333-5>

Dhuria S V, Hanson L R, Frey II W H. Intranasal delivery to the central nervous system: mechanisms and experimental considerations[J]. *Journal of pharmaceutical sciences*, 2010, 99(4): 1654-1673.

Dhuria S V, Hanson L R, Frey II W H. Intranasal delivery to the central nervous system: mechanisms and experimental considerations[J]. *Journal of pharmaceutical sciences*, 2010, 99(4): 1654-1673.

Diamond D M, Campbell A M, Park C R, et al. The temporal dynamics model of emotional memory processing: a synthesis on the neurobiological basis of stress-induced amnesia, flashbulb and traumatic memories, and the Yerkes-Dodson law[J]. *Neural plasticity*, 2007.

Diaz-Aparicio I, Paris I, Sierra-Torre V, et al. Microglia actively remodel adult hippocampal neurogenesis through the phagocytosis secretome[J]. *Journal of Neuroscience*, 2020, 40(7): 1453-1482.

Diaz-Jimenez D, Kolb J P, Cidlowski J A. Glucocorticoids as regulators of macrophage-mediated tissue homeostasis[J]. *Frontiers in immunology*, 2021, 12: 669891.

Dulewicz M, Kulczyńska-Przybik A, Mroczko P, et al. Biomarkers for the diagnosis of Alzheimer's disease in clinical practice: The role of CSF biomarkers during the evolution of diagnostic criteria[J]. *International Journal of Molecular Sciences*, 2022, 23(15): 8598.

Eisenhauer PB, Johnson RJ, Wells JM, Davies TA, Fine RE. Toxicity of various amyloid beta peptide species in cultured human blood-brain barrier endothelial cells: increased toxicity of Dutch-type mutant. *J Neurosci Res*. 2000; 60(6): 804-810.

Fardet L, Flahault A, Kettaneh A, et al. Corticosteroid-induced clinical adverse events: frequency, risk factors and patient's opinion[J]. *British Journal of Dermatology*, 2007, 157(1): 142-148.

Fischer H J, Finck T L K, Pellkofer H L, et al. Glucocorticoid therapy of multiple sclerosis patients induces anti-inflammatory polarization and increased chemotaxis of monocytes[J]. *Frontiers in immunology*, 2019, 10: 1200.

Fourgeaud L, Través P G, Tufail Y, et al. TAM receptors regulate multiple features of microglial physiology[J]. *Nature*, 2016, 532(7598): 240-244.

Freiherr J, Hallschmid M, Frey W H, et al. Intranasal insulin as a treatment for Alzheimer's disease: a review of basic research and clinical evidence[J]. *CNS drugs*, 2013, 27: 505-514.

Gate D, Saligrama N, Leventhal O, Yang AC, Unger MS, Middeldorp J, Chen K, Lehallier B, Channappa D, De Los Santos MB, McBride A, Pluvinaige J, Elahi F, Tam GK, Kim Y, Greicius M, Wagner AD, Aigner L, Galasko DR, Davis MM, Wyss-Coray T. (2020). Clonally expanded CD8 T cells patrol the cerebrospinal fluid in Alzheimer's disease. *Nature*. 577(7790):399-404.

Gray J D, Kogan J F, Marrocco J, et al. Genomic and epigenomic mechanisms of glucocorticoids in the brain[J]. *Nature Reviews Endocrinology*, 2017, 13(11): 661-673.

Greicius M D, Srivastava G, Reiss A L, et al. Default-mode network activity distinguishes Alzheimer's disease from healthy aging: evidence from functional MRI[J]. *Proceedings of the National Academy of Sciences*, 2004, 101(13): 4637-4642.

Grundke-Iqbal I, Iqbal K, Tung Y C, et al. Abnormal phosphorylation of the microtubule-associated protein tau (tau) in Alzheimer cytoskeletal pathology[J]. Proceedings of the National Academy of Sciences, 1986, 83(13): 4913-4917.

Gulyaeva N V. Glucocorticoid regulation of the glutamatergic synapse: mechanisms of stress-dependent neuroplasticity[J]. Journal of Evolutionary Biochemistry and Physiology, 2021, 57(3): 564-576.

Gulyaeva N V. Glucocorticoids orchestrate adult hippocampal plasticity: growth points and translational aspects[J]. Biochemistry (Moscow), 2023, 88(5): 565-589.

Haass C, Kaether C, Thinakaran G, et al. Trafficking and proteolytic processing of APP[J]. Cold Spring Harbor perspectives in medicine, 2012, 2(5).

Halliday, Matthew R., et al. "Accelerated pericyte degeneration and blood–brain barrier breakdown in apolipoprotein E4 carriers with Alzheimer's disease." Journal of Cerebral Blood Flow & Metabolism 36.1 (2016): 216-227.

Hanisch U K, Kettenmann H. Microglia: active sensor and versatile effector cells in the normal and pathologic brain[J]. Nature neuroscience, 2007, 10(11): 1387-1394.

Hardy J A, Higgins G A. Alzheimer's disease: the amyloid cascade hypothesis[J]. Science, 1992, 256(5054): 184-185.

Hardy J, Selkoe D J. The amyloid hypothesis of Alzheimer's disease: progress and problems on the road to therapeutics[J]. science, 2002, 297(5580): 353-356.

Hauser P S, Narayanaswami V, Ryan R O. Apolipoprotein E: from lipid transport to neurobiology[J]. Progress in lipid research, 2011, 50(1): 62-74.

Hench P. Effects of cortisone in the rheumatic diseases[J]. Lancet (London, England), 1950, 2(6634): 483-484.

Heneka M T, Carson M J, El Khoury J, et al. Neuroinflammation in Alzheimer's disease[J]. *The Lancet Neurology*, 2015, 14(4): 388-405.

Heneka M T, McManus R M, Latz E. Inflammasome signalling in brain function and neurodegenerative disease[J]. *Nature Reviews Neuroscience*, 2018, 19(10): 610-621.

Höglinger G U, Litvan I, Mendonca N, et al. Safety and efficacy of tilavonemab in progressive supranuclear palsy: a phase 2, randomised, placebo-controlled trial[J]. *The Lancet Neurology*, 2021, 20(3): 182-192.

Hong S, Beja-Glasser V F, Nfonoyim B M, et al. Complement and microglia mediate early synapse loss in Alzheimer mouse models[J]. *Science*, 2016, 352(6286): 712-716.

Hua C, Buttgereit F, Combe B. Glucocorticoids in rheumatoid arthritis: current status and future studies[J]. *RMD open*, 2020, 6(1): e000536.

Huang Y W A, Zhou B, Wernig M, et al. ApoE2, ApoE3, and ApoE4 differentially stimulate APP transcription and A β secretion[J]. *Cell*, 2017, 168(3): 427-441. e21.

Huang Y, Happonen K E, Burrola P G, et al. Microglia use TAM receptors to detect and engulf amyloid β plaques[J]. *Nature immunology*, 2021, 22(5): 586-594.

Iliyasu M O, Musa S A, Oladele S B, et al. Amyloid-beta aggregation implicates multiple pathways in Alzheimer's disease: Understanding the mechanisms[J]. *Frontiers in neuroscience*, 2023, 17: 1081938.

Iqbal K, Liu F, Gong C X, et al. Tau in Alzheimer disease and related tauopathies[J]. *Current Alzheimer Research*, 2010, 7(8): 656-664.

Jack Jr C R, Andrews J S, Beach T G, et al. Revised criteria for diagnosis and staging of Alzheimer's disease: Alzheimer's Association Workgroup[J]. *Alzheimer's & Dementia*, 2024.

Jawhar, S., Trawicka, A., Jenneckens, C., Bayer, T. A., & Wirths, O. (2012). Motor deficits, neuron loss, and reduced anxiety coinciding with axonal degeneration and intraneuronal A β aggregation in the 5XFAD mouse model of Alzheimer's disease. *Neurobiology of Aging*, 33(1), 196.e29-40.

Jevtovic-Todorovic, V., Absalom, A. R., Blomgren, K., Brambrink, A., Crosby, G., Culley, D. J., ... & Ikonomidou, C. (2013). Anaesthetic neurotoxicity and neuroplasticity: an expert group report and statement based on the BJA Salzburg Seminar. *British Journal of Anaesthesia*, 111(2), 143-151.

Jiménez-García L, Mayer C, Burrola P G, et al. The TAM receptor tyrosine kinases Axl and Mer drive the maintenance of highly phagocytic macrophages[J]. *Frontiers in Immunology*, 2022, 13: 960401.

Keren-Shaul H, Spinrad A, Weiner A, et al. A unique microglia type associated with restricting development of Alzheimer's disease[J]. *Cell*, 2017, 169(7): 1276-1290. e17.

Khalil M, Teunissen C E, Otto M, et al. Neurofilaments as biomarkers in neurological disorders[J]. *Nature Reviews Neurology*, 2018, 14(10): 577-589.

Knezevic E, Nenic K, Milanovic V, et al. The Role of Cortisol in Chronic Stress, Neurodegenerative Diseases, and Psychological Disorders[J]. *Cells*, 2023, 12(23): 2726

Labzin, L. I., Heneka, M. T., & Latz, E. (2018). Innate immunity and neurodegeneration. *Annual Review of Medicine*, 69, 437-449.

Lee CYD, Landreth GE. The role of microglia in amyloid clearance from the AD brain. *J Neural Transm*. 2010; 117:949–60.

Lee V M Y, Goedert M, Trojanowski J Q. Neurodegenerative tauopathies[J]. *Annual review of neuroscience*, 2001, 24(1): 1121-1159.

Lemke G, Burstyn-Cohen T. TAM receptors and the clearance of apoptotic cells[J]. *An-*

nals of the New York Academy of Sciences, 2010, 1209(1): 23-29.

Li Y, Schindler S E, Bollinger J G, et al. Validation of plasma amyloid- β 42/40 for detecting Alzheimer disease amyloid plaques[J]. *Neurology*, 2022, 98(7): e688-e699.

Liddel S A, Guttenplan K A, Clarke L E, et al. Neurotoxic reactive astrocytes are induced by activated microglia[J]. *Nature*, 2017, 541(7638): 481-487.

Lilly E. Donanemab Significantly Slowed Cognitive and Functional Decline in Phase 3 Study of Early Alzheimer's Disease[J]. Press release, 2023.

Liu Y, Walter S, Stagi M, et al. LPS receptor (CD14): a receptor for phagocytosis of Alzheimer's amyloid peptide. *Brain*. 2005; 128:1778–89.

Lue L F, Schmitz C T, Serrano G, et al. TREM 2 Protein Expression Changes Correlate with Alzheimer's Disease Neurodegenerative Pathologies in Post-Mortem Temporal Cortices[J]. *Brain pathology*, 2015, 25(4): 469-480.

Lui, H., Zhang, J., Makinson, S. R., Cahill, M. K., Kelley, K. W., Huang, H. Y., ... & Akama-Garren, E. H. (2016). Progranulin deficiency promotes circuit-specific synaptic pruning by microglia via complement activation. *Cell*, 165(4), 921-935.

Lupien S J, De Leon M, De Santi S, et al. Cortisol levels during human aging predict hippocampal atrophy and memory deficits[J]. *Nature neuroscience*, 1998, 1(1): 69-73.

Mawuenyega KG, Sigurdson W, Ovod V, et al. Decreased Clearance of CNS β -Amyloid in Alzheimer's Disease. *Science*. 2010; 330:1774–1774.

McAlpine C S, Park J, Griciuc A, et al. Astrocytic interleukin-3 programs microglia and limits Alzheimer's disease[J]. *Nature*, 2021, 595(7869): 701-706.

Mejía-Vilet J M, Ayoub I. The use of glucocorticoids in lupus nephritis: new pathways for an old drug[J]. *Frontiers in medicine*, 2021, 8: 622225.

Mitra R., Sapolsky R.M. (2008) Acute corticosterone treatment is sufficient to induce anxiety and amygdaloid dendritic hypertrophy. *Proc Natl Sci USA*. 105:5573-8.

Mohamed N V, Herrou T, Plouffe V, et al. Spreading of tau pathology in Alzheimer's disease by cell-to-cell transmission[J]. *European Journal of Neuroscience*, 2013, 37(12): 1939-1948.

Morales I, Farias G, Maccioni R.B. *Neuroimmunomodulation* 2010; 17: 202- 204.

Morioka S, Kajioaka D, Yamaoka Y, et al. Chimeric efferocytic receptors improve apoptotic cell clearance and alleviate inflammation[J]. *Cell*, 2022, 185(26): 4887-4903. e17.

Mullard A. FDA approves third anti-amyloid antibody for Alzheimer disease[J]. *Nature reviews. Drug discovery*, 2024.

Mummery C J, Börjesson-Hanson A, Blackburn D J, et al. Tau-targeting antisense oligonucleotide MAPTRx in mild Alzheimer's disease: a phase 1b, randomized, placebo-controlled trial[J]. *Nature medicine*, 2023, 29(6): 1437-1447.

Neher J J, Emmrich J V, Fricker M, et al. Phagocytosis executes delayed neuronal death after focal brain ischemia[J]. *Proceedings of the National Academy of Sciences*, 2013, 110(43): E4098-E4107.

Nelson, Peter T., et al. "Correlation of Alzheimer disease neuropathologic changes with cognitive status: a review of the literature." *Journal of Neuropathology & Experimental Neurology* 71.5 (2012): 362-381.

Nerius M, Haenisch B, Gomm W, et al. Glucocorticoid therapy is associated with a lower risk of dementia[J]. *Journal of Alzheimer's Disease*, 2020, 73(1): 175-183.

Neumann H, Kotter M R, Franklin R J M. Debris clearance by microglia: an essential link between degeneration and regeneration[J]. *Brain*, 2009, 132(2): 288-295.

Nilsberth C, Westlind-Danielsson A, Eckman C B, et al. The 'Arctic' APP mutation (E693G) causes Alzheimer's disease by enhanced A β protofibril formation[J]. *Nature neuroscience*, 2001, 4(9): 887-893.

Noetzelin S, Breville G, Seebach J D, et al. Short-term glucocorticoid-related side effects and adverse reactions: a narrative review and practical approach[J]. *Swiss Medical Weekly*, 2022, 152(0102): w30088-w30088.

Novak P, Kovacech B, Katina S, et al. ADAMANT: a placebo-controlled randomized phase 2 study of AADvac1, an active immunotherapy against pathological tau in Alzheimer's disease[J]. *Nature aging*, 2021, 1(6): 521-534.

O'Leary T P, Brown R E. Visuo-spatial learning and memory deficits on the Barnes maze in the 16-month-old APPswe/PS1dE9 mouse model of Alzheimer's disease[J]. *Behavioural brain research*, 2009, 201(1): 120-127.

Oakley H, Cole S L, Logan S, et al. Intraneuronal β -amyloid aggregates, neurodegeneration, and neuron loss in transgenic mice with five familial Alzheimer's disease mutations: potential factors in amyloid plaque formation[J]. *Journal of Neuroscience*, 2006, 26(40): 10129-10140.

Ouanes S, Popp J. High cortisol and the risk of dementia and Alzheimer's disease: a review of the literature[J]. *Frontiers in aging neuroscience*, 2019, 11: 43.

Palop J J, Mucke L. Synaptic depression and aberrant excitatory network activity in Alzheimer's disease: two faces of the same coin?[J]. *Neuromolecular medicine*, 2010, 12: 48-55.

Pardridge W M. Drug transport across the blood-brain barrier[J]. *Journal of cerebral blood flow & metabolism*, 2012, 32(11): 1959-1972.

Paresce DM, Ghosh RN, Maxfield FR. Microglial cells internalize aggregates of the Alz-

heimer's disease amyloid beta-protein via a scavenger receptor. *Neuron*. 1996; 17:553–65.

Pike C J, Carroll J C, Rosario E R, et al. Protective actions of sex steroid hormones in Alzheimer's disease[J]. *Frontiers in neuroendocrinology*, 2009, 30(2): 239-258.

Raina P, Santaguida P, Ismaila A, et al. Effectiveness of cholinesterase inhibitors and memantine for treating dementia: evidence review for a clinical practice guideline[J]. *Annals of internal medicine*, 2008, 148(5): 379-397.

Rawal S, Yagi T, Boyd P, et al. Safety, Pharmacokinetics and Immunogenicity of Single and Multiple Ascending Doses of the Anti-Tau Therapeutic Antibody E2814: A Phase 1, First-In-Human (FIH) Study in Healthy Subjects[J]. *Alzheimer's & Dementia*, 2023, 19: e082752.

Reardon S. Alzheimer's drug donanemab: what promising trial means for treatments[J]. *Nature*, 2023, 617(7960): 232-233.

Reisberg B, Doody R, Stöffler A, et al. Memantine in moderate-to-severe Alzheimer's disease[J]. *New England Journal of Medicine*, 2003, 348(14): 1333-1341.

Reitz, C., and Mayeux, R. (2014). Alzheimer disease: Epidemiology, Diagnostic Criteria, Risk Factors and Biomarkers. *Biochemical pharmacology* 88, 640-651.

Ros-Bernal F, Hunot S, Herrero M T, et al. Microglial glucocorticoid receptors play a pivotal role in regulating dopaminergic neurodegeneration in parkinsonism[J]. *Proceedings of the National Academy of Sciences*, 2011, 108(16): 6632-6637.

Salvador E, Shityakov S, Förster C. Glucocorticoids and endothelial cell barrier function[J]. *Cell and tissue research*, 2014, 355: 597-605.

Sasaguri H, Nilsson P, Hashimoto S, et al. APP mouse models for Alzheimer's disease preclinical studies[J]. *The EMBO journal*, 2017, 36(17): 2473-2487.

Schaefer P W, Grant P E, Gonzalez R G. Diffusion-weighted MR imaging of the brain[J]. Radiology, 2000, 217(2): 331-345.

Scheimann J R, Mahbod P, Morano R, et al. Deletion of glucocorticoid receptors in fore-brain GABAergic neurons alters acute stress responding and passive avoidance behavior in female mice[J]. Frontiers in behavioral neuroscience, 2018, 12: 325.

Scheltens, P., Blennow, K., Breteler, M. M. B., de Strooper, B., Frisoni, G. B., Salloway, S., & Van der Flier, W. M. (2016). Alzheimer's disease. The Lancet, 388(10043), 505–517.

Schlepckow K, Monroe K M, Kleinberger G, et al. Enhancing protective microglial activities with a dual function TREM 2 antibody to the stalk region[J]. EMBO molecular medicine, 2020, 12(4): e11227.

Schweingruber N, Reichardt S D, Lühder F, et al. Mechanisms of glucocorticoids in the control of neuroinflammation[J]. Journal of neuroendocrinology, 2012, 24(1): 174-182.

Selkoe D J, Hardy J. The amyloid hypothesis of Alzheimer's disease at 25 years[J]. EMBO molecular medicine, 2016, 8(6): 595-608.

Selkoe D J. Alzheimer's disease is a synaptic failure[J]. Science, 2002, 298(5594): 789-791.

Selkoe D J. Soluble oligomers of the amyloid β -protein impair synaptic plasticity and behavior[J]. Behavioural brain research, 2008, 192(1): 106-113.

Selkoe, D.J. (2001). Alzheimer's disease: genes, proteins, and therapy. Physiological reviews 81, 741-766.

Seo N, Kim G H, Noh J E, et al. Selective regional loss of cortical synapses lacking pre-synaptic mitochondria in the 5xFAD mouse model[J]. Frontiers in Neuroanatomy, 2021, 15: 690168.

Shimba A, Ikuta K. Glucocorticoids regulate circadian rhythm of innate and adaptive immunity[J]. *Frontiers in immunology*, 2020, 11: 2143.

Shin J, Park S, Lee H Y, et al. Thioflavin-positive tau aggregates complicating quantification of amyloid plaques in the brain of 5XFAD transgenic mouse model[J]. *Scientific reports*, 2021, 11(1): 1617.

Shorey C L, Mulla R T, Mielke J G. The effects of synthetic glucocorticoid treatment for inflammatory disease on brain structure, function, and dementia outcomes: A systematic review[J]. *Brain Research*, 2023, 1798: 148157.

Shulman M, Kong J, O’Gorman J, et al. TANGO: a placebo-controlled randomized phase 2 study of efficacy and safety of the anti-tau monoclonal antibody gosuranemab in early Alzheimer’s disease[J]. *Nature Aging*, 2023, 3(12): 1591-1601.

Siller N, Kuhle J, Muthuraman M, et al. Serum neurofilament light chain is a biomarker of acute and chronic neuronal damage in early multiple sclerosis[J]. *Multiple Sclerosis Journal*, 2019, 25(5): 678-686.

Smit T, Deshayes N A C, Borchelt D R, et al. Reactive astrocytes as treatment targets in Alzheimer's disease—Systematic review of studies using the APPswePS1dE9 mouse model[J]. *Glia*, 2021, 69(8): 1852-1881.

Spiga F, Walker J J, Terry J R, et al. HPA axis-rhythms[J]. *Comprehensive physiology*, 2011, 4(3): 1273-1298.

Spires-Jones T L, Hyman B T. The intersection of amyloid beta and tau at synapses in Alzheimer’s disease[J]. *Neuron*, 2014, 82(4): 756-771.

Stevens, B., Allen, N. J., Vazquez, L. E., Howell, G. R., Christopherson, K. S., Nouri, N., ... & Barres, B. A. (2007). The classical complement cascade mediates CNS synapse elimination. *Cell*, 131(6), 1164-1178.

Stewart CR, Stuart LM, Wilkinson K, et al. CD36 ligands promote sterile inflammation through assembly of a Toll-like receptor 4 and 6 heterodimer. *Nat Immunol.* 2010; 11:155–61.

Suárez-Calvet, M. et al. Novel tau biomarkers phosphorylated at T181, T217 or T231 rise in the initial stages of the preclinical Alzheimer's continuum when only subtle changes in A β pathology are detected. *EMBO Mol. Med.* 12, e12921 (2020).

Tariot P N, Farlow M R, Grossberg G T, et al. Memantine treatment in patients with moderate to severe Alzheimer disease already receiving donepezil: a randomized controlled trial[J]. *Jama*, 2004, 291(3): 317-324.

TauRx. (2023). Initial data of LUCIDITY study. Retrieved from <https://taurx.com/news-insights/initial-data-of-lucidity-study>

Teng E, Manser P T, Pickthorn K, et al. Safety and efficacy of semorinemab in individuals with prodromal to mild Alzheimer disease: a randomized clinical trial[J]. *JAMA neurology*, 2022, 79(8): 758-767.

Terry, R. D., Masliah, E., Salmon, D. P., Butters, N., DeTeresa, R., Hill, R., Hansen, L. A., & Katzman, R. (1991). Physical basis of cognitive alterations in Alzheimer's disease: synapse loss is the major correlate of cognitive impairment. *Annals of Neurology*, 30(4), 572-580. doi:10.1002/ana.410300410

Terwel D, Steffensen KR, Verghese PB, et al. Critical role of astroglial apolipoprotein E and liver \times receptor- α expression for microglial A β phagocytosis. *J Neurosci.* 2011; 31:7049–59.

Timmermans S, Souffriau J, Libert C. A general introduction to glucocorticoid biology[J]. *Frontiers in immunology*, 2019, 10: 1545.

Tong R. AAIC 2023: Blood Tests for Detecting Alzheimer Disease Show Promise[J].

Blood, 2023.

U.S. Food and Drug Administration. (2023, July 13). FDA converts novel Alzheimer's disease treatment to traditional approval. Retrieved from <https://www.fda.gov/news-events/press-announcements/fda-converts-novel-alzheimers-disease-treatment-traditional-approval>

Ulrich J D, Ulland T K, Mahan T E, et al. ApoE facilitates the microglial response to amyloid plaque pathology[J]. Journal of Experimental Medicine, 2018, 215(4): 1047-1058.

Umoh V A. Chronic Obstructive Pulmonary Disease (COPD): A Review of the Clinical Management[J]. Nigerian Health Journal, 2013, 13(1): 7-17.

Unger, Michael Stefan, et al. "CD8+ T-cells infiltrate Alzheimer's disease brains and regulate neuronal-and synapse-related gene expression in APP-PS1 transgenic mice." Brain, Behavior, and Immunity 89 (2020): 67-86.

Van Dyck C H, Swanson C J, Aisen P, et al. Lecanemab in early Alzheimer's disease[J]. New England Journal of Medicine, 2023, 388(1): 9-21.

Van Dyck C H, Tariot P N, Meyers B, et al. A 24-week randomized, controlled trial of memantine in patients with moderate-to-severe Alzheimer disease[J]. Alzheimer Disease & Associated Disorders, 2007, 21(2): 136-143.

Vandevyver, S., Dejager, L., Tuckermann, J., & Libert, C. (2013). New insights into the anti-inflammatory mechanisms of glucocorticoids: An emerging role for glucocorticoid-receptor-mediated transactivation. Endocrinology, 154(3), 993-1007.

Varesi A, Carrara A, Pires V G, et al. Blood-based biomarkers for Alzheimer's disease diagnosis and progression: an overview[J]. Cells, 2022, 11(8): 1367.

Vermunt L, Sikkes S A M, Van Den Hout A, et al. Duration of preclinical, prodromal, and dementia stages of Alzheimer's disease in relation to age, sex, and APOE genotype[J].

Alzheimer's & Dementia, 2019, 15(7): 888-898.

Viho E M G, Buurstede J C, Mahfouz A, et al. Corticosteroid action in the brain: the potential of selective receptor modulation[J]. Neuroendocrinology, 2019, 109(3): 266-276.

Walker L C. A β plaques[J]. Free neuropathology, 2020, 1.

Wang S, Mustafa M, Yuede C M, et al. Anti-human TREM2 induces microglia proliferation and reduces pathology in an Alzheimer's disease model[J]. Journal of Experimental Medicine, 2020, 217(9): e20200785.

Wang X, Su B, Zheng L, et al. The role of abnormal mitochondrial dynamics in the pathogenesis of Alzheimer's disease[J]. Journal of neurochemistry, 2009, 109: 153-159.

Wang Y, Mandelkow E. Tau in physiology and pathology[J]. Nature reviews neuroscience, 2016, 17(1): 22-35.

Wang Z, Meng S, Cao L, et al. Critical role of NLRP3-caspase-1 pathway in age-dependent isoflurane-induced microglial inflammatory response and cognitive impairment[J]. Journal of neuroinflammation, 2018, 15: 1-12.

Warburton E C, Brown M W. Neural circuitry for rat recognition memory[J]. Behavioural brain research, 2015, 285: 131-139.

Whitwell, Jennifer L. "Progression of atrophy in Alzheimer's disease and related disorders." Neurotoxicity research 18.3-4 (2010): 339-346.

Williams S, Ghosh C. Neurovascular glucocorticoid receptors and glucocorticoids: implications in health, neurological disorders and drug therapy[J]. Drug discovery today, 2020, 25(1): 89-106.

Wisniewski, H.M., Ghetti, B., and Terry, R.D. (1973). Neuritic (senile) plaques and filamentous changes in aged rhesus monkeys. Journal of neuropathology and experimental

neurology 32, 566-584.

Wolfe C M, Fitz N F, Nam K N, et al. The role of APOE and TREM2 in Alzheimer' s disease—current understanding and perspectives[J]. International journal of molecular sciences, 2018, 20(1): 81.

Wong W. Economic burden of Alzheimer disease and managed care considerations[J]. The American journal of managed care, 2020, 26(8 Suppl): S177-S183.

World Health Organization. Ageing and health. <https://www.who.int/news-room/fact-sheets/detail/ageing-and-health> (2022).

Wu, T. et al. Complement C3 is activated in human AD brain and is required for neurodegeneration in mouse models of amyloidosis and tauopathy. Cell Rep. 28, 2111–2123 (2019).

Xia M X, Ding X, Qi J, et al. Inhaled budesonide protects against chronic asthma-induced neuroinflammation in mouse brain[J]. Journal of neuroimmunology, 2014, 273(1-2): 53-57.

Xie, Z., Dong, Y., Maeda, U., Alfille, P., Culley, D. J., Crosby, G., & Tanzi, R. E. (2006). The common inhalation anesthetic isoflurane induces apoptosis and increases amyloid β protein levels. Anesthesiology, 104(5), 988-994.

Xu Y, Yang Y, Chen X, et al. NLRP3 inflammasome in cognitive impairment and pharmacological properties of its inhibitors[J]. Translational Neurodegeneration, 2023, 12(1): 49.

Yang R, Yu Y. Glucocorticoids are double-edged sword in the treatment of COVID-19 and cancers[J]. International journal of biological sciences, 2021, 17(6): 1530.

Zlokovic B V. The blood-brain barrier in health and chronic neurodegenerative disorders[J]. Neuron, 2008, 57(2): 178-201.

8. Supplement

Effects of intranasal Budesonide treatment in the 5xFAD mouse model of AD.

S1. Effect of intranasal Budesonide treatment in the cognition of 5xFAD mouse model of AD

After long-term intranasal Budesonide treatment (from 1.5 to 6 months old), female 5xFAD mice did not exhibit impairment in the alternatig Y-maze. No differences were observed among the four treatment groups. In the novel object recognition test, female 5xFAD animals showed a trend of impairment compared to wt control animals. With intranasal Budesonide treatment, 5xFAD mice performed significantly better compared to sham treated 5xFAD, spending more time exploring the novel object. In the Barnes maze, a similar pattern was observed: female 5xFAD animals showed a trend of impairment compared to wt control animals, which was significantly mitigated by intranasal Budesonide treatment, as evidenced by more time spent in the target zone during the probe trail. (**Figure S1**)

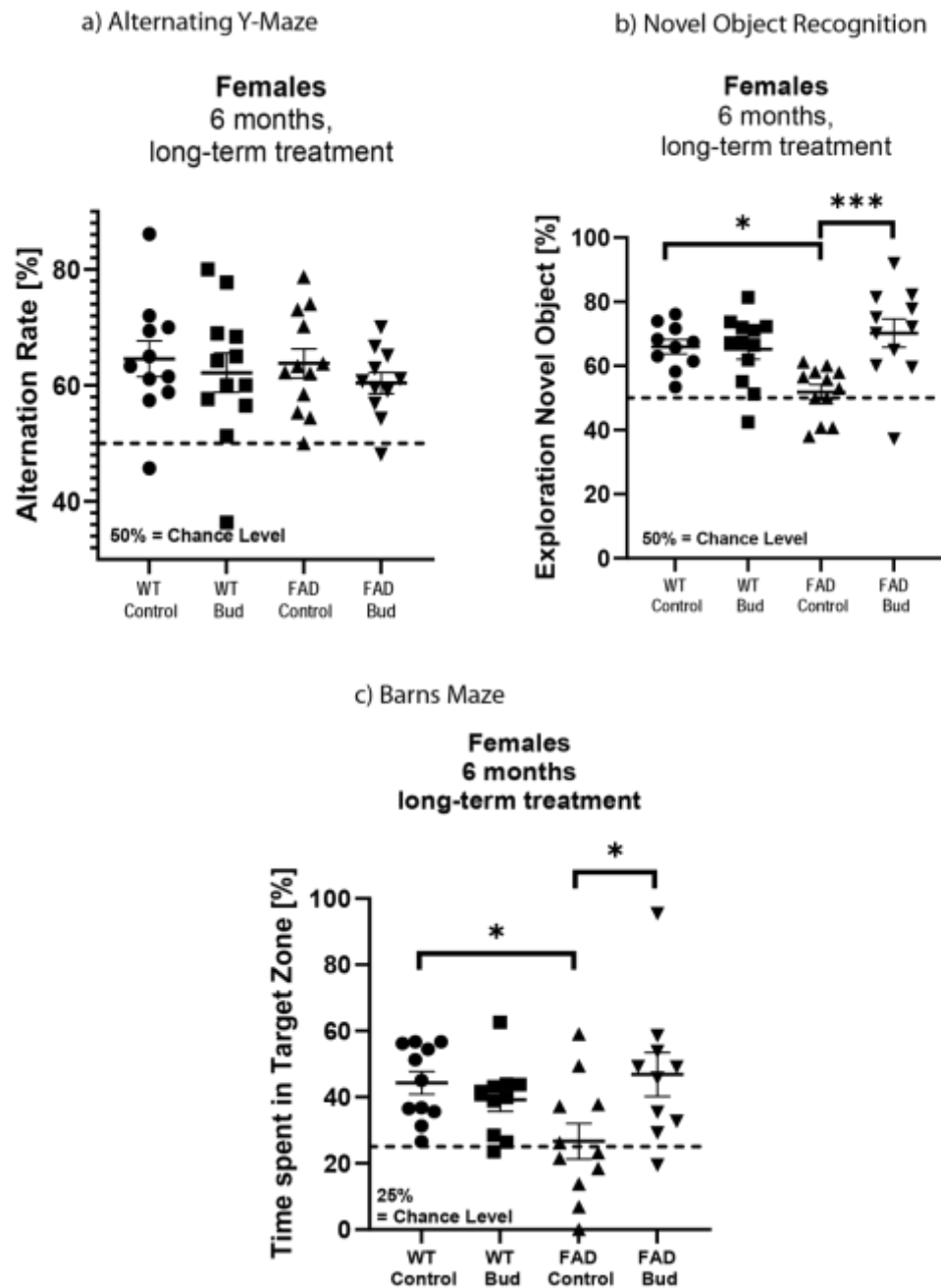


Figure S1: Behavior experiment results summary of 6 month long-term intranasal Budesonide treated female mice. a) Alternation rate analysis of alternating Y-maze. b) Percentage of time mice explore novel object in novel object recognition test. c) Percentage of time spent in the target zone during the test trail of Barnes maze. Data are presented as mean \pm SEM; ordinary one-way ANOVA followed by Sidak's multiple comparisons test, * $p \leq 0.05$.

S2. Effect of intranasal Budesonide treatment on amyloid pathology of 5xFAD mouse model of AD

To investigate the effect of intranasal Budesonide treatment on amyloid pathology in 5xFAD mice, female mice were treated from 1.5 months to 6 months of age. After behavioral testing, the mice were sacrificed at 6 months old. Since the cortex and hippocampus are brain regions affected early in the 5xFAD mouse model by amyloid pathology, the prefrontal cortex, CA1, subiculum, and entorhinal cortex were analyzed using immunohistochemistry staining with the 6E10 antibody, which specifically binds to amino acid residues 1-16 of the beta-amyloid peptide, a major component of amyloid plaques in Alzheimer's disease

The number of 6E10-positive plaques per region of interest (ROI) did not show significant differences in the prefrontal cortex, subiculum, and entorhinal cortex, but there was a trend towards a reduction in the CA1 region of Budesonide-treated 5xFAD mice compared to the untreated group. Additionally, the total area of 6E10-positive staining per ROI was quantified, revealing no significant effect of Budesonide treatment in any of the four regions analyzed (**Figure S2**).

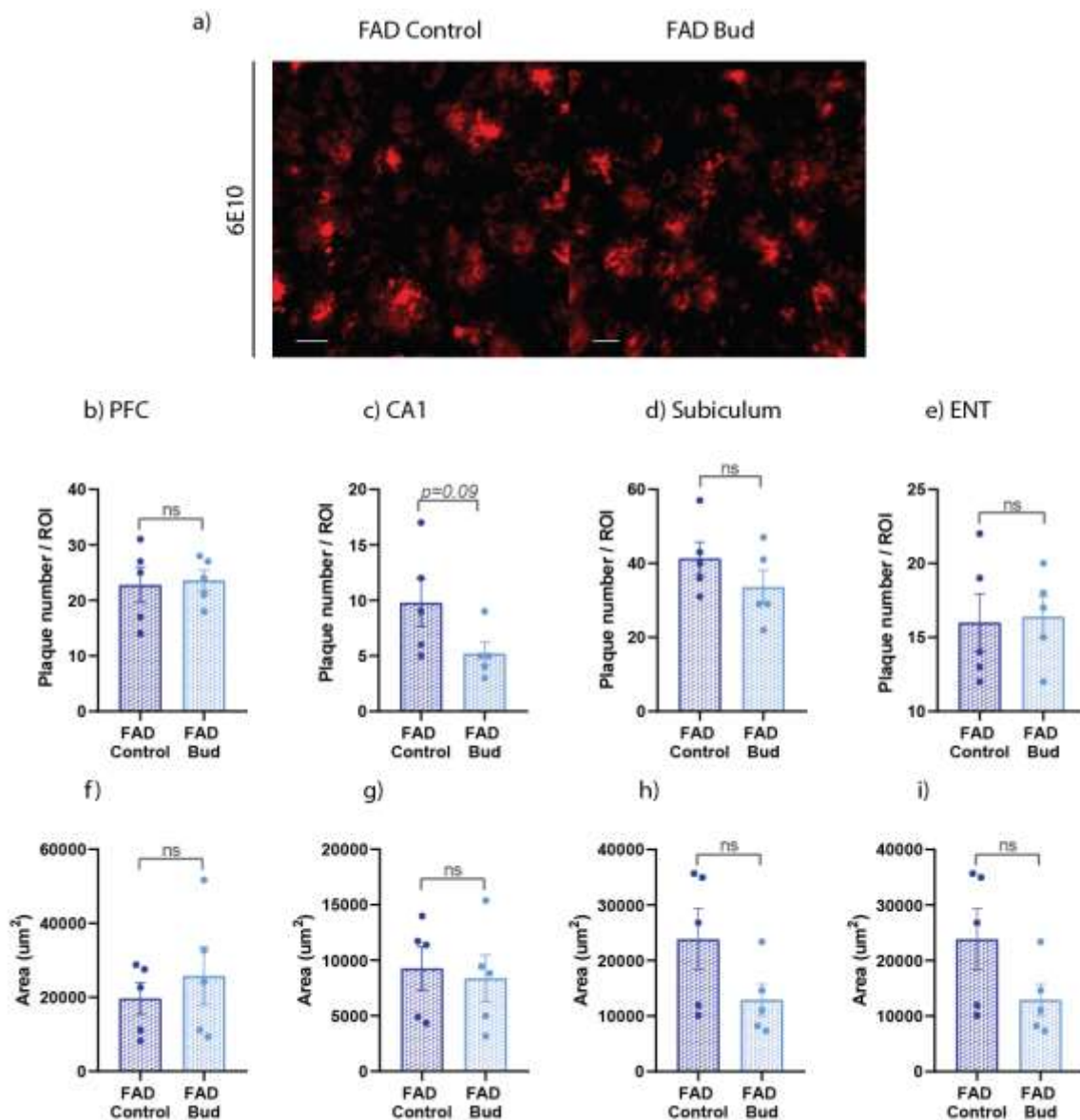


Figure S2: Long term Intranasal Budesonide treatment effect on amyloid pathology of female 5xFAD mouse model of AD.

a) Example image of 6E10 immunohistochemistry staining on brain sections of 6 month old Budesonide treated and control 5xFAD mouse model. Example image was taken from subiculum. Scale bar: 20 μm . b-e) Quantification of 6E10 positive plaque numbers in prefrontal cortex (PFC, b), CA1 (c), subiculum (d) and entorhinal cortex (e). f-i) Quantification of 6E10 positive plaque area in prefrontal cortex (PFC, f), CA1 (g), subiculum (h) and entorhinal cortex (i). For both analyses $n=5$ animals two hemispheres from each

animal was included. Data are presented as mean \pm SEM from t test.

S3 Effect of intranasal Budesonide treatment on neurodegeneration development of 5xFAD mouse model of AD.

Since Budesonide treated 5xFAD mice showed a significant improved performance in several behavior tests. Next we wanted to elucidate whether Budesonide has treatment effect on neurodegeneration development of 5xFAD mice. One of the most prominent hallmarks of AD is neuronal loss in hippocampus. Therefore we quantified neuronal numbers by immunohistochemistry of NeuN antibody at subiculum of our mouse model.

S3.1 Neuronal loss was not reduced upon long term intranasal Budesonide treatment

By 6 months of age, female 5xFAD mice reveal a significant loss of neurons (50%) in the subiculum region of hippocampus compare to wt mice, female 5xFAD mice received intranasal Budesonide treatment from 1.5 to 5 months did not show significant altered neuronal loss, no different was seen for wt mice received same treatment. (**Figure S3**)

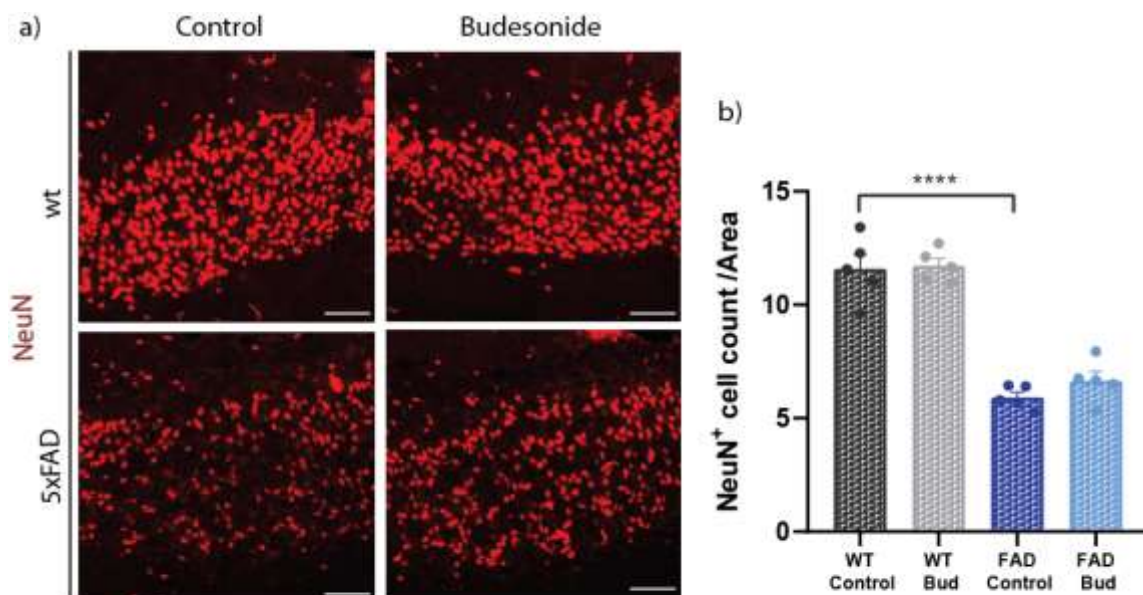


Figure S3: Long term intranasal Budesonide treatment effect on neuronal loss of 5xFAD mice at 6 month.

a) Representative images of 6 month old female mice subiculum stained for NeuN (red). Scale bar = 50 μ m. b) Neuronal loss quantified in subiculum of 6 month female mice. N=5. Data are presented as mean \pm SEM; ordinary one-way ANOVA followed by Sidak's multiple comparisons test, ****p \leq 0.0001.

S3.2 Neurofilament light chain (NfL) was not reduced upon long term intranasal Budesonide treatment

To further analyze effect of intranasal Budesonide treatment on neuronal and axonal damage of 5xFAD mouse model, NfL concentration was detected from plasma sample.

By 6 months of age, plasma of female 5xFAD mice showed significant higher concentration of NfL compare to wt mice, female 5xFAD mice received intranasal Budesonide treatment from 1.5 to 5 months did not show significant altered NfL concentration, also no different was seen for wt mice received same treatment. (**Figure S4**)

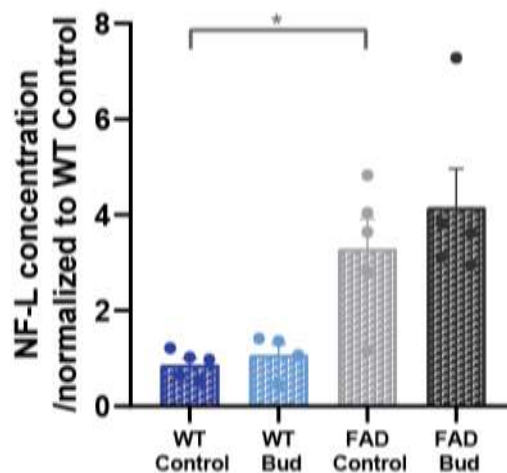


Figure S4: Quantification of Neurofilament light chain (Nf-L) concentration in the plasma of wt and 5xFAD mice upon long-term intranasal budesonide treatment. Nf-L was not altered upon long term intranasal Budesonide treatment at 6 month. N \geq 4. Data are presented as mean \pm SEM; ordinary one-way ANOVA followed by Sidak's multiple comparisons test, *p \leq 0.1, **p \leq 0.01. (Sample measured by Pauline Bongard)

9. Acknowledgments

First and foremost, I would like to express my deepest gratitude to my supervisor, Prof. Dr. Anja Schneider, for providing me with the opportunity to undertake my doctoral studies in her esteemed group. Your scientific guidance has been invaluable, and you have been a role model for me as a successful female scientist and medical doctor, embodying experience, kindness, and fairness. Your support has been a beacon of inspiration, and I am profoundly thankful for the wisdom and encouragement you have imparted.

I extend my heartfelt thanks to Prof. Gabor Petzold, Prof. Jochen Walter, and Prof. Mikael Simons for their willingness to be in my thesis committee. Your guidance throughout the progress of my study and the valuable advice you provided for my project have been instrumental in shaping my research and academic journey.

A special thank you goes to the animal caretakers at DZNE Bonn for their dedicated care of the mice. Your hard work and commitment have been crucial to the success of this research. I am also immensely grateful to Ireen and Hans from the Light Microscope Facility (LMF) at DZNE in Bonn for their exceptional efforts and solution-oriented support, which have been pivotal in advancing my work.

I would like to express my sincere appreciation to Dr. Kristin Oberländer for supervising and guiding me through my daily training as a scientist. Your patience, professional experience, and steadfast support in both my work and personal life have been remarkable. You have been a great role model for me and a kind person who unites the group and supports everyone. Your mentorship has been a cornerstone of my development, and I am deeply grateful for your guidance and friendship.

My gratitude also extends to everyone in the AG Schneider group. Thank you for creating an amazing, friendly, and professional working environment. This is truly precious, and I will always remember how fortunate I was to be part of this group. Special thanks to

Christian for being a fantastic technician, always supportive and excellent in his work. Also, thank you to Anna, Eva, Tanja, Heba, Sophie, Loic, Madhurima, and Selcuk for being wonderful colleagues and making the office a lot of fun. Your camaraderie and collaboration have made this journey enjoyable and enriching.

I also want to thank my friends who have supported and encouraged me during the highs and lows of my PhD journey. Thank you, Alina, Annika, Komal, Angela, Lily, and Sophie, for the wonderful times outside of the lab and for sharing the ups and downs as PhD students. Your friendship has been a source of strength and joy. And to Samuel, I am incredibly grateful to have you in my life, always bringing me joy and peace. Your constant support has been my anchor.

Finally, I would like to thank my family for their steadfast support and trust. You have always given me the strength to move forward. Your encouragement and belief in me have been my foundation.

I am deeply appreciative of everyone who has been part of this journey. Thank you for contributing to this incredible adventure and for being part of my life.

10. Publications

Yang X, Hutter M, Goh WW, Bureik M (2017) CYP4Z1 - A Human Cytochrome P450 Enzyme that Might Hold the Key to Curing Breast Cancer. *Current Pharmaceutical Design* 23, 2017. <https://doi.org/10.2174/1381612823666170207150156>

Song Y, **Yang X**, Li Z, Zhao Y & Fan A (2014) Label-free chemiluminescent ATP aptasensor based on graphene oxide and an instantaneous derivatization of guanine bases. *Biosensors and Bioelectronics* 51, 232-237. <https://doi.org/10.1016/j.bios.2013.07.039>